A Finite Element Modelling Strategy for Suture Anchor Devices

A thesis submitted for the degree of Doctor of Philosophy

Christopher M. Hughes

Brunel University
School of Engineering and Design

March 2014

"Consider again that dot."

-   Carl Sagan

Abstract

Suture or bone anchors are used to reattach a tendon or ligament after it has been torn away from the bone. Anchors provide secure attachments to bone during trauma or reconstructive surgery, holding the ligament or tendon in place and potentially allowing greater mobility during recovery.

Computer modelling techniques are used to investigate both established bone anchor technology, such as threaded implants, and emerging technologies such as cement augmentation or sonic-fusion. Sonic fusion is an ultrasound-assisted anchoring method which has recently been introduced in low load maxillofacial applications, and is expected to be used in other low load applications such as hallux valgus alignment procedures and suture attachment.

Threaded anchors were examined using two Finite Element (FE) models of human cancellous bone, representing both "normal" and "weaker" bone. Simulation and analysis revealed the critical nature of modelling the microstructure of bone. Changing the direction of loading in the model leads to significant changes in the response of the construct, and this cannot be represented in continuum models, or in physical models using artificial cancellous bone. Rapid prototyping (RP) using 3d printing was used for validation of the FE models. While this method has previously been implemented to create physical bone models, testing an assembly model and comparing it to FE results for inclined loading had not been attempted. RP models were created of the threaded anchor in both "normal" and "weaker" bone, and a sonic fusion model in the normal bone was also created. These models were then subjected to mechanical testing. Results produced from the simulation correlated with the physical results.

The importance of a cortical layer was re-confirmed. At the apparent densities simulated, engagement with the cortical layer increases pull-out force

dramatically. Engaging the anchor even with a thin cortical layer can produce a significant improvement to pull-out strength.

Novel sonic fusion FE models were created from a CT scan of animal bone, and the geometry for both the sonic-fusion pin and bone were taken from the CT scan. Computer generated geometry was used to build pin concepts of varying shapes. It was shown that if good engagement is made with bone, as in the case of all of the concepts created, then sonic fusion can produce a good holding power - comparable with that of a threaded anchor. The results showed that sonic-fusion requires less drill penetration into the bone, meaning less of the inherent bone structure is removed – vital for patients with poor bone quality.

Bone cement models were investigated. Bone augmentation models were created, and the addition of cement demonstrated an improvement in anchor holding power. The research showed that there are benefits to using FEA as a tool to evaluate the mechanical aspects of cement distribution. The results proved the hypothesis that augmentation will likely increase the holding power of anchor, and its distribution will affect pull-out significantly.

This work has created a method for modelling and evaluating both established and novel bone anchor technology in CT bone geometry, a procedure which could be expanded to other bone implants. It has been validated using the innovative approach of rapid prototyping.

Acknowledgements

I wish to thank the following people who have helped me get to this stage and offered their support throughout the project:

At Brunel University: Chris for his guidance, motivation and time. Keith for his help during testing and for the cups of tea. Philippe and Rhona for their help getting me started and showing me it can be finished.

Stryker for sponsoring the project and giving me invaluable guidance throughout, especially Astrid, Gert, and Torben. Philip for his enthusiasm and dependable input.

My Family for shaping who I am.

My Friends for letting me be myself: Alice, Andre, Bernie, Cakey, Charlie, Chilli, Clare, Dan, Dave, Ed, Gary, George, James, Joe, Jonny, Liz, Matt, Moeva, Noona, Oli, Rachel, Sophia, Tim, Tom, Tom, Will and Vijay, and especially Will and Wilf.

Juliet, Dave, Mary and Tom for an act of kindness I will never forget.

Amy for putting up with a student all these years, and all she has given me in life.

Declaration

I confirm that the intellectual content of this research presented in this thesis is the original work of the author, save for any express acknowledgements, references and bibliographies cited in the work. This work or any part thereof has not previously been presented in any form to any institutional body whether for another degree, award or other purposes.

This project was carried out at the School of Engineering and Design, Brunel University, under the supervision of C. J. Brown.

Contents

List of Figures

List of Tables

Acronyms and Abbreviations Used

ACL – Anterior Cruciate Ligament

BV/TV – Bone Volume/Total Volume

CaP – Calcium Phosphate

CPC – Calcium Phosphate Cement

CAD – Computer Aided Design

CFD – Computational Fluid Dynamics

C(A)T – Computed (Axial) Tomography

FDA – Federal Drug Administration

HA – Hydroxyapatite

HPC – High Performance Computing

FEA – Finite Element Analysis

FEM – Finite Element Method

MRI – Magnetic Resonance Imaging

NHS - National Health Service

OFC - Osteitis Fibrosa Cystica

PLA – Polylactide

PLDLLA – Poly(L-lactide-co-D,L-lactide)

PMMA – Polymethylmetharcrylate

PU – Polyurethane

RP – Rapid Prototyping

SD – Standard Deviation

SLA – Stereo-Lithography

SLS – Selective Laser Sintering

SMI - Structure Model Index

Tb.Th – Trabecular Thickness

Tb.SP – Trabecular Spacing

WHO – World Health Organisation

Equations

$$(1)\ \sigma_{ult} = 68\dot{\varepsilon}^{0.06}\rho^2$$

$Where:\ \sigma_{ult} = Ultimate\ Tensile\ Strength\ (Pa)$

$\dot{\varepsilon} = strain\ rate$

$\rho = density\ (kgm^{-3})$

$$(2)\ v = \sqrt{E/\rho}$$

$Where:\ v = velocity\ of\ sound\ (ms^{-1})$

$E = Young's\ Modulus\ (Pa)$

$and\ \rho = density\ (kgm^{-3})$

$$(3)\ F_s = S \times A_s = \left(S \times L \times \pi \times D_{major}\right) \times \{0.5 + 0.57735[d/p]\}$$

$Where:\ F_s = Predicted\ shear\ failure\ force\ (N)$

$S = Material\ ultimate\ shear\ stress\ (MPa)$

$A_s = Thread\ shear\ area\ (mm^2)$

$L = Length\ of\ thread\ engagement\ (mm)$

$D_{major} = Major\ diameter\ (mm)$

$d = Thread\ depth\ (mm)$

$p = Thread\ pitch\ (mm)$

$$(4)\ Pure\ Penalty:\ F_{normal} = k_{normal}x_{penetration}$$

$$(5)\ Augmented\ Lagrange:\ F_{normal} = k_{normal}x_{penetration} + \lambda$$

$F_{normal} = Force\ (N)$

$k_{normal} = constant$

$x_{penetration} = displacement\ (m)$

$\lambda\ is\ an\ internally\ calculated\ term\ that\ augments\ the\ penalty\ calculation$

1 Introduction

Tendon or ligament tear is a common injury, leading to pain and potentially lengthy recovery times for the patient. For example, in the United States alone there are estimated to be 150,000 anterior cruciate ligament (ACL) injuries each year (Gordon & Steiner, 2004).

In the event of severe tendon or ligament tear, bone anchors are used to provide secure attachments to bone during trauma surgery, holding the ligament or tendon in place. The use of bone anchors may therefore allow a patient greater mobility during recovery. This thesis describes the use of computer modelling techniques that are used to investigate both established bone anchor technology, such as threaded implants, and emerging technologies such as cement augmentation or sonic-fusion.

Bone anchors are similar in structure to bone screws, but have the addition of a suture eyelet. They are also smaller in size (typically 5mm diameter), and predominantly produced with a tapered thread to aid insertion.

Historically, screws have been used more prevalently in surgery than bone anchors (6-8 screws are generally required per procedure compared with only 1-2 anchors), so knowledge of the holding power of screws is comparably well researched due to the greater frequency of use, as are the influences that affect screw pull-out. This is the load at which the screw fails.

The general equation for screw pull-out can be used in a continuum of any size, but with bone anchors inserted in cancellous (internal "spongy") bone this is less appropriate – due to the smaller size of anchors (typically a 5 mm diameter) and the open, porous bone structure. When using a small implant, such as a bone anchor, even a 1mm difference in placement position can lead to significant variance in pull-out strength due to this heterogeneous structure. The risk of pull-out increases further if low density osteoporotic cancellous bone is encountered (Chapman, 1996).

When bone anchors fail, their subsequent pull-out and replacement requires further surgery. This failure may occur after many months of physiotherapy and recovery, and can be very distressing – and painful for the patient.

By furthering the research into suture anchors' performance in bone, the aim is to improve the holding power of bone anchors, reducing the incidence of pull-out.

In addition to established threaded anchor technologies, emerging technologies; sonic-fusion and cement augmentation, are also examined and compared with the conventional anchor application procedure.

Sonic-fusion is an ultrasound-assisted anchoring method which has recently been introduced in low load maxillofacial applications (Müller-Richter *et al.*, 2011; Aldana *et al.*, 2009). In the long term it is intended to compete with conventional resorbable and metal screw systems in supporting fixation of cortical bone fragments.

Laboratory research is being carried out into suture anchoring using sonic fusion, rather than traditional titanium anchors (Schneider *et al.*, 2012). The technique applies ultrasonic energy onto a polymer implant inducing heat by generating shearing forces at the contact interface between implant and bone. Within seconds the polymer re-solidifies, forming a strong and uniform interface between implant and bone. Biomechanical data (Meyer *et al.*, 2006) demonstrates that this kind of anchoring provides enhanced stability which may reduce the risk of implant migration.

Sonic-fusion technology has not been computer modelled previously and is a novel aspect to the research.

In addition to sonic-fusion, bone cement models will be presented. Bone augmentation products have been available for some time; two common types of bone cement are Polymethylmetharcrylate (PMMA) and calcium phosphate (CaP). Historically the use of PMMA cement has been unpopular due to the heat generated during curing, resulting in cell necrosis(Gundapaneni & Goswami,

2014). More recently, Calcium Phosphate based augmentation products have been developed, and while these are primarily defined as non-load-bearing, the effects of using them to fill voids around critical screws in cancellous bone is under investigation. Early trials have shown positive results, and it is likely that such products will gain Federal Drug Association (FDA) approval in the near future – hence their inclusion in this research.

Testing these osteosynthetic devices in human bone is out of scope for this project but there are some alternatives. Polyurethane foam is used as a common substitute for bone and is frequently examined in laboratory evaluations. It comes in different forms that correspond to the varying mechanical qualities of bone. It is produced in both open and closed pore structures. Open-pore foams are commonly used to substitute lower apparent density (weaker) bone. Unfortunately its pore size is larger than that found in human bone, meaning it is unsuitable for small implants as they often have insufficient material to engage to. Closed-pore foams are not suitable for testing augmentation products as the cement or polymer cannot flow through the material.

Another option would be to use animal bone but as animals are usually slaughtered at a young age, their good bone quality means it can be unsuitable for testing. This is because this research investigates whether the implant is also suitable for weak or osteoporotic bone – not just healthy bone.

It can be argued that the best medium to test the suitability of anchors to be used in humans - is human bone. However, physically testing human bone is more expensive and there are additional ethical considerations. Furthermore, testing human bone is often destructive, unlike computer modelling, such as Finite Element Analysis (FEA) where the same piece of bone can be tested infinitely.

The main objectives of this research are to model physical systems using FEA. This technique calculates the stresses and strains in implanted devices and the

surrounding bone. FEA is a well-established tool for simulating loads upon the musculoskeletal system (Simpson *et al.*, 2008). Previously, solid models were used to simulate the internal "spongy" bone but it is now possible to take real micro-geometry of bone from CT scans.

As software and hardware improves and becomes more affordable, more realistic models can be produced. Even within the relatively short timeframe of this research, the models used have developed from simplified structures to 3d models of human cancellous bone taken from micro CT scans.

This advancement in technology means less laboratory work is required - and hopefully less pre-clinical work will be required in the future.

1.1   Contribution to the body of knowledge

- An innovative method of modelling cancellous bone using frictional contacts. A description of the method used to create a 3d mesh suitable for simulation

- Substantiation of the FEA models created by 3d printing of replica models and mechanically testing them - Rapid prototype models have revealed variations in reaction force with results aligning with those of FEA

- The first detailed anchor study carried out with FEA – what affects the holding power of bone anchors?

- A study of the use of bone cement with anchors and showing how its use can greatly improve the holding power of an anchor

- Simulation of sonic fusion models and showing that sonic fusion currently provides no strength advantage over a threaded anchor but looks to reduce stress applied to the bone.

1.2   Thesis Outline

In this thesis established spiral anchors are investigated first, and then the emerging technologies are examined: sonic-fusion and augmentation. Validation methods are also explored and tested.

Chapter 2 gives background information on the relevant subjects; including bone properties and histology, bone substitutes, implant technology, and computer modelling methods.

Chapter 3 discusses the path to the modelling technique used, how the process was refined using preliminary models and knowledge on finite element modelling.

Chapter 4 studies a traditional spiralled anchor and examines the effect of adjusting the bone density and the thickness of the cortical layer. It also looks at the importance of modelling frictional contact.

Chapter 5 continues these studies by looking at suture pull in all directions and also includes additional side studies looking at bone orientation and thread taper.

Chapter 6 investigates sonic fusion and looks at the methods of modelling it, arising with a suitable comparable method.

Chapter 7 compares a sonic fusion model to an appropriate predicate device.

Chapter 8 provides evidence towards validation. Physical models were produced using 3d printing and were physically tested and compared to the FEA models.

Chapter 9 looks at the use of augmentation, by adding idealised cement geometry to the FEA models.

Chapter 10 collates the findings of the previous chapters, discussing the results and observations. A recommendation of further work is also made.

2 Review of the Literature

2.1 Overview

This thesis addresses the problem of torn connective tissue and its repair. Most commonly this affects tendons but also ligaments. If a tendon becomes torn it must be reattached to reinstate function. The most widespread surgical method to enable repair is to insert an anchor into the bone and reattach the tendon by suturing it to the anchor, therefore anchoring it to the bone (Barber, 2006). Most anchors are threaded and thus screwed into the bone. As connective tissue is predominately located near joints, anchors are generally inserted on or near the condyles (rounded heads) of long bones. However the strong cortical layer here is thinner. At the epiphysis (ends) of the femur for example, the cortical layer can be less than 1mm thick (Jee, 2001). Due to this lack of stronger cortical bone in this region, fixation into cancellous bone is of greater interest to researchers of these devices.

Not all implants are threaded; other types of anchors work by creating an interference (friction) fit with the bone; a hole is drilled, the anchor inserted, and then expanded physically. Performances of both types of anchors are clearly dependent on the structure of the surrounding bone.

New anchor designs are primarily tested using mechanical methods (Barber, 2008); investigating these types of implants frequently involves the use of a polymer bone substitute, with progression to animal and human bone for more detailed evaluations.

Modern evaluation methods also make use of computer modelling. At present there is limited published work utilising computer models on anchors. However simulations involving larger threaded implants are available and descriptions of models using micro-CT scans are beginning to appear in the literature.

Although the threaded anchor design has been used for decades, technological developments are leading to a greater understanding of the devices. A decade

ago computer models of bone were all solid continua. This evolved into simplified lattice modelling and now it is possible to model the cancellous bone structure from CT scans. However, creating a model detailed enough to simulate the mechanics of large problems, such as multiple lag screws in bone with full cortical and cancellous geometry, is currently out of scope of most research grade computers. Smaller models can be produced, and as anchors are typically in the range of 3-6mm in diameter, they are manageable to simulate with CT models.

Considerable research has been carried out on the effect of larger thread screws in solids and their holding power can generally be calculated to a reasonable degree (Chapman *et al.*, 1996). Work done on larger threads can also be accurately scaled down to calculate smaller thread screws inserted into a solid.

However, far less research has been done to investigate the efficacy of a small thread screw fitted into a porous material – such as the cancellous bone used to fit bone anchors.

Current improvements to anchors are focused on filling the porous area with a stiff substrate, be that through the use of injectable cement or melting a polymer into the porous bone using ultra-sonic vibrations.

This chapter examines the background of the investigation and has been structured in three sections:

- Bone and its properties relevant to this study
- Anchors and other relevant implants
- Engineering methods available for anchor research.

2.2 Skeletal System

The role of the skeletal system is primarily mechanical; it provides support, protects vital organs (e.g. thoracic cage), and allows movement, but it also has the crucial functions of blood cell production, mineral and lipid storage, and endocrine regulation.

An infant human has just over 300 bones in their body. Over time as some bones fuse and growth stops the adult bone count becomes 206. Traces of bone fusion can be seen in the adult skeleton, particularly at the metaphysis of long bones where the epiphyseal line is present. In the human skeleton there are five main bone groups:

- *Long bones* are found in the appendicular skeleton (limbs); they are long, generally cylindrical and typically have two heads (condyles) at either end. The femur, clavicle and the phalanges are all examples of long bones

- *Short bones* are generally cuboid in shape and found in the limb extremities, e.g. carpals and tarsals

- *Flat bones* often protect the internal organs and include the cranium and scapula. They contain mostly red marrow, and are therefore the largest producers of blood cells in the body, unlike long bones which possess both red and yellow marrow

- *Irregular bones* are non-uniform in shape and include the vertebrae and some facial bones. They primarily consist of cancellous bone with a thin cortical shell

- *Sesamoid bones* are embedded within tendons; they protect tendons and prevent them from collapsing. The patella (knee-cap) is a sesamoid bone

Another type of bone that can form are *Intra-Suturual* bones otherwise known as *Wormian bones.* They are small flat irregular shaped bones that form between the flat bones of the skull. They are a marker for some bone diseases and may indicate the presence of brittle bone disease (Glorieux, 2008). They are not

included in the main five bone groups as they are not present in the majority of people.

2.3   Bone Structure
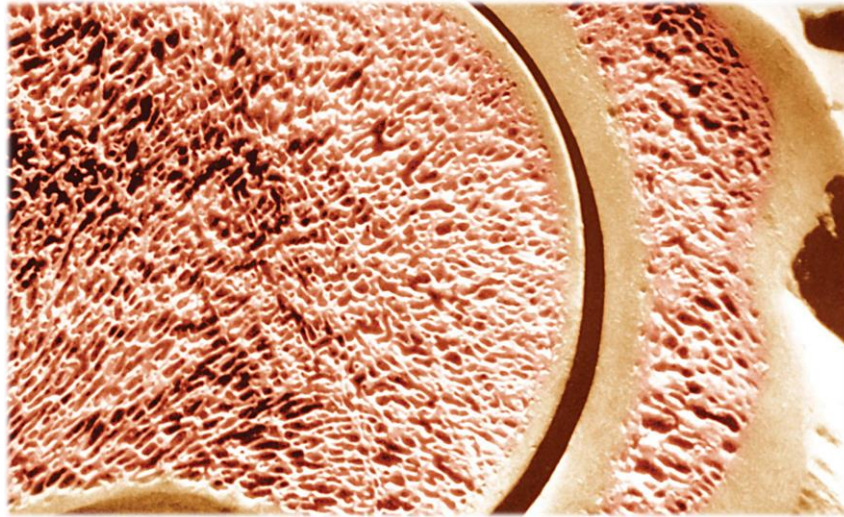
Figure 2-1: Desiccated bone of the Glenohumeral joint, showing cortical shells and inner cancellous bone (http://medicalpicturesinfo.com/cancellous-bone, 10/09/2011)

2.3.1   Cortical and Cancellous Bone

Cortical bone is the compact outer layer which forms the shell of a bone. In long bones it is thickest on the diaphysis (shaft) of the bone, sometimes up to approximately 10mm on the femur (Jee, 2001). At the epiphysis the cortical layer may thin out significantly to less than 1mm on the femur (this can be observed in Figure 2-1). Cortical bone accounts for approximately 80% of the total skeletal mass. It is made up of osteons and interstitial tissue. Cancellous bone accounts for the remaining 20% and is the internal "spongy" bone; it is formed of a lattice of rods and/or plates called trabeculae. The volume fraction of cancellous bone is varied and depends on gender, age, race and environmental factors. The pores of cancellous bone are mostly filled with marrow. Cortical bone (Figure 2-2a) only contains microscopic channels and varies from approximately 2% to 3% porosity in young healthy adults. Cancellous bone varies from 70% to 80% porosity (Jee, 2001). Not all bones have 20% cancellous bone, for example vertebrae are 38%

cancellous, while long bones are less than 10% cancellous. Cancellous bone density is approximately 1.874 g/cm^3 and cortical 1.914 g/cm^3. Cancellous bone has a lower density because it remodels (the histological process of removing and replacing bone cells) at a faster rate which leads to a lower calcium content (Jee, 2001).
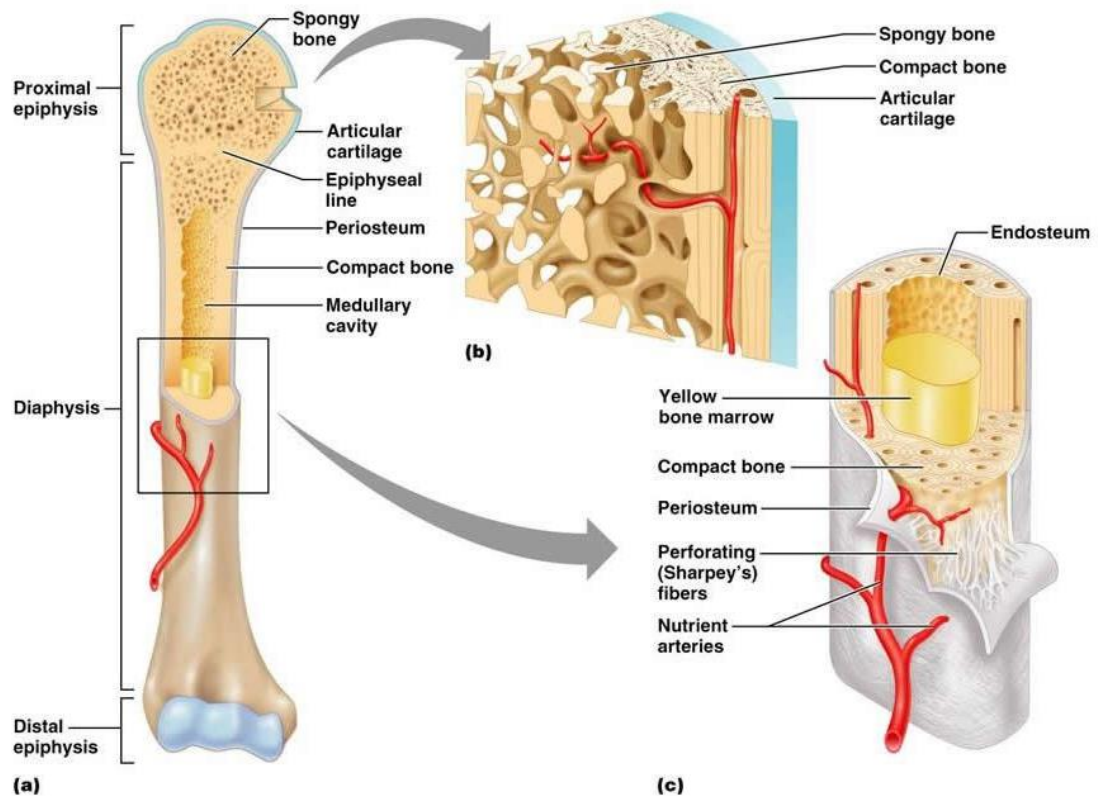
Figure 2-2: Anatomy of Long Bones

(http://classconnection.s3.amazonaws.com/436/flashcards/844436/jpg/long_bone131907191 5389.jpg)

Wolff's Law is the theory (not law) that over time bone will adapt to the loads it is placed under (Goodship & Cunningham, 2001). This theory is debated for its origins, accuracy and exact working. Nevertheless it is true that bone does adapt under various magnitudes and patterns of loading. The main interest in bone re-modelling theory is under what conditions bone adapts. Studies have found that bone mass does not increase under light regular exercise e.g. running (Judex and

Zernicke, 2000), but it will increase under heavy regular exercise as seen in galloping horses (Firth *et al.*, 1999) or under diverse loading such as in a squash player's wrist. It is also true that the trabecular structure of cancellous bone will align along the principal stress trajectories that the bone is subjected to. The main use of understanding how bone re-models under stress is to obtain a reduction in healing times and to minimise additional stress on the bone by good implant positioning. Some loading is important, otherwise stress shielding can occur (Jee, 2001). Stress shielding when a reduction in bone volume occurs due to lack of stimulus during remodelling.

2.3.2 Marrow

Bone marrow is vital tissue and consists of two types: red and yellow. Yellow marrow is made up of mostly fat; it is not present at birth but its presence increases with age to approximately 50% of the total marrow in adults. Red marrow is primarily made up of haematopoietic tissue (tissue in which blood cells are formed). Most yellow marrow is found in the diaphysis of long bones, whilst red marrow is found mainly in flat bones and in cancellous bone. Mechanically it provides negligible support. However it is important to consider its material properties when inserting implants. At 37 °C and under no shear stress marrow has an average viscosity of 0.037 Nsm^{-2} (Davis, 2006), which is 37 times greater than water and in the order of ten times greater than blood. Cements or implants that solidify rapidly encounter greater resistance in living bone than in desiccated bone, and therefore may not penetrate as far due to this high viscosity.

2.3.3 Osteon

The osteon or Haversian system (Figure 2-3) is the main structural unit of cortical bone. Typically an osteon is a cylinder about 200 μm in diameter and runs parallel to the long axis of the bone. An osteon consists of a tube or Haversian canal surrounded by about 20 to 30 concentric layers or lamellae of compact bone tissue. Between each layer lies a cement line, around 1 to 2 μm thick. Within the central canals are nerve fibres, blood vessels, lymphatics and other

loose connective tissue. The length of each canal is around 10 mm; they are interconnected perpendicularly by Volkmann's canals, thus forming a network of tissue (Jee, 2001). Osteons are around 70% of cortical bone volume, the remainder is interstitial bone which is formed from remnants of partially resorbed osteons.
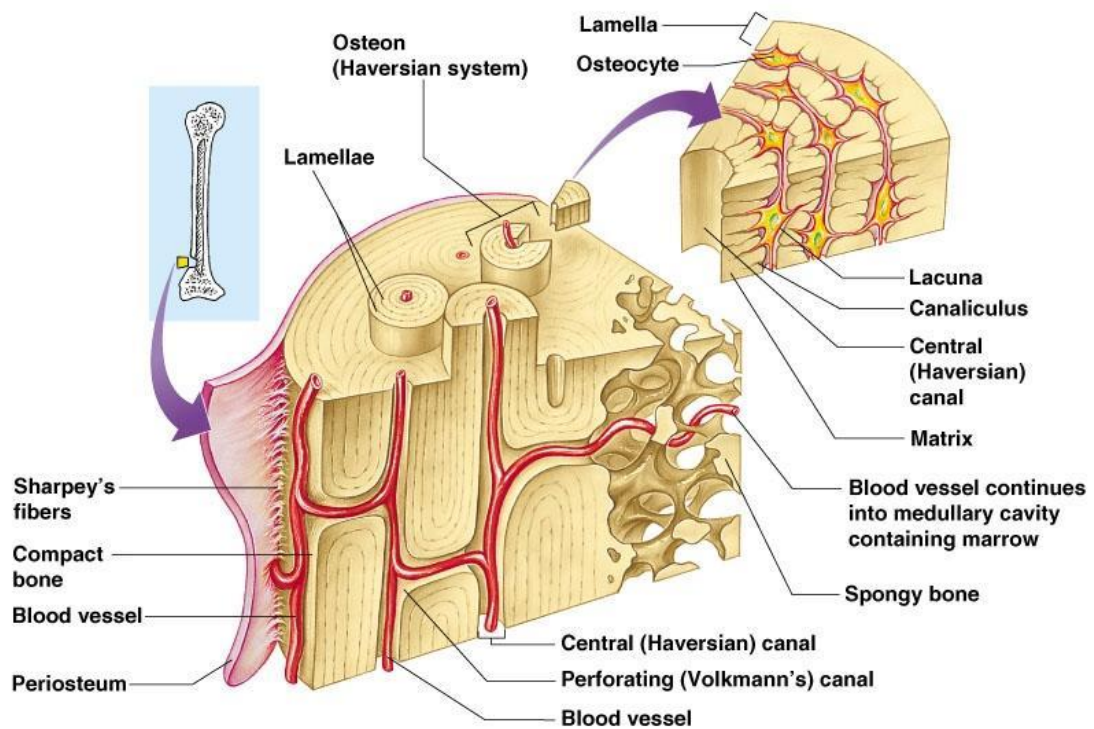
Figure 2-3: Diagram of the Haversian system and its surrounding elements (http://classconnection.s3.amazonaws.com/795/flashcards/1195795/jpg/compact_bone13293 5142174.jpg)

2.3.4 Bone Histology

Bone remodelling is the process which maintains bone; old bone cells are removed (resorption) and are replaced (ossification). In humans after 2 to 3 years, infant or woven bone is replaced with secondary or lamellar bone. Once woven bone has been replaced the mean age of cortical bone is 20 years and 1 to 4 years for cancellous bone (Jee, 2001). Remodelling is vital in maintaining healthy bone by removing damaged cells and adapting bone architecture to regional stresses bone remains healthy. However over time more cells are

removed than created, leading to a reduction in density and overall bone width thus decreasing bone strength. The key types of bone cells involved in bone resorption and remodelling are:

- *Bone-Lining* cells cover bone surfaces and can be activated into osteoblasts. Although these cells do not divide, they do secrete growth factors which trigger osteoblast progenitor proliferation. Bone-lining cells also act as an ion barrier and therefore have a role in mineral homeostasis (Miller, 1989).

- *Osteoblasts* are the single nucleus bone building cells responsible for ossification. They synthesise, and then secrete the bone matrix (osteoid) which is 90% collagen and 10% non-collagenous protein. Once this matrix is formed into an organised structure, it is then mineralised primarily by calcium and phosphate ions. Osteoblast cells decrease with age, which is part of the reason for bone density decreasing with age.

- *Osteocytes* are mature bone cells, and they each entirely occupy a lacuna (pocket). Osteocytes are old osteoblasts which are left behind in lacunae as bone formation occurs; they differentiate from osteoblasts as they have lost most of their organelles (the sub-units of a cell). They are the most abundant in bone cells, and are responsible for stabilising mineral content in the region. They are able to sense local tissue damage and possibly mechanical loading via fluid movement (Ehrlich, 2002).

- *Osteoclasts* are large (20 to 100 μm wide) multi-nucleic cells and are responsible for bone resorption. Active osteoclasts are usually found in cavities on the bone's surface, where organic compounds are soluted by secreting various enzymes and digest mineral compounds by secreting H^+ ions (Jee, 2001).

- *Osteoprogenitor* cells are the precursors to osteoblasts and are classified as stem cells. They are most active during bone growth, but also activate during fracture repair.

2.3.5 Collagen

Collagen is the most abundant protein in mammals, making up 25-35% of the total protein amount (Di Lullo *et al.*, 2002). It is a key molecule providing strength to and between cells, it is found in tendons, ligaments, bones and skin, as well as many other tissue types. Collagen has a high tensile strength to due to its structure – generally in the form of fibrils (fibres less than 10 μm in diameter). Its mechanics depend on the arrangement of these fibrils. In tendons it is found in the form of tightly packed parallel arrangements, whereas in the skin it is found as a cross network of fibres.

Author's Note: Section 2.3 frequently makes use of information provided in chapter 1 of the Bone Mechanic's Handbook, authored by Webster S. S. Jee, and edited by S. C. Cowin. If required a more in depth explanation of bone tissue physiology and histology can be found in this excellent text.

2.4 Bone Disease and Healing

There are many skeletal diseases affecting the strength of bones. Osteoporosis is the most relevant to this project as it affects approximately 5% of the British population (NHS online, 2010). Other relevant diseases which affect bone strength and are therefore of interest are also described briefly.

2.4.1 Osteoporosis

Osteoporosis (derived from the Greek "bone" and "pore") is a skeletal disease which results in a surplus of osteoclast activity. This can lead to an increase in cortical porosity up to approximately 12% and cancellous porosity to over 90%, therefore significantly weakening the bone. The World Health Organisation (2003) definition of osteoporosis is a -2.5 T-score standard deviation from the mean, where the mean is a T-score of a young adult Caucasian woman. T-scores between -1.0 and -2.5 (WHO, 2003) are defined as osteopenia. When fractures are present in osteoporotic bone it is described as severe osteoporosis. In the UK Approximately 3 million people are thought to have osteoporosis and 230,000 fractures a year are attributed to the disease (NHS online, 2010). For Europe and the USA combined that figure rises 10 fold to 2.3 million fractures annually (WHO, 2003).

The risk of osteoporosis increases with a variety of factors, the common ones being: age, decreased gonadal steroids (i.e. the reason for post-menopausal women having a much higher rate of osteoporosis), nutrition (e.g. low calcium and vitamin D diet), drug use (legal drugs such as tobacco and alcohol, and illegal drugs such as heroin), disease, and medication (including hormone treatment and SSRI anti-depressants (Diem, 2007)). The onset of osteoporosis can be delayed by lifestyle changes e.g. exercise, and by a variety of drugs, most commonly from the bisphosphonates group (Abtahi, Tengvall & Aspenberg; 2010). However, bisphosphonates can also have significant side effects.

2.4.2 Other Less Common Bone Diseases

Osteopetrosis (derived from the Greek "bone" and "stone") can be described as pathologically opposite to osteoporosis, instead of a surplus of osteoclast activity in osteopetrosis there is an osteoclast dysfunction (Sandor, 2007). This lack of bone resorption results in more brittle bones than normal and in mild cases this may cause no problems, but in more severe cases it can lead to bone deformation, fractures and narrowing of the bone marrow cavities. These symptoms show the importance of the resorption function and how an imbalance opposite to that of osteoporosis can also cause severe complications.

Osteomalacia (derived from the Greek "bone" and "softness") is commonly known in children as rickets. It is the weakening of bone due to deficient bone mineralisation in turn due to inadequate amounts of phosphorous and calcium. The most common reason for this is a lack of Vitamin D. Common symptoms include weakening and bending of bones leading infamously to genu varum or "bandy-legs" in children. Treatment is relatively straight forward with administration of Vitamin D.

Osteitis fibrosa cystica (OFC) is a disorder in which the sufferer has an elevated number of osteoclasts caused by overactive parathyroid glands. This over-activity of osteoclasts results in weakening of bone as the bone tissue is replaced with fibrous tissue resulting in bone tumours. It can also be treated using Vitamin D but more severe cases require a parathyroidectomy (parathyroid gland removal) and/or bone transplantation (Wysolmerski & Insogna, 2008).

Paget's disease of bone is a condition affecting adults in which there is a higher rate of bone turn-over. This higher rate results in erratic bone growth which may lead to other complications such as: arthritis, cardiovascular issues (due to more blood vessels in the bone), hearing loss and kidney stones. Due to the range and number of complications each patient requires a variety of drug (principally bisphosphonates) and surgical treatments (Ralston, 2013).

2.4.3 Fracture Repair

The principal reason for any type of medicine is to improve on the body's own healing time. Orthopaedic medicine does this via bone fixation. Once re-alignment has been carried out, the body's healing process can continue on an effective path. There are two main types of fracture repair; direct (primary) and indirect (secondary). Indirect fracture involves the formation of "callus" which forms a natural splint, stabilising the fracture region (Goodship & Cunningham, 2001). This happens in three phases:

- *Reactive Phase*: Immediately after fracture vasoconstriction occurs, decreasing blood flow to the area. Then a haematoma forms, killing all blood cells within it, however fibroblasts survive and begin to replicate forming granulation tissue. The reactive phase also includes swelling of the adjacent tissue, providing increased support and protection to the bone underneath (Brighton, 1986).

- *Reparative Phase*: Osteoblasts in the periosteum (outer membrane lining bone) begin to gather around the fracture, forming woven bone. Fibroblasts within the granulation tissue develop into chondroblasts (cartilage forming cells), forming hyaline cartilage. The cartilage and bone tissue grows until it eventually joins and spans the fracture gap, forming a fracture callus. Endochrondral ossification (mineralisation of the hyaline cartilage) then begins. This process combined with bony substitution of the woven bone forms lamellar bone in the form of cancellous bone (Goodship & Cunningham, 2001).

- *Remodelling Phase*: The cortical layer begins to form. Osteoclasts resorb some of the trabecular bone, before osteoblasts deposit the new compact layer. This is the longest phase and it may take up to five years to before the bone returns near to its original geometry (Wheeless, 2001).

Direct fracture repair follows a similar three phase process but only happens under conditions of rigid stabilisation (i.e. under device or plate fixation) when

one fragment of bone matrix comes into direct contact with another (Cowin, 2001). The crucial difference is instead of a callus "splint" being formed via the osteoblasts in the periosteum an intra-cortical "bridge" of woven bone is produced (Perren, 1979).

2.5 Mechanical Properties of Bone

Due to the heterogeneous nature of cancellous bone its mechanical properties vary broadly. Bone modulus has a strong correlation with volume fraction, but it is also dependant on the trabecular orientation or "grain" of the bone and the tissue properties (Keaveny, 2001). Volume fraction or porosity is most commonly used as a measurement of bone health because it can be measured using non-invasive techniques and it has a strong correlation to bone modulus. It is inversely and exponentially proportional to modulus, with a common relation being (Carter & Hayes, 1977):

$$(1) \; \sigma_{ult} = 68\dot{\epsilon}^{0.06}\rho^2$$

$$Where: \sigma_{ult} = Ultimate \; Tensile \; Strength \; (Pa), \dot{\epsilon} = strain \; rate,$$

$$and \; \rho = density \; (kgm^{-3})$$

Additionally, yield stress can be estimated from volume fraction and has linear relationship with the bone's elastic modulus (Keaveny, 2001). As the volume fraction of cancellous bone changes over a cross section, so does its modulus. It can vary in orders of magnitude, as the bone alters in porosity over a section (Figure 2-4).
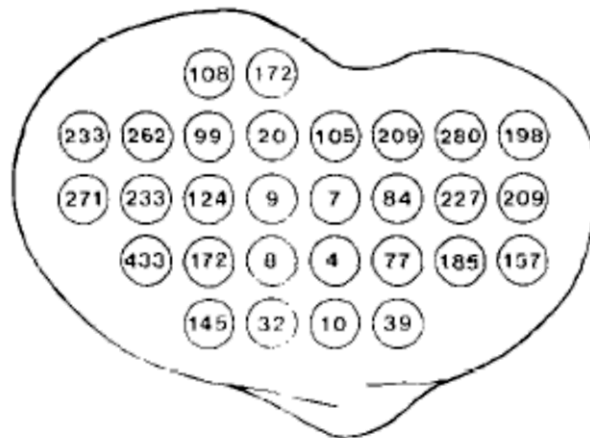
Figure 2-4: Elastic moduli from a proximal transverse section of a human tibia. Values are in MPa (Goldstein, 1983)

Anisotropy is when a material's property (or properties) varies directionally. In the case of bone, mechanical anisotropy is of interest. Anisotropic effects are due to the architecture of the bone, and are primarily dependant on the grain direction (Figure 2-5). Bone develops this grain due to the adaptive remodelling effect (as described in Wolff's Law). Trabecular orientation explains the majority of deviation from the Carter & Hayes (1977) density relationship, whilst the remaining deviation can be accounted for by variation in tissue properties. It was previously though that anisotropy increased with age (Hodgkinson, 1990). However it now seems that this is not now the case. Sugita *et al*. (1999) published results showing that bone with a mean patient age of 79.9 was less anisotropic than bone samples from younger patients. However Snyder *et al*. (1993) provided an earlier reason for this effect, showing that with decreasing apparent density, vertical trabeculae are resorbed at twice the rate of horizontal trabeculae, so the data is potentially in conflict.
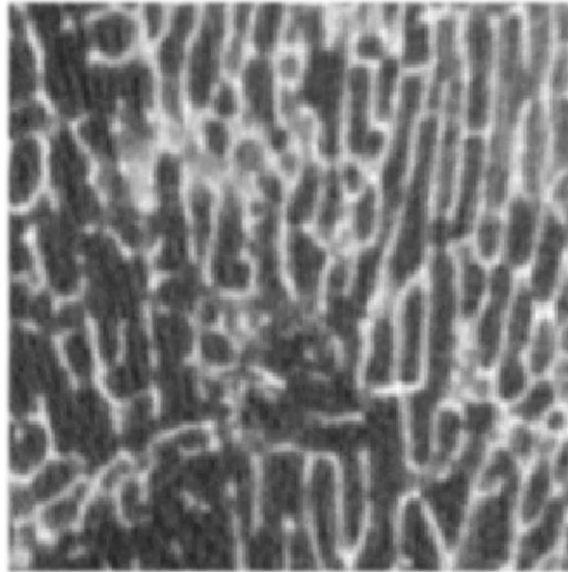
Figure 2-5: CT scan of ovine bone, showing the varying grain direction and differing porosity. Photographed areas is 14 mm by 14 mm (Author's own image)

Care should be taken when discussing the mechanical properties of cancellous bone, as there are two different categories of mechanical properties. There is a set of "global" anisotropic mechanical properties which is dependent on the density, grain structure and tissue properties. There is also the "specific" mechanical property which only measures the tissue properties and is isotropic in cancellous bone.

Explaining variation in cancellous strength and modulus is useful. However it does not answer the question of what values should be chosen for productive engineering situations. Measuring cancellous bone's specific modulus is difficult due to its micro-structure; values measured for human bone have been in the range from 3.7 GPa via 3-point bending (Kuhn *et al.,* 1989) to 20.7 GPa via ultrasound, using the relationship (Rho *et al.,* 1993):

$$(2) \quad v = \sqrt{E/\rho}$$

$$Where: v = velocity\ of\ sound\ (ms^{-1}), E = Bulk\ Modulus\ (Pa),$$

$$and\ \rho = density\ (kgm^{-3})$$

Values can be obtained in different ways; modern methods include ultrasound and nano-indentation, but previously have included buckling, tension and 3-point bending tests. Mechanical tests have the drawback of attempting to measure small pieces, which are irregular in shape and may have large relative indentations. For these reasons visco-elastic testing often gives lower elastic moduli compared to the more modern methods of ultrasound and nano-indentation (although these methods also have their drawbacks e.g. ultrasound cannot be used to determine strength characteristics). Variations in these test results means determining a value for cancellous bone's elastic modulus may be difficult and to an extent idiosyncratic. Values between 12-18 GPa are generally accepted (Currey, 2003), but values outside this range are not necessarily incorrect. The Poisson's ratio for cancellous bone is often considered isotropic, and is typically taken as 0.3 (Turner *et al.*, 1999) because the variation is a small effect.

Cortical bone is anisotropic which is due to the lamellar structure which forms during growth. Typical values when measured acoustically for the elastic modulus in human long bone are in general 20 GPa longitudinal and 13.4 GPa transverse (Ashman *et al.*, 1984). Turner *et al.* (1999) had similar results when measuring acoustically: 20.55 ± 0.21 GPa longitudinally and 14.91 ± 0.52 GPa transversally. However their results were 10-20% higher when using nano-indentation. Turner *et al.* (1999) put this down to the fact that the acoustically measured samples were allowed to re-hydrate before testing, indicating the two techniques would give similar results if carried out under the same conditions. This shows that the average Young's modulus for cortical bone is not significantly different from the specific modulus of cancellous bone.

2.6   Animal Bone

Animal bone is often used in device studies, mainly due to availability and lower cost, although studies which monitor live animals (mainly fracture repair studies) will cost significantly more and incur greater ethical questions. Animal bone is

useful for carrying out comparative studies for devices in healthy bone. However there are some limitations. Generally animals are slaughtered at a young age, therefore having bone with high strength and stiffness properties and thus cannot be compared to human osteoporotic bone. Figure 2-6 shows the difference between animal (bovine) and low-density human bone. Drugs may be used to chemically age the animal bone, but this increases cost and raises very serious scientific ethical questions. Where possible it is optimal to use human cadaver bone to compare human implants. This is even more important for osteoporotic focused devices. For implants with drug or other coatings it is essential in vivo studies must be carried to understand the complex biology.
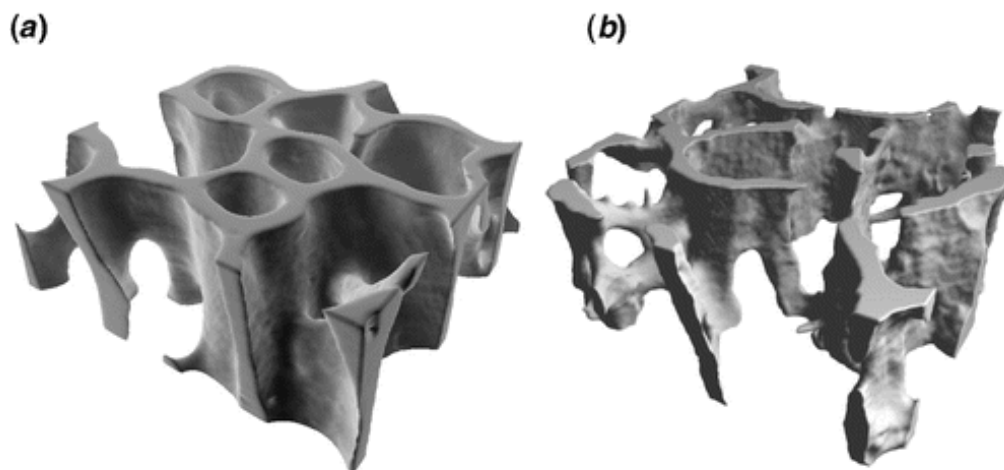
Figure 2-6: Volume rendering (20-µm resolution) of (a) bovine proximal tibial, (b) human proximal tibial. Both specimens have the same bulk dimensions (3 × 3 × 1 mm³). Keaveny (2001)

The focus of the previous sections has been on cancellous bone rather than cortical bone. This is because there is only very thin layer of cortical bone present at the epiphysis of long bones where anchors are predominately inserted, leaving cancellous bone as the predominant bone type to fix in to (Barber, 2006). Furthermore, occasionally the cortical layer is removed during surgery to promote healing in the area, only leaving cancellous bone.

2.7 Tendons And Ligaments

Tendons are the tough fibrous tissues that connect muscle to bone rather than ligaments which connect bone to bone. Both are mostly made-up of parallel collagen fibres closely packed together which stretch and undergo tensile loading. Tendon comes from the Latin *tendere*, "to stretch".

2.7.1 Tendon and Ligament Reconstruction

Under heavy or sustained load tendons can become unattached from the bone. This is commonly known as a tendon tear. Two of the most common areas for severe tendon or ligament tears are the shoulder and knee; specifically the rotator cuff and the anterior cruciate ligament (ACL). If the tear is not severe, non-operative treatment involving physical therapy aided by drugs and ice packs may be used. More relevant to this project is the reconstruction of severely torn tendons which are reattached by inserting a bone anchor or anchors and suturing the torn tendon to it/them. In the case of a rotator cuff (muscle and tendon group in the shoulder) repair anchors are frequently inserted at 45° (Mazzocca, Cole & Rome, 2002) and separated by 5-8mm if two or more are needed.

2.8 A Brief History of Surgical Implants

The first surgical implants discovered date back to 600 AD and are in the form of false teeth made from shells by the ancient Mayan population. During the Middle Ages (as with most scientific and cultural progression) not much headway was made and it wasn't until after the Renaissance era development in orthopaedic surgery happened. Orthopaedics is the branch of surgery relating to the musculoskeletal system derives from the Greek words "orthos" meaning correct and "paideion" meaning child. It was coined by Nicholas Andry in 1741 for the title of his book; *Orthopaedia: or the Art of Correcting and Preventing Deformities in Children*. The first orthopaedic institute was opened forty years later in 1780 by Jean-Andre Venel, and focused in the treatment of skeletal deformities in children. The birth of widespread orthopaedics can be said to have

happened in the mid to late 19th century due to two major innovations; the plaster of Paris cast devised by a Dutch military surgeon, Antonius Mathysen, and the discovery of carbolic acid as an antiseptic by the British surgeon, Joseph Lister. The pioneering of antiseptic techniques allowed surgeons to insert sterile metal implants, greatly reducing infection during surgery, which was a major cause of death post-surgery at the time. In 1883, sixteen years after Lister first published his work on suppuration (the discharge of pus) in the Lancet, orthopaedic screws and plates for internal fixation were devised by surgeon W.A. Lane. They were first used in 1886 by German surgeon, Dr. H. Hansmann, however these early plates were made from vanadium steel which was later deemed to be incompatible with body tissue. Before stainless steel was created in the in 1910s, ivory and nickel plated screws were used by Themistocles Gluck in 1910 to create the first ball and socket hip joint.

Modern Surgery started in the First World War, 6.5 million people were left invalid in France and 20 million people are estimated to have been wounded in total. This gave surgeons a huge challenge and experimental surgical theatres became common in both military field hospitals and civilian hospitals. After the First World War and the growth of X-ray photography, rapid progress in implants began to be made. By 1926, stainless steel was used as the main material for implants and orthopaedic companies such as Zimmer were being formed. In 1930 the Steinman pin or Kirschner wire (now known as the K-wire), a metal rod for internally securing fractures was used and made popular by Lorenz Bohler. In 1939 Gerhard Kuntscher first used an intramedullary (IM) nail to treat long bone fractures which allowed patients (mainly soldiers at that time) to return to normal activity in a much shorter time frame due to the metal implant carrying a proportion the load. After World War Two, IM nails were discovered in returning prisoners of war and quickly adapted around the world to treat long bone fractures. An extract from Time magazine of March 12, 1945 read:

"At England General Hospital in Atlantic City last week was a wounded soldier with a strangely mended femur (thighbone). The man had been treated by the

Germans, his captors. When the broken bone failed to heal, after weeks of conventional treatment, the soldier was operated on. He was mystified to find that his only new wound was a 2½-inch incision above the hipbone. Two days later, the German surgeons told him to move his leg; a few days after that, they told him to walk. He did. He has walked ever since. After his exchange, U.S. Army doctors X-rayed the soldier's leg. They were amazed at what they saw: a half-inch metal rod of some kind had been rammed down the thighbone through the marrow for three-quarters of the bone's length, thus supplying a permanent, internal splint."

A decade later saw the first ACL reconstruction and the introduction of titanium alloys in orthopaedic implants. The 1960s saw the first total hip replacement by John Charnley who pioneered the use of a cemented polyethene cup to replace a worn socket.

Recent relevant developments include: medical imaging, cement, polymers and to some extent scaffolding and robotics. The invention of Magnetic Resonance Imaging (MRI) and Computed Tomography (CT) could be argued as having the largest impact as it has enabled clinicians to diagnose disease quicker with no invasion (bar x-ray energy) and scientists to better understand the human body. One fragment of this is the ability to distinguish tissue types from layered images and build 3d models from the image slices. This allows surgeons to have much more information before they go into surgery, even allowing them to handle rapid prototyped models before a procedure. It also allows companies to produce tailored implants for a superior fit and for engineers and scientists to simulate natural processes such as blood flow through the heart or externally implemented effects such as bone implants.

2.9 Surgical Screw fixation

Although this text will focus mainly on suture anchors, surgical bone screws are also of relevance as a greater body of research has been carried out into the interaction of screws with bone. Screw stability is clearly important but it is awkward to measure, therefore the most common measure is pull-out force.

When predicting implant failure, screw pull-out strength is most commonly assessed, and therefore is the most valid to consider; Chapman *et al*. (1996) gave an evaluation of the equation given by Oberg *et al*. in the Machinery's Handbook (1987):

$$(3)\ F_s = S \times A_s = \left(S \times L \times \pi \times D_{major}\right) \times \{0.5 + 0.57735[d/p]\}$$

Where:

$$F_s = Predicted\ shear\ failure\ force\ (N)$$
$$S = Material\ ultimate\ shear\ stress\ (MPa)$$
$$A_s = Thread\ shear\ area\ (mm^2)$$
$$L = Length\ of\ thread\ engagement\ (mm)$$
$$D_{major} = Major\ diameter\ (mm)$$
$$d = Thread\ depth\ (mm)$$
$$p = Thread\ pitch\ (mm)$$

Chapman *et al*. compared the relationship using three different densities of polyurethane (PU) foam, and came to the following conclusions:

a) *Screws embedded in porous materials within the range of densities and shear strengths of cancellous bone shear the internal threads in the material during pull-out.*

b) *Experimental bone screw pull-out strength is highly correlated to that predicted for machine screws.*

c) *The pull-out strength in porous material is governed by the factors laid out in the equation by Oberg et al.*

d) *Increasing thread shape factor increases screw purchase in a porous material.*

e) *Cannulated screws tested had a lower pull-out that the equivalent non-cannulated screw, although this was probably due to the increase minor diameter due to cannulation.*

f) *Tapping in porous media decrease screw pull-out, because the removal of material effectively increases the minor diameter.*

It should be stated that some studies have found have found a good correspondence to the mechanical properties of bone to PU foam (Gibson & Ashby, 1988). However at lower densities (below $0.16g/cm^3$) the behaviour may not necessarily correspond well due to the increasing anisotropy and heterogeneity (Patel, Shepherd & Hukins; 2008).

2.10 Current Suture Anchors and their use

Suture anchors are generally small screws or plugs with eyelets and a suture attached. They are smaller but similar in design to bone screws but instead of being used for bone fracture repair they are commonly used to secure tendons or ligaments to bone. A typical use would be a rotator cuff repair or anterior cruciate ligament reconstruction.

Suture anchors are generally judged by their pull-out strength and factors which affect this such as bearing area are considered when designing them. All suture anchors cannot be compared directly as they are designed for different operational procedures. Some may be for use in open surgery in the foot while others may be for arthroscopic surgery in the shoulder.

2.10.1.1 Anchor Types
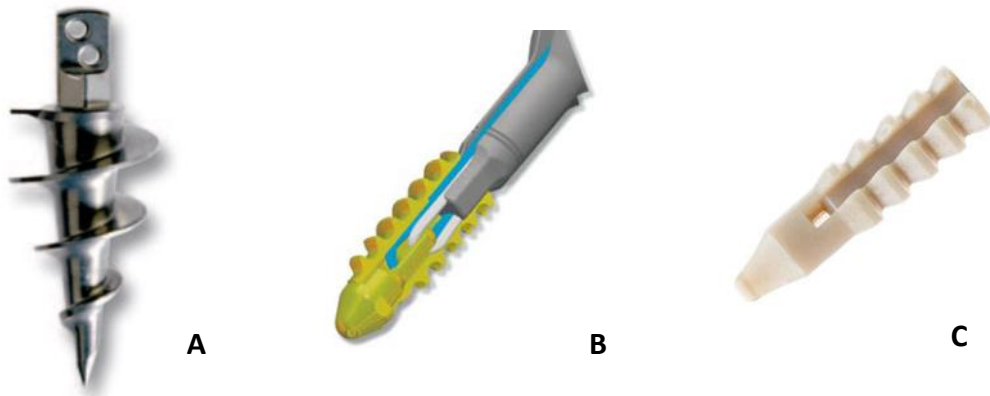
Figure 2-7: from left to right: Stryker Titanium Wedge Anchor (A), Coviden Herculon Anchor (B), Smith & Nephew Kinsa Anchor (C)
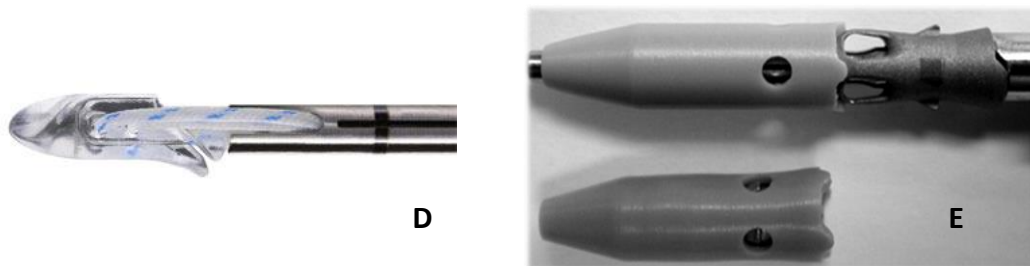
Figure 2-8: from left to right: Stryker XCEL Anchor (D), DePuy-Mitek Versalock Anchor (E)

Figure 2-7 and Figure 2-8 show the main five types of anchor in use. There are a few other new designs or anchor designs which have been and gone due to low uptake or technological developments.

The most common type of anchor is a threaded spiral (A). It is the most popular type and manufactured by a large number of companies and therefore available in many different forms. The main differences between them are external and internal diameters, length, taper and pitch. Some thread pitches are variable, having a tighter pitch at the distal end of the anchor to compensate for the denser cortical bone. The principal material used for these anchors is titanium alloy.

A different but similar type of anchor is the threaded helix type (B). This particular anchor has performed well under in vitro static conditions, and the

model shown achieved the highest pull-out strength in a laboratory evaluation using porcine bone (Barber, 2006). In the 2008 study by Barber the five anchors with the highest pull-out force were all of this design.

Another form of anchor is the push-fit type (C). The one pictured has ridges on the side, but they are also available with studs. This type of anchor often has a low pull-out force due to small area engagement with the bone (Barber, 2008).

Anchors also come in toggle (D) or expandable types (E). Once inserted the toggle anchor head or barb flexes and catches on the cancellous bone (Barber, 2008). When anchored the surgeon rotates off the inserter until it breaks free. The expandable anchor shown expands radially by longitudinal compression after insertion under mechanical force, creating an interference fit.

Traditionally, titanium alloy has been used for anchor material due to its high strength but more frequently polymers are being used as their material strength improves (Barber, 2006 & 2008). Polyether-ether-ketone (PEEK) is a now a common polymer used in anchor design due to its radio-luminance, high strength and relatively soft (compared to titanium alloys) structure, allowing surgeons to drill through if revision surgery is required. Bio-absorbable and bio-degradable anchors are also becoming increasingly popular as their material strength grows with improved manufacturing processes (Tan *et al.*, 2006). A bio-absorbable material chemically breaks down in the body, and is eliminated. A bio-degradable material breaks down, but there is no proof of elimination.

The previous section made reference to Chapman *et al.*'s (1996) equation for predicting pull-out force. Another similar method of predicting pull-out force is bearing area. Bearing area is the area where a surface *may* come into loading with the bone, i.e. if a screw was being pulled out of bone, the bearing area would be the co-directional top thread surface. Without the use of CAD software the bearing area can be approximated using the equation:

Bearing area = Revolutions x Circumference x Thread Width

Yakacki *et al*. (2008) observed the effect of change in bearing area in PU foam for all types of anchors (threaded spiral to push-fit types). Yakacki *et al*. found a good correlation between bearing area and pull-out in a range of PU foam densities. However in cadaver the results were not so clear cut with large standard deviations observed. This deviation could be due to varying local density causing wider variation in contact area and localised stiffness.

Drill or awl size is another factor to consider in the prediction of pull-out forces of anchors; however a specific study has not been carried out into the effect of this factor so currently no proven relationship exists, although it can clearly be stated that if a pre-drilled hole is too large in diameter it will cause a reduction in holding strength as Chapman *et al*. stated in their 1996 study.

Table 2-1: Cancellous Trough Loads to failure (Barber, 2006)

Anchor	Tests	Mean force (N)	SD (N)	Range (N)
SpiraLok	10	289.5	74.3	192.0–436.5
Bio-Corkscrew FT	10	259.9	47.5	211.8–369.7
BioRaptor 2.9	10	198	74.2	55.2–310.5
BioZip	11	358.9	25.6	304.3–404.8
Herculon	10	821.4	179.5	504.4–1007
TwoVo	10	513.8	94	397.4–727.2
ThreeVo	10	335.4	78	171.5–437.0
Impact	10	201.1	87	47.0–273.4
AxyaLoop Ti 3.0	10	335.26	135.6	72.9–514.7
AxyaLoop Ti 5.0	10	457.76	91.8	307.6–628.6
AxyaLoop Ti 6.5	9	453.7	58.1	376.1–551.2
AxyaLoop PLLA 3.0	9	124.76	56.2	46.2–190.25
AxyaLoop PLLA 5.0	10	395.1	33.4	324.5–433.0
AxyaLoop PLLA 6.5	9	384.56	70	264.1–462.3
ParaFix Ti 3.0	10	335.26	135.6	72.9–514.7
ParaFix Ti 5.0	10	457.76	91.8	307.6–628.6
ParaFix Ti 6.5	9	453.7	58.1	376.1–551.2
ParaSorb PLLA 3.0	9	124.76	56.2	46.2–190.25
ParaSorb PLLA 5.5	10	395.1	33.4	324.5–433.0
ParaSorb PLLA 6.5	9	384.56	70	264.1–462.3

Using the equation given by Chapman *et al.* it should be the case that pull-out force keeps increasing as the thread diameter keeps increasing but as can been seen in Table 2-1, results showed no increase in mean pull-out force when increasing maximum diameter from 5.0 mm to 6.5 mm. However there was a significant increase when going from 3.5 mm to 5.0 mm diameter. This suggests that the mean force alone does not tell the whole story, as the larger anchors predominantly tended to fail at the suture eyelet rather through pull-out or cut-out, causing less damage to the bone and possibly allowing for suture re-attachment.

Suture strength has increased significantly over the past ten years and along with the introduction of "knotless anchors" suture failure is now uncommon. In fact anchors placed too deep can cause failure due to the high-tensile suture cutting through cancellous bone. (Norris *et al.*, 2010). As anchor pull-out or cut-out is undesirable for a patient an argument can be made for designing a suture break force to allow for re-attachment rather than re-insertion.

2.11 Injectables

A clear method of improving any threaded fix should be the use of an adhesive or cement, especially in a weak and porous structure such as osteoporotic bone. Increased cancellous porosity has been shown to decrease screw stability where the cortical bone plays a critical role in screw holding power (Seebeck *et al.*, 2005). Polymethylmetharcrylate (PMMA) was first proposed by Mueller in 1962 as a method for bone augmentation, it was proved to provide quick setting stability (Bartucci *et al.*, 1985) but it has poor bio-compatibility. Currently calcium phosphate (CaP) cement is being increasingly used to augment bone due to its good bio-compatibility and strength (Wikerøy *et al.,* 2010). Cement is typically mixed by hand and quickly (due to its fast setting time) delivered by a pre-injection or via a cannulated screw.

2.12 Sonic Fusion

Sonic Fusion was first mentioned at a 1971 surgical conference in the then USSR. A single paragraph described the technique:

"A new method of osteosynthesis was investigated by V. A. Polyakov and M. V. Volkov (Moscow).Electrical oscillations, produced by an ultrasonic generator are applied to a magnetostrictive sheath which converts them into mechanical vibrations. At operation, the fragments of bone are located, a thin layer of liquid "solder" is applied to the ends, and the closely fitted fragments are "welded" by an ultrasonic wave guide; i.e., an ultrasonic osteosynthesis is performed. Another variant is the ultrasonic "welding" of bone chips or powdered bone into one conglomerate. A bone defect can be replaced by this method. The lecturers attempted ultrasonic osteosynthesis of fractures of various long bones and patella, and also in pseudarthroses of the ulna, after removal of benign bone tumours, etc. This method is relatively safe and does not lead to complications. Regeneration of the bone tissue occurs in the usual length of time. It is considered that ultrasonic bone "welding," like ultrasonic bone "cutting," is a promising method." (Geselevich, 1971)

After this conference publications on the subject cannot be found. However in 1999 a similar technology was used for bonding timber. In 2000 the wood welding technology was evaluated for medical use, and since then the technology has been developed.

2.12.1 The Sonic Fusion Process

The current sonic fusion process follows these steps:

1) The surgeon firsts taps a hole with a small clearance of approximately 0.05mm diametrical clearance
2) The pin is attached to an end of a sonotrode (a tool producing ultrasonic vibrations), and while applying minimal downward force, an active ultrasound signal drives the pin into the cancellous bone

3) Contact between the pin and bone creates shearing forces under ultrasonic vibrations (Langhoff *et al.*, 2009), causing the pin to liquefy (reaching temperatures up to 180°C) and infiltrate into the voids of the cancellous bone, forcing out the marrow in the pore space.

4) The thermoplastic cools within a few seconds, solidifying and creating a steady fix.

Figure 2-9 shows steps two to four of the process.
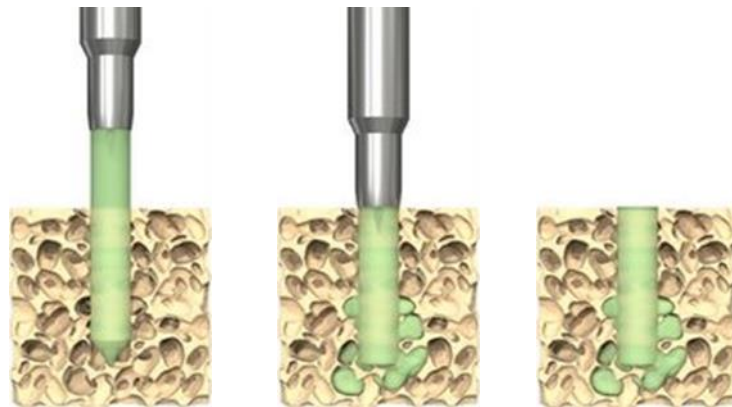
Figure 2-9: The bone welding process (http://www.spinewelding.ch/technology/)

Under *in vitro* conditions local temperatures of approximately 180°C have shown to be reached. Although these temperatures are high, due to rapid cooling of the material only a 7-8°C transient rise is observed (Langhoff *et al.*, 2009) which is on the 45°C threshold for bone tissue injury (Li *et al.*, 1999). As it is on the threshold negligible cell necrosis or tissue inflammation is observed (Langhoff *et al.*, 2009). The reason for the low transient temperature rise is due to the polymer used which is generally poly[lactic acid] (PLA). Although PLA has desirable thermal properties it is primarily used because it is bio-degradable.

The strength of PLA varies widely and depends on such factors such as crystallinity and method of manufacturing. Its shear strength is generally between 80-500 MPa and its Young's modulus is a more consistent 2.7 GPa (Black, 1992). Although it is suitable for some orthopaedic applications it does

not have the stiffness or strength of titanium alloy so is not currently used for higher load applications such as locking plates or nails.

2.12.2 Applications

To date the sonic fusion process has been used in humans in low load applications, primarily maxillofacial (Müller-Richter *et al*., 2011) but laboratory research is being carried out into suture anchoring with sonic fusion rather than traditional titanium anchors (Schneider *et al*., 2012)

2.13 Finite Element Analysis

Finite Element Analysis (FEA) is used through-out the engineering industry, from the concept design stage to post analysis of a critical failure. Frequently designs have to be compromised due to operational necessity and FEA can be used as a tool to find an acceptable limit or reveal under or over design. The exponential growth of computing power along with advancements in medical imaging has led to increasingly complex simulations being analysed in shorter time periods and now large models with numerous components under frictional surface interaction can be simulated, creating more possibilities for the engineer.

One of these possibilities is to apply the analysis method to the human body. The benefits of this are great. A wide range of simulations can now be run which could currently never be possible to measure in the laboratory, e.g. crash test simulation of a muscular-skeletal model (Danelson *et al.*, 2009) or stresses on a hip replacement (Jonkers *et al.*, 2008). These simulations help the engineer to understand what mechanisms and loads the body is subjected to when undergoing extreme or regular loading allowing for designs to be adapted from the results. It also can mean a reduction in the number or duration of pre-clinical trials and testing due to preliminary concepts being evaluated virtually, rather than undergoing numerous and expensive laboratory tests.

2.13.1 The Finite Element Method

The Finite Element Method (FEM) divides the solid into a finite number of elements and uses simultaneous equations to approximate displacements and forces for the whole body, Stolarski (2006) describes the steps of direct FEM as:

1) Discretization: Division of the object to a finite number of elements.
2) Selection of Element type: e.g. four noded quad elements.
3) Derivation of Element Stiffness Matrices: Determine force and displacement in each element, and the element stiffness matrix.
4) Assembly of Stiffness Matrices into the Global Stiffness Matrix: Relates to forces and displacements of the whole body.

5) Re-arrangement of The Global Stiffness Matrix: Introducing mechanical and geometrical boundary conditions into the global matrix, re-arranging for known and unknown variables, and setting up the simultaneous equations.

6) Derivation of Unknown Forces and Displacements: Solving unknown variables in the simultaneous equations.

7) Compute Strains & Stresses: With the displacements found, strains and stresses can be transformed using strain-displacement & stress-strain relationships:

Force ← *Equilibrium* → Stress ← *Elasticity* → Strain ← *Compatibility* → Displacement

Stress concentration is often the most relevant and important output for the engineer to observe, showing locations were the design is most susceptible to failure. The analogy of fluid flow can be applied to stress concentration, as where stress cannot occur i.e. a void; the stress must increase in areas around it. Stress concentration is due to these changes in the flow of stress because of "*discontinuities in continuum and contact forces*" (Young & Budynas, 2002).

Previously stress concentration was studied using experimental measuring, photo-elastic observations and relatively basic but technologically solvable equations. The FEM along with computing growth has allowed incredibly complex problems to be solved, causing a growth in FEA applications.

2.13.2 Bone Representation

There are a range of geometries and material models ranging in complexity available to create approximations of cancellous bone. These range from continuum models to geometry imported from micro-CT scans. It should also be noted that without the correct loading and contact parameters, results will be unusable however accurate the mesh.

2.13.2.1 Continuum Modelling

Figure 2-10: Solid block created in Solidworks® representing cancellous bone

This is the simplest and fastest solving method of representing bone. It evidently works well with cortical bone but has limitations when modelling cancellous bone. Material anisotropy can be added to the material properties, and this can work well for uni-axial loading. However from experience under combined loading or varying load situations the model can become inaccurate due to the complex nature of cancellous bone.

2.13.2.2 Variable Density Modelling

This technique makes use of the modulus-density relationship. Chen *et al* (2002) set the density of each individual element using the relationship: *ρ = x + y(CT), where CT relates to the grey scale value.* The density value in turn is related to the elastic modulus: *E= x ρ^y.* Using this technique it is possible to create a continuum model with variable mechanical stiffness. This technique has the benefit of creating continuum geometry, thus simplifying the mesh but still having varying stiffness. Although even elements with zero value grey scale will have some density and thus some stiffness, it also creates unnecessary elements which limit the volume which can be solved.

2.13.2.3 Lattice Modelling

Melchels *et al.* (2010) evaluated various architectures for lattice modelling including; cube, diamond, gyroid, and an irregular salt-leached structure. Although the purpose of the paper was to evaluate structures for tissue

scaffolding, it also provided a useful analysis of how different structures with the same porosity behave. The paper showed that for the same porosity a cubic structure will have a higher stiffness than a gyroid structure. Melchels *et al.* also demonstrated variable porosity modelling, which would be able to mimic the range of stiffness found in a cross section of bone.

This method of F.E analysis allows the user to set different global material materials by changing the geometry not just the material properties. Importantly it can produce a bearing area similar to bone. However it is difficult to decide on appropriate geometry to simulate real bone due to its heterogeneous nature and therefore it is also difficult to validate these structures

2.13.2.4   *High-Resolution Modelling*
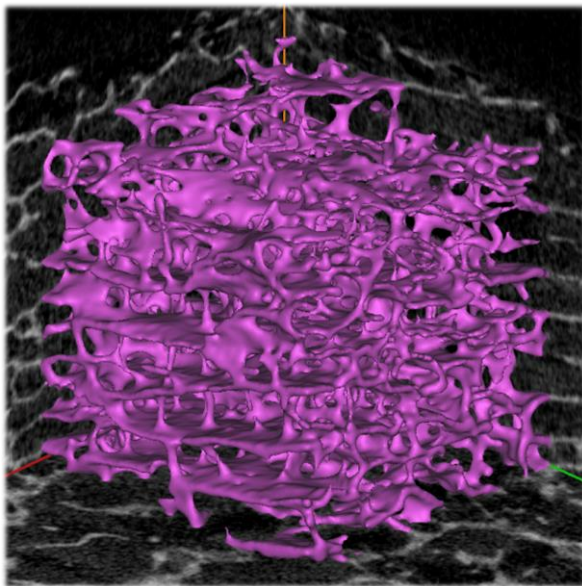
Figure 2-11: 3D Model created from CT scans using Mimics® software

Using CT manipulation software it is possible to create a high resolution 3d geometric model of bone. This model can then be meshed and set-up for FEA. This is currently the most accurate method of simulating bone geometry, and therefore often produces the most relevant and interesting results. However because of the intricate nature of bone it is time consuming and demanding to set-up and run. It also incurs significant financial cost due to the software and hardware requirements.

Wirth, Muller and van-Lenthe (2012) published a paper comparing discrete (CT models) and continuum bone models. They found a strong difference in bone-

implant stiffness between the two bonded models in both high and low density structures. Due to their findings they came to the conclusion that continuum models are of limited use for peri-implant analyses. Furthermore, if they had used a frictional contact for the models they would have found further differences between a discrete model and a continuum model.

Virtual high resolution geometries have also been modelled (Donaldson *et al.,* 2008). Virtual models are useful due to the difficulty of obtaining suitable physical samples. Donaldson *et al.* (2008) modelled various determinants of mechanical properties; trabecular connectivity, size, and spacing and then compared the elastic response of different models. The models produced different responses but were not compared to physical bone samples. If further research effort went in to produce reliable and accurate virtual models it could prove incredibly useful. It would allow anyone to create desired models based on factors such as gender, age, weight etc. – negating the hunt for suitable bone samples to be found and scanned.

2.14 CT Image Measurements

Bone strength depends on the amount of bone tissue and on the microarchitecture of bone (Dalen *et al.,* 1976, Ciarelli *et al.,* 1991). Therefore it is useful to analyse the structure to predict and understand how strength differs. Volume fraction (Bone Volume / Total Volume) is the most apparent commonly observed due it being easily calculated in the laboratory or by most modelling software. Other important but less readily calculable properties are trabecular thickness (Tb.Th) and spacing (Tb.Sp) which provide further insight into the bone structure. The thickness is calculated at any point as the diameter of the greatest sphere that fits within the structure and which contains the point (Dougherty and Kunzelmann, 2007).

Another property to consider but to use cautiously is the structure model index (SMI). It is a method for calculating the plate-like or rod-like geometry of trabecular bone. It uses the change in surface area as volume increases

infinitesimally to calculate SMI, which is calculated on a scale from 0 to 4. SMI = 0 for plate-like structures, 3 for rod-like and 4 for solid spheres. Unfortunately the SMI is negative for concave surfaces, which are common in trabecular bone, making results difficult to interpret and therefore often unusable. From the author's experience calculating the SMI has a tendency to be more tractable on smaller samples.

All the properties described can now easily be calculated using an add-on of Image-J® software, Bone-J developed by Doube *et al.* (2010). The software uses binary images of CT scan slices to calculate properties. As the images are binary there is no grey-scale option and care must be taken when importing the precise pixels used, otherwise incorrect values will be out-putted.

2.15 Physical Substitutes

Animal bone is frequently used as a substitute to human bone but artificial substitutes which have no ethical issues are also available, the most common being polyurethane (PU) foam. PU foam is widely available and is used in many industrial applications. One of the main producers of PU foam bone substitute is Sawbones®, who produce a variety of open and closed cell foams in different densities. Open pored foams are of a greater interest geometrically to those studying osteoporotic bone and have shown to have similar Young's Modulus values (0.08–0.93 MPa for the 0.09 gcm^{-3} foam and from 15.1–151.4 MPa for the 0.16 and 0.32 gcm^{-3} foam) and strength but fatigue life of PU foam has shown to be lower than that of cancellous bone (Patel, 2008).

Stiffness and strength are very important but are obviously not the only criteria when considering a suitable substitute. Figure 2-12 shows the contrast in structure of human bone and a closed pore sawbones. Thickness analysis using Bone J (Doube *et al.*, 2010) in Table 2-2 shows the difference in trabecular thickness and spacing between two closed pore PU foams, one open pore PU foam and human bone. The trabecular thickness analysis reveals that perhaps the 0.32 g cm^{-3} closed pore type would be a suitable match but looking at the

BV/TV value it reveals that it has a 57% increase in volume over the human bone rendering it unsuitable.

The 0.2 gcm^{-3} has an approximate pore size of Ø 1.4mm and contains few inter-locking pores compared to the trabecular bone which in this case is plate like and has a mean trabecular spacing of 0.75mm.
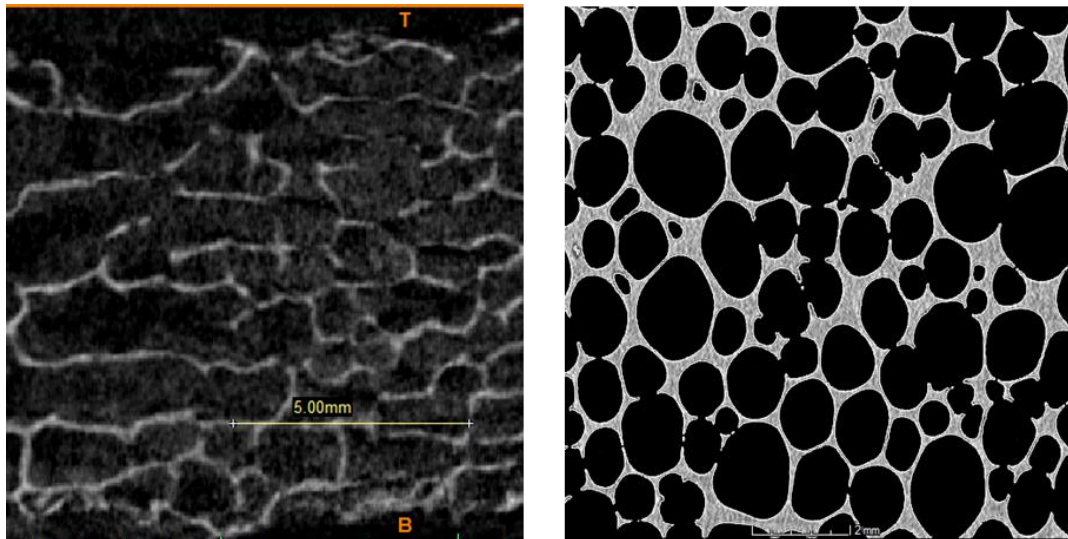
Figure 2-12: Comparison of Human Trabecular Bone with 17.5 BV/TV (left) and Saw Bones 0.2 gcm^{-3} (right) – Both images are 10 mm in dimension

Table 2-2: Trabecular Analysis of three sawbones types compared to human bone, carried out using ImageJ (Doube et al., 2010)

Image Set	Saw Bones Type	Tb.Th Mean	Tb.Th Std Dev	Tb.Th Max	Tb.Sp Mean	Tb.Sp Std Dev	Tb.Sp Max	BV/TV
1	0.32 g cm^{-3} Closed	0.166	0.058	0.395	0.758	0.242	1.794	27.60%
2	0.20 g cm^{-3} Closed	0.097	0.030	0.224	1.038	0.378	1.882	19.20%
3	0.24 g cm^{-3} Open	0.205	0.077	0.500	2.404	0.704	3.259	13.30%
Human Bone	17.5 BV/TV	0.19	0.063	0.48	0.756	0.298	1.65	17.50%
All values in mm except BV/TV								
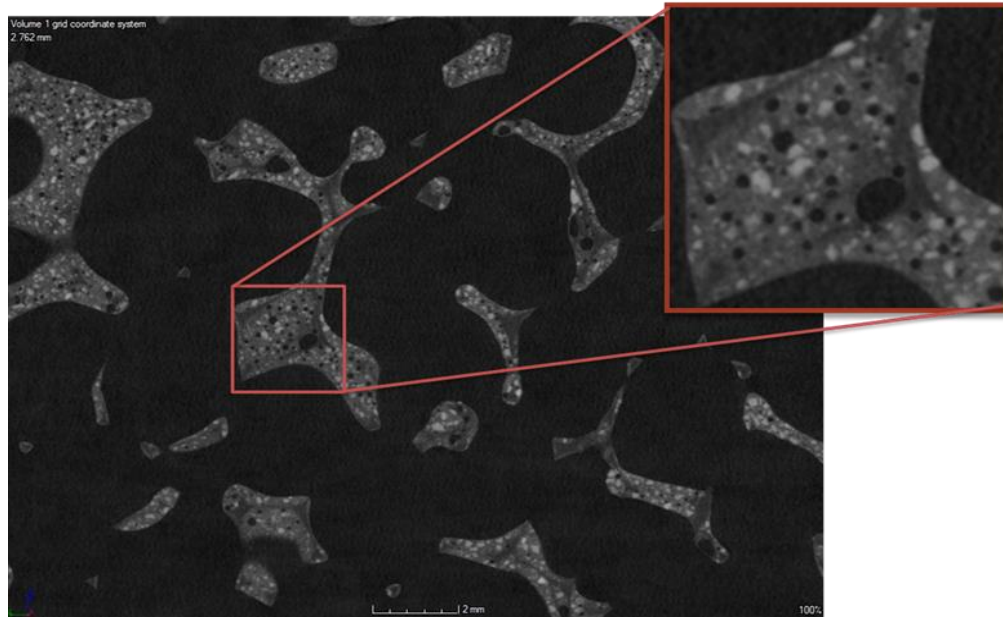
Figure 2-13: CT scan of 0.24 g cm^{-3} Open Pore SawBones, measurement line at bottom is 2mm

The alternative option with PU foams is to use open pore rather than closed pore. Figure 2-13 shows the open pore structure sample has an inhomogeneous microstructure which gives misleading results in the thickness and spacing analysis in Table 2-2. Looking at Figure 2-13 it can be seen that the trabecular spacing is too large to create a meaningful implant simulation, just as with physical testing, and therefore is unsuitable for simulation. Observation of these factors shows that for small implants PU foam is of little relevance to this investigation especially when combined with a substance that sets in vitro. For larger implants where pore size or type is of less consequence they can be more relevant. Patel, Shepherd and Hukins (2008) concluded that "*PU foam of density 0.16 g.cm-3 may prove suitable as an OP cancellous bone model when fracture stress, but not energy dissipation, is of concern*". Of course there is a certain paradox in creating a suitable laboratory test material to a set standard which matches the heterogeneous qualities of cancellous bone. With small implants such as anchors this is why it is important to test or simulate in real bone.

2.16 Validation

All FEA results should have some form of validation but some simulations will better represent the physical compared to others, i.e. a plate under tensile loading can be replicated very well, but when replicating a screw in cancellous bone educated assumptions in FEA must be made (e.g. mechanical effects from marrow can be ignored). Validation has always been difficult with detailed cancellous models, to validate the models physically one method would be to:

1) Scan a suitable piece of bone

2) Scan the implant in the bone

3) Load the implant and record the stiffness

4) Scan an implant under loading in bone or at least at the end of loading

5) Replicate this through CT-manipulation software, mesh creation software and FEA software

6) Compare the results. Stiffness can be easily be compared, but geometry changes should also be examined.

This method would have to be repeated on multiple samples to an acceptable correlation. Although this method is valid, previous work carried out showed it to be very intricate in set-up leading to a greater chance of error, as well as being costly and impossible to repeat on the same piece of bone (Bennani-Kamane, 2013). An alternative to real bone is to use 3d printing (rapid prototyping) to produce scaled models of the bone geometry. Rapid prototyping has a few advantages over testing in actual bone: It allows for the model to be scaled up, making it easier to work with; Each model can be reproduced as many times as required; Eroded (and any other) models created in CT manipulation software can be produced and compared to the original model via testing. The only restrictions are cost and access to testing equipment.

Rapid prototyping has been used in the past to determine the effects of computer modelled bone loss with promising results (McDonell *et al.*, 2009) but it has not been used to validate FEA assembly models. This may be because rapid prototyping has previously been prohibitive due to cost (Approximately £600 in

2010 for a small 50mm x 50mm x 50mm polymer model) or 3d printing method used. Stereo-lithography (SLA) is one of the most affordable and widespread methods of 3d printing available. It uses a UV laser to cure layers of photo-reactive liquid polymers on top of each other. This additive manufacturing technique has been evaluated in the past but found to produce models with unacceptably high levels of stiffness anisotropy due to the layering method of manufacturing (Bennani-Kamane, 2013). Recently an alternative 3d printing method – Selective Laser Sintering (SLS) has come down in cost nearly a magnitude in order (now less than £100 for a 50mm x 50mm x 50mm polymer model) due to growth in the industry, and patents beginning to lapse. SLS uses a laser to sinter powdered material together, this powder can be polymer, metal, and even composite. This is still a layer manufacturing method but it produces models with lower, acceptable anisotropy which are suitable for replicating bone geometry.

Pull-out tests are one form of validation, but they require multiple models to be sourced and tested. Multi-directional non-destructive testing is an alternative method which does not require as many models. If an anchor is loaded horizontally rather than vertically then reaction forces from any direction on the horizontal plane can be compared to see if ratios of change match i.e. if the force ratio given in FEA is a 2:1 ratio comparing opposing directions, will the physical model also produce a similar ratio? This method of validation is presented later in this thesis and makes use of SLS to produce scaled cancellous bone models.

3   Modelling and Techniques

3.1   Introduction

This chapter describes the software, and techniques used within the software to model human bone. Some of this ground will be well trodden and some of it will be new. The whole process is included here because it is the basis of the project.

First, three different types of modelling were investigated: continuum, lattice, and high (or micro) resolution modelling. The objective of looking at different types of modelling was to find the most suitable technique for this project. Eventually high resolution modelling was chosen due to the reasons laid-out in this chapter. Once the modelling method had been chosen a process had to be established.

The final process is largely dictated by the technology and resources available. Subsequently the technique used has evolved and been refined over the course of the project. The process described here is the current method used to model the cancellous and cortical elements of the bone. This chapter will also provide the reasoning behind the mesh and contact settings used.

The software used to import a CT scan and create a mesh from it was Mimics®, which is produced by Materialise®. The cortical layer may be considered solid and can be created from any CAD package, in this case it was Solidworks® produced by Dassault Systems®. The finite element software used was Workbench® (on a High Performance Computing (HPC) licence) which is developed by ANSYS®.

3.2   Proof of Concepts

The problem under investigation can be simplified down to a screw inserted into a block. However, in reality the problem is greatly complicated by it being necessary to use a small screw and having to insert it into a material full of holes. To determine the best method to examine the problem a methodical comparison of continuum, lattice and CT models was undertaken.

3.2.1 Preliminary Studies

Continuum (solid) models require rudimentary modelling skills and are straightforward to solve, allowing for the most number of models to be created and solved compared to lattice and CT models.
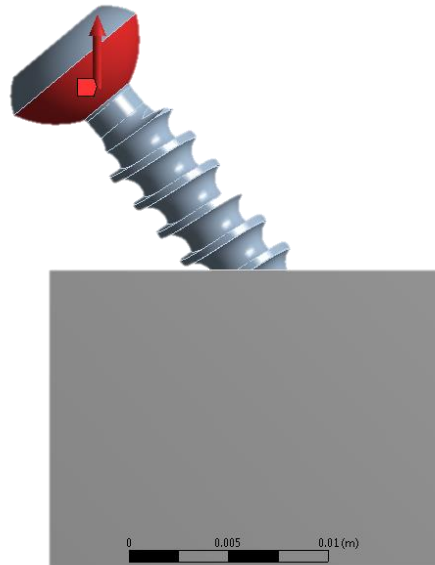
Figure 3-1: Set- up of model investigation pull-out vs. insertion angle

Figure 3-1 shows the loading of a continuum investigation based on a paper by Patel, Shepherd & Hukins (2010). Here a screw is inserted at angles 0, 10, 20, 30 and 40° and then displaced upward 1mm (shown in red). It allows for quick investigation into the geometric effects of anchor design e.g. thread angle. Here the peak reaction force is examined against insertion angle. The peak reaction force is the maximum force value observed at the applied displacement. Figure 3-2 shows that for this particular screw design there is a small increase in force reaction at 10° and a 25% reduction in reaction force from 20° to 40°.

Figure 3-2: Plot of Screw Insertion Angle vs. Pull-out force at 1mm
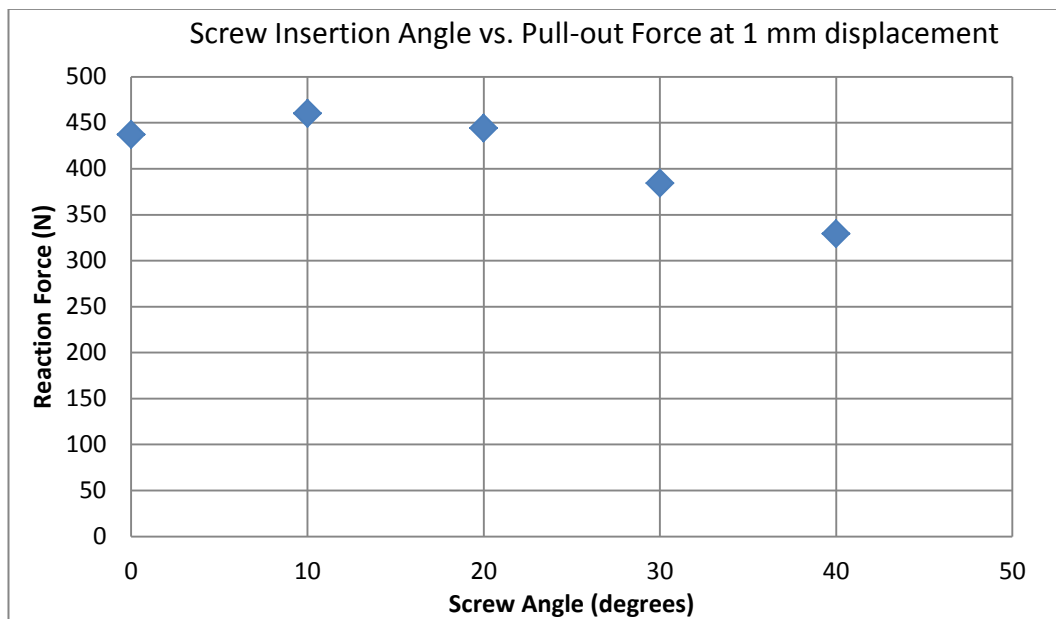
This small study shows that solid models are useful for quick studies, producing a basic evaluation for different loading applications or different designs. However when compared to a CT model, the differences become clear.

Figure 3-3 shows the difference in deformation between two identically loaded anchors, one in a continuum and the other in a CT model. In this simulation the bone is restrained on the four vertical sides and the anchor has a linear ramped displacement applied of 0.2 mm applied to the top of the anchor (eyelet geometry is removed). It can clearly be seen that there is a difference in the location of deformation and therefore where the areas where the bone is under loading – in fact the peak displacement is five times the value in the CT model compared to the solid model.
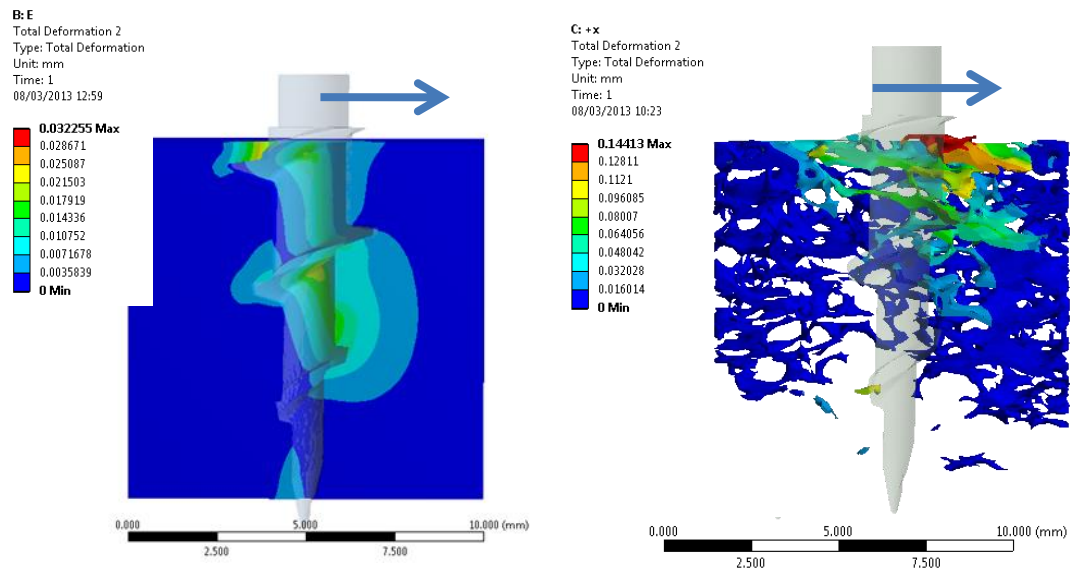
Figure 3-3: Contrast of a continuum and CT model, arrows show the direction of loading: 0.02mm displacement

However, the method should be not disregarded completely and for larger models it makes sense (and may only be possible) to utilise continuum models. For example, if significant cortical bone over cancellous bone is present (e.g. the shaft of the femur) it is sensible just to model the cortical bone – Modelling the cancellous bone here would be time consuming and would add little to the stiffness of the model. It is also necessary to model devices in a continuum to get an understanding of their mechanisms and importantly as controls to be compared against the behaviour in cancellous bone.

Lattice modelling uses repeating shapes to form a framework; cube, rod, diamond, sphere and gyroid shapes are common. The aim is to replicate some of the bulk mechanical properties as bone, primarily bulk elastic moduli but also volume and the mechanical effects observed in trabecular bone, such as variation in pull-out.
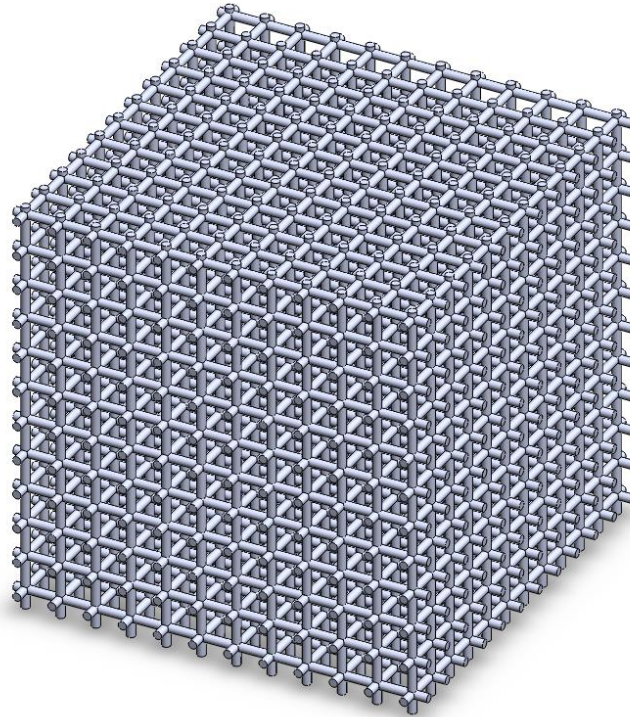
Figure 3-4: Rod Lattice model with a BV/TV of 11.6%, model size is 10 mm x 10 mm x 10 mm.

Lattices of rods were examined first, as they were reasoned to have similarities with more rod-like trabecular bone and because 2D grid models had been previously examined (Bennani-Kamane, 2013). Rod lattices provide good adjustability when producing a model with the required apparent density, either by adjusting the spacing or the diameter of the rods. Figure 3-4 shows a rod lattice model with uniform rod diameter (0.2 mm) and spacing (0.85mm centre to centre) in 3 orthogonal directions. These dimensions produce a model with 11.6% BV/TV – it is easy to adjust the volume by changing the diameter or spacing. By changing the BV/TV value it allows the bulk modulus to be affected and give some variability with pull-out within the structure. For example in the case given if you reduced the rod diameter, you would also reduce the bulk modulus. However bulk modulus can be adjusted in a continuum and the variability deviation is low and predictable – unlike cancellous bone. Therefore they were not investigated further. Although not investigated in this project with augmentation, because rod structures have an open structure they would also be suitable for producing models with cement.
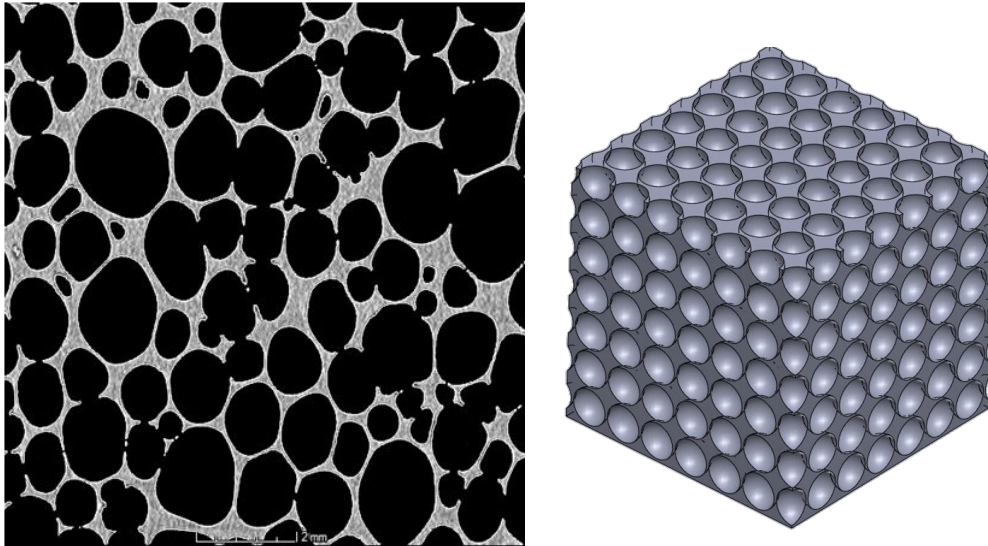
Figure 3-5: Closed pore PU foam CT image (left) and idealised CAD model of a spherical lattice (right).

After observing the spherical structure of Sawbones® PU foam in micro-CT images (Figure 3-5 - left) it was decided that a lattice could be created by removing spheres from a solid to replicate the structure. Although not replicating bone it could possibly replicate the materials used in mechanical testing and experimentation. However, using this technique it proved more difficult to produce models with medium to low apparent densities (<12%). Ultimately it was discounted as its weakest point always lies at the thinnest point – equidistant between the spheres. This meant failure would always occur at the thinnest point closest the thread, creating a model which was of little interest due to its predictability.

Producing lattice models and assemblies is evidently faster than creating models from CT scans, but interestingly solve times in FEA for lattice models are no faster than that of CT models. The similar solve times are likely due to the similar complexity in contact areas i.e. there are many different contact points, opposed to a single contact surface for a continuum model. Validation of these models was also very difficult, of course bulk moduli can be compared but this can also be done with continuum models. It is evident that lattice modelling could not be compared to the intricacy and complexity of trabecular bone, and arguably could

be said to be less relevant than continuum models due to the difficulties over validation.

3.3 Modelling Strategy and Technique

3.3.1 Imaging

After arriving at the conclusion that modelling real bone would be the most relevant, a process has been established. This started by finding a suitable human bone sample to undergo a scan. Animal bone is readily available with common species being ovine and porcine. However due to the lack of bone maturity in these animals they are often unsuitable for use. Therefore, although obtaining human bone is more difficult and costly it is the clear choice for sample selection. Samples obviously vary so care should be taken before performing an image scan.

For micro-imaging tissue samples in three dimensions only two processes are viable, CT (Computed Tomography) and MRI (Magnetic Resonance Imaging). A CT scan is usually used for bone because it provides greater detail in denser material, whereas MRI is better suited to soft tissue. CT scanning also offers better resolution, currently as low as 0.5 μm (SkyScan®, Belgium, 2014), while μMRI has approximately a lowest resolution of 25 μm in high strength magnetic fields (MicroMRI Inc., USA, 2014). If performing an in-vivo CT scan the patient will receive a high radioactive dose – the frequencies of CT scans performed annually per person are limited. Most samples undergoing μCT will be scanned in vitro due to the high radiation doses required for higher resolution imaging and due to machine design – MRI does not produce any radiation but μMRI does require higher energy compared to standard resolution MRI. CT offers two other benefits over MRI, it is less expensive and a full body scan can be completed in seconds rather than minutes.

A micro-CT (μ-CT) scanner must be used to obtain sufficient resolution of cancellous bone; a typical pixel size would be 0.02 mm x 0.02 mm with a 0.02 mm distance between image "slices". Typically the volume produced would be

approximately 20 mm x 20 mm x 20 mm, but this is dependent on the object's geometry. Using the numbers given this would result in each slice containing around a million pixels but the whole image set containing one thousand million pixels – or one giga-pixel.

3.3.2 Modelling Technique

Once the image slices have been imported and analysed by the software (Mimics®) a 3d shell can be created. The first stage is to select the pixels within the corresponding Hounsfield (grey) scale for the tissue being studied – this is called "thresholding". The top left image in Figure 3-6 shows the pixels used for the cancellous model highlighted in purple – this is called a mask. Thresholding selects all the pixels within a given range, allowing for different material or tissue selection. Bone is a comparatively straight forward tissue to threshold as it is a relatively dense tissue it gives clear boundaries to be selected. Soft tissue, e.g. marrow can be difficult to distinguish against implanted polymers due to similar densities. Distinguishing between the marrow and polymer is better done visually rather than with set Hounsfield values. Metal alloys are clear to distinguish, although some materials can cause image diffraction. Shot-peened titanium alloy is known for this interference effect.
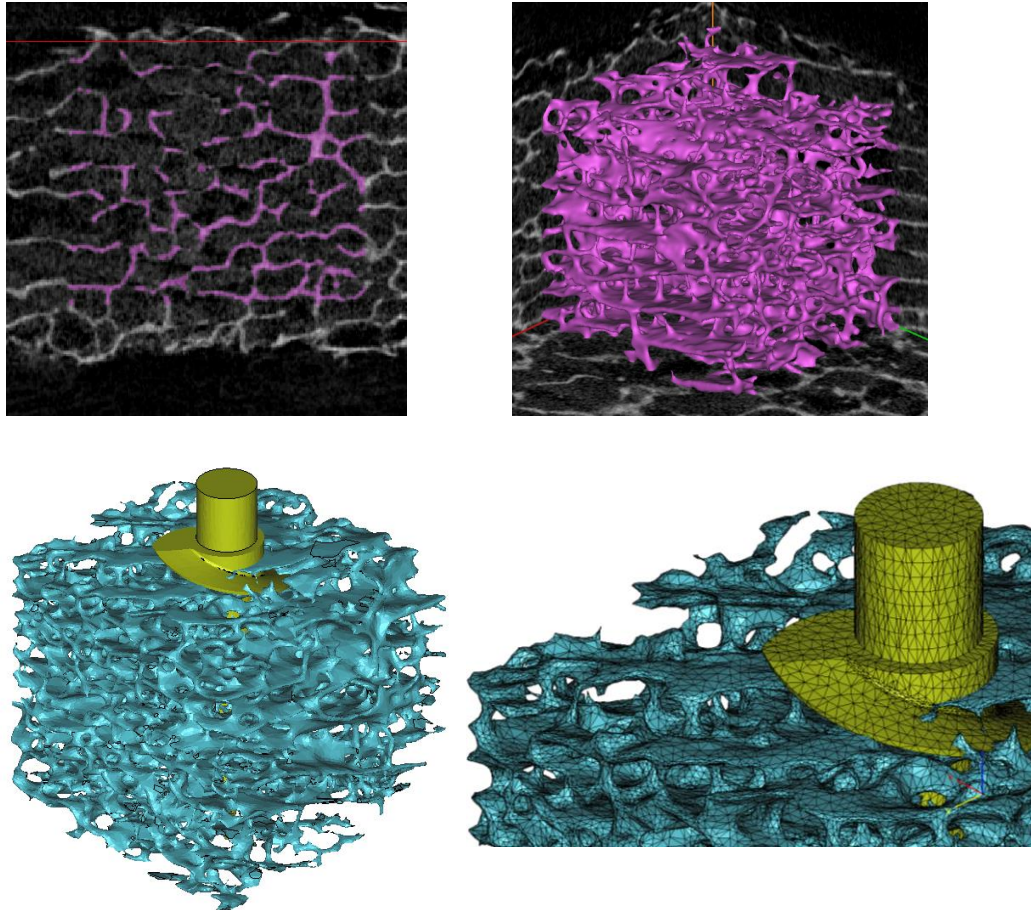
Figure 3-6: Stages of modelling: From CT scan to assembly mesh

The next image (top right) in Figure 3-6 shows the smoothed 3d shell or "mask" produced from the image slices, it is made up of voxels (3-Dimensional pixels). At this stage options such as smoothing are available. Smoothing helps to reduce model distortion produced by the square profile of the pixels, although care must be taken not to de-feature the bone by over smoothing – this can be checked visually.

The 3d mask is then tessellated to produce a rudimentary surface mesh made up of shell elements. This mesh is automatically produced, (although with some user element control) but due to the geometry being extremely faceted it requires meshing manually afterwards. Manual meshing is the time consuming process of individually deleting intersecting and duplicate elements but it is necessary to produce a successful mesh. Manual meshing requires some interpretation, and requires some investment to become skilled at. At the meshing values used that

represent several elements for the perimeter of each trabecular strut, the remaining patching operation for some hundreds of elements can be completed in several hours. However, experience has dictated that the use of any finer mesh would result in a disproportionate number of manual operations that would in turn take several weeks to implement, and would consequently lead to greater uncertainty about the representation of the geometry. Once an acceptable surface mesh has been produced a volume mesh of the cancellous structure can be automatically created.

The next stage shown in the bottom left in Figure 3-6 is to insert the chosen implant in the desired position and create an assembly. A Boolean operation is performed to insert the implant; in practice a hole is often drilled or tapped, for anchors it was not necessary to model this as the anchor would always end up overlapping the pre-insertion volume. Again, intersecting or overlapping elements must be deleted and replaced with acceptable elements. Finally (lower right image, Figure 3-6) once the shell mesh contains no intersecting or overlapping elements a volume mesh can be created of the assembly for export into the desired FEA software, in this case ANSYS ®.

A complete step by step procedure, including settings and values used is given in Appendix A

Due to the intricacy of the geometry it can currently only be exported as a mesh and not CAD geometry. This is because CAD is vector based, meaning each feature must be based on a mathematical expression rather than set data values as in the case of mesh files. As the level of detail needed is very high there would be an overwhelming number of mathematical expressions produced in this case. This has the drawback of limiting the ability to make changes to the geometry readily and not being able to make mesh adjustments within FE software.

3.3.3 Mesh Options

Throughout the whole modelling and meshing process decisions must be made to produce a working and efficient model. The process described above took numerous trial and error attempts using varying settings to get to an acceptable

working stage. One of the main decisions was choosing element size; a balance between accuracy and time. Figure 3-7 shows the visual difference between four meshes with a tenfold increase in elements each time from left to right. The far left image shows a mesh which is unrecognisable, the next image shows an image which is discernible as a person, whilst the next image can be distinguished as Beethoven. The final image on the far right is the clearest image but also contains ten times the number of elements of the previous model for little gain. This visual approach can be applied to modelling bone, giving an idea of feature retention and element quality.

60
triangles

600
triangles

6000
triangles

60000
triangles
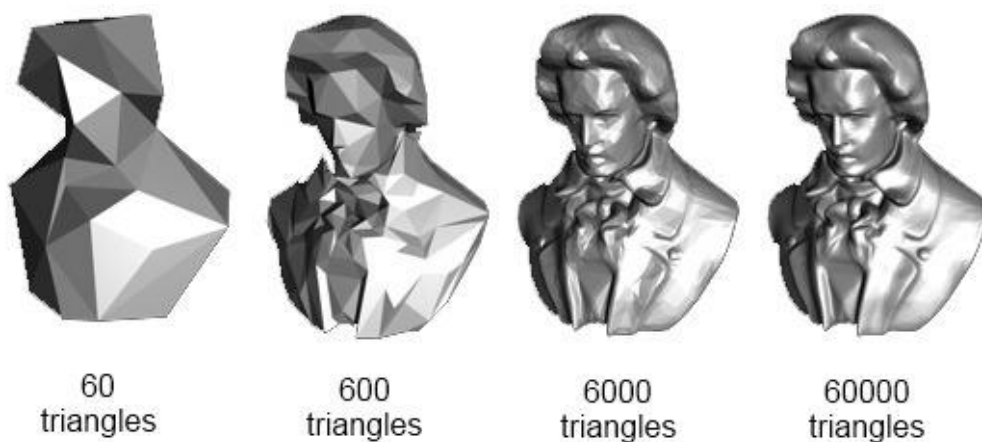
Figure 3-7: Element size and effect, four meshes with a tenfold increase each time from left to right (http://cdn.overclock.net/a/a4/a4a47b78_ChsSwUE.png)

As well as visual checking stress or displacement convergence should also be looked at. However, stress convergence tests are difficult for these models. Approximately one million volume elements are used for a piece of healthy cancellous bone occupying a bulk volume of 1100 mm^3 (just over 10mm x 10mm x 10mm), and each of these models can take significant time (of the order of days) to load and solve. This number of elements is close to the limit of computational ability available to the author at this time. Hence significant further refinement is not achievable as it would involve using a considerably smaller piece of bone around the screw. Further coarsening is not acceptable, as the mesh is graded to give adequate geometric definition of the screw/bone interface – a factor which experience dictates is important to give a solution with

the contact elements used. Larger elements may lead to a failure to produce any solution.

Suitable meshing values were discovered after trial and error attempts. Mesh assessment included visual evaluation (feature retention), ability to import (too many elements would not import), and ability to solve (too few elements would often create contact solve issues). Once suitable values were found the mesh creation process and settings remained constant throughout to ensure like for like was always being compared.

The final mesh creation settings were:

- *Shape quality threshold: 0.3* – this sets the desired quality of triangles, the value is the ratio of triangle height to base. In this case no triangle had a base: height value less than 0.3
- *Maximum geometrical error: 0.01* – this is the maximum deviation between the part's surface before and after automatic re-meshing
- *Maximum edge length: 0.2 mm* – which sets a limit on the length of edges of triangles created.

3.4   Loading
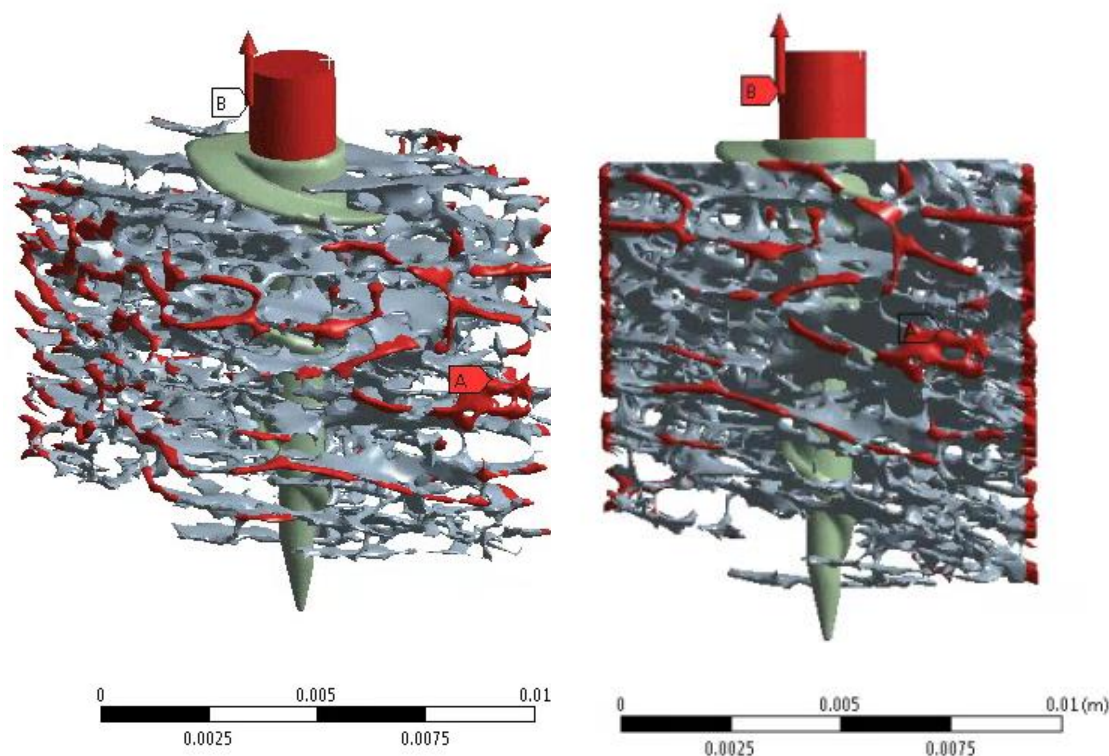
Figure 3-8: Loading conditions for the majority of solutions

Figure 3-8 shows the loading conditions used for the majority of cases examined. All cases presented in this thesis will have the same loading conditions unless otherwise stated. The cancellous bone is fully restrained on the four vertical sides of the sample (Label A) in all Cartesian directions. A case could be made to also restrain the base of the bone, but especially in the case of lower apparent density bone there is little material to restrain - as can be observed in Figure 3-8 in the right image.

The anchor (Figure 3-8) had a displacement applied to the simplified top. Eyelet geometry was removed in all cases to simplify the model. Eyelet geometry was not considered a point of failure as the suture would fail before any deformation occurred to the eyelet (Barber, 2008).

3.5 Contact parameters

Contact is arguably the next important configuration stage after loading the model correctly but it requires more technical consideration when selecting parameters.

Figure 3-9 shows the purpose of penetration. It is important because only elements in contact can transmit compressive normal forces and tangential friction forces. However if penetration is too high then the bodies can pass straight through one another.
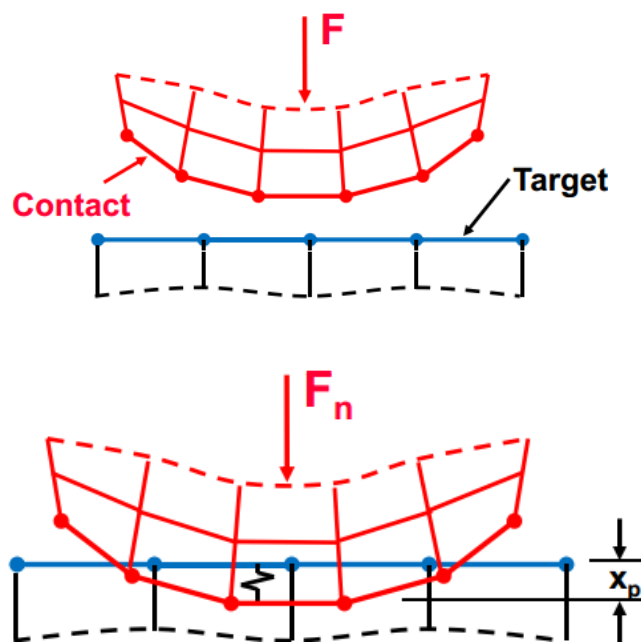
Figure 3-9: Penetration of Target (Ansys® Mechanical Structural Nonlinearities Notes)

Pure Penalty contact formulation was used for all simulations, although Augmented Lagrange can also been used for non-linear problems. Pure Penalty was chosen because although it is more sensitive to contact stiffness settings, it is more likely to converge or converge with fewer iterations. The formulation for both is as follows:

$$(4) \ Pure \ Penalty: F_{normal} = k_{normal} x_{penetration}$$

$$(5) \ Augmented \ Lagrange: F_{normal} = k_{normal} x_{penetration} + \lambda$$

$Where \ \lambda \ is \ an \ internally \ calculated \ term \ that \ augments \ the \ calculation$
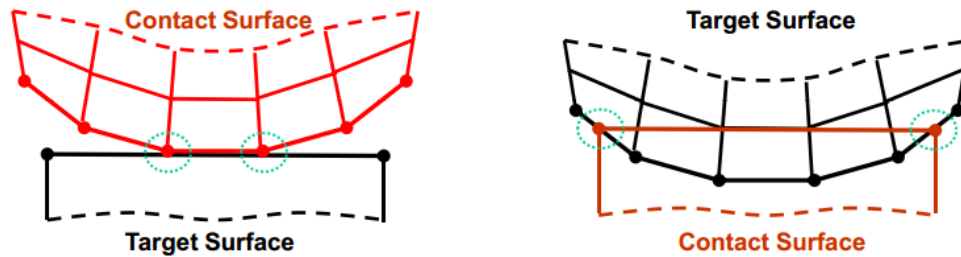
Figure 3-10: Asymmetric behaviour (Ansys® Mechanical Structural Nonlinearities Notes)

The stiffer material was always set as the target mesh (Figure 3-10) to ensure only the metal anchor was allowed to penetrate the bone or only the bone was allowed to penetrate the polymer anchor.

3.5.1 Friction and other contact types

For contact simulation there is a choice between bonded and frictional interaction. Bonded contact prevents any movement over the surfaces and therefore solves with fewer iterations. Frictional contact allows for sliding between bodies and for the bodies to come in and out of contact, and crucially for shear forces to develop between the two bodies. Frictional contact was chosen for anchor problems to produce a more accurate model – as there is no evidence of bonded contact between bone and anchor.

Figure 3-11 shows a plot of peak reaction force vs. friction coefficient for an anchor in cancellous bone. It can be seen that there is a large increase in reaction force between 0.32 and 0.35 but a small increase from 0.35 to 0.6. For this reason any value below 0.35 was not used. A value of 0.6 was chosen as it produced reliable solve times and consistent reaction force results, unlike a value of 0.32, which fluctuated greatly depending on the mechanism of pull-out – This is shown further in chapter 4. A value of 0.6 is also consistent with the literature (Grant *et al.*, 2007).

Figure 3-11: Plot of peak reaction force of an anchor in a CT model vs. friction coefficient, 1 represents bonded
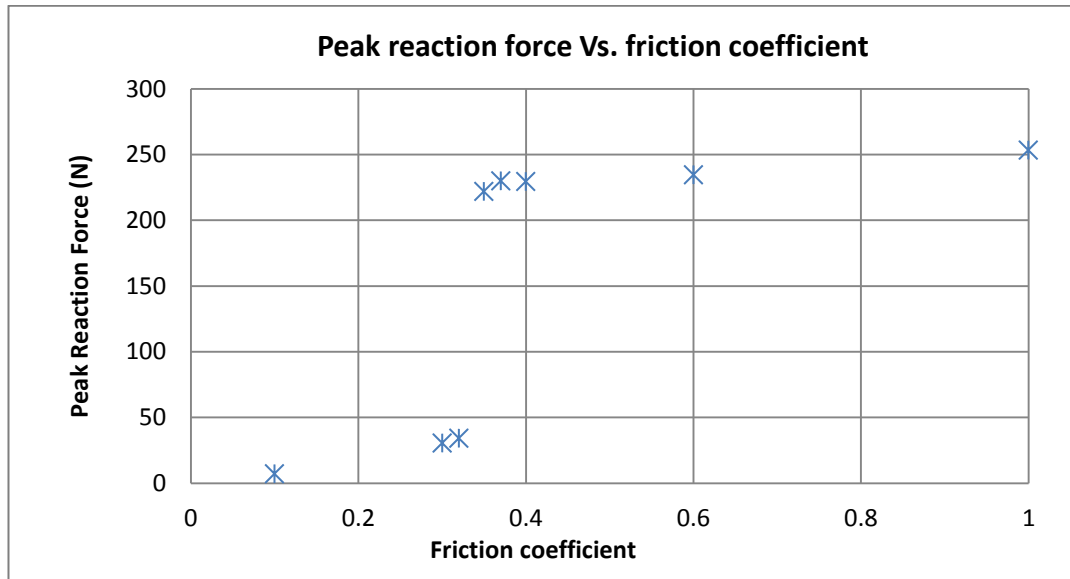
Contact stiffness was set to 0.01. Although this is a low value which allows greater penetration to occur, it was necessary to apply for the solution to converge. Even with a value of 0.01 and 60 sub-steps set, complex simulations still took over 3000 iterations to solve. A larger contact stiffness of 1 is indicated to produce more "accurate" models but small preliminary studies found the peak stress to be less than 2% different. Stiffness was updated each iteration.

Table 3-1: Summary of Contact Parameters

Parameter	Value/Setting
Friction Coefficient	0.6
Behaviour	Auto Asymmetric
Formulation	Pure Penalty
Normal Stiffness Factor	0.01
Update Stiffness	Each Iteration
Pinball Region	Auto Detection Value

3.5.2 Element types

One limitation of the software used to produce the meshes – Mimics® 3Matic and the software used to import the meshes – Ansys® FE Modeller is the compatibility with 10 node tetrahedral (tet10) elements. Although tet10 element meshes could be produced, they could never be imported into the FE software – the software developers supplied no solution or explanation to this, although it may be due to mismatching of element numbering between software suites. For this reason 4 node tetrahedral elements with 6 degrees of freedom at each node were used during simulation. The element type in Ansys is SOLID72.

4 Factors affecting the pull-out of a titanium spiral anchor

4.1 Introduction

This chapter presents the findings of the investigation into some of the factors affecting pull-out of an idealised spiral anchor. It also further discusses the materials and methods used to create an assembly CT model. This enables an assessment of the relevance of cancellous bone properties, while also identifying the important effect of the cortical shell (Seebeck *et al.*, 2005). To observe the consequence of aging bone, two pieces of human cancellous bone have been modelled, representing both "normal" and "weaker" bone. The effect of increasing cortical thickness is examined both when the anchor is not engaged with the cortical shell, and also when it is engaged. In practice, loads are applied through a suture which means that different loading angles can be applied to the direction of pull-out, and this feature is also examined.

4.2 Materials and Methods

Ansys® (Workbench version 13.0) was used to implement all the F.E. analyses. F.E. modelling has evolved two common alternative strategies for detailed modelling of cancellous bone. The first strategy uses voxels to create the building blocks of cancellous bone and assembles the voxels as a solid, while the second builds solids by modelling the surfaces and interpolates the surface from a series of slices to form a solid. To determine pull-out loads for implants it is important to model the interacting surfaces of bone and implant, and so this latter procedure is adopted here.

4.2.1 Geometry

A disc of bone was extracted from the femoral head of a cadaver (adult female) and images were taken (μCT 1076, SkyScan, Belgium). The bone has been orientated so that the upper surface (Figure 4-1) is parallel and near to the cortical shell. The "local" apparent bone density measured by the ratio of Bone

Volume (BV) to Total Volume (TV) (BV/TV) decreases through the depth of the sample. The CT scan data was imported and processed using Mimics® (Materialise Mimics version 14.0) software to create surfaces, and hence a volume of cancellous bone. The bone image was cropped and a 10 x 10 x 10.5 mm cancellous bone model created.

From the original volume, bone of different densities can be created by modifying the threshold values in the software (Hara *et al.*, 2002; Kim *et al.*, 2007). For this study two densities of bone have been created; one by smoothing a closely approximated geometry of the original bone (right, Figure 4-1), and the other by eroding the smoothed geometry (left, Figure 4-1) to give a bone of lower apparent density (Guo & Kim, 2002; van der Linden *et al.*, 2002). This method was chosen instead of finding two pieces of bone with naturally different BV/TV, as it enables a direct comparison between two similar bone structures. Tables 1 and 2 below give the trabecular thickness and spacing measurements for both cancellous bone models (Doube *et al.*, 2010). The smoothed bone model had an overall apparent bone density of 17.5%, and this might represent normal or healthy cancellous bone, while the eroded model had an overall apparent bone density of 8.3%, and this might be more appropriately described as weak or osteopenic bone. This study is limited to this particular bone structure. For the sample with the lower BV/TV ratio, the SMI is 2.56, while for the higher ratio the SMI is 2.03. This was calculated using ImageJ 1.46 with BoneJ plugin 1.3.1 (Doube *et al.*, 2010; Hildebrand & Ruegsegger, 1997). Figure 4-2 shows a plotted trabecular thickness of the 17.5% BV/TV bone using a thermal spectrum, the left image is the bone viewed from above and the right image is the bone viewed from below, the image was created using the BoneJ plugin 1.3.1 (Doube *et al.*, 2010).
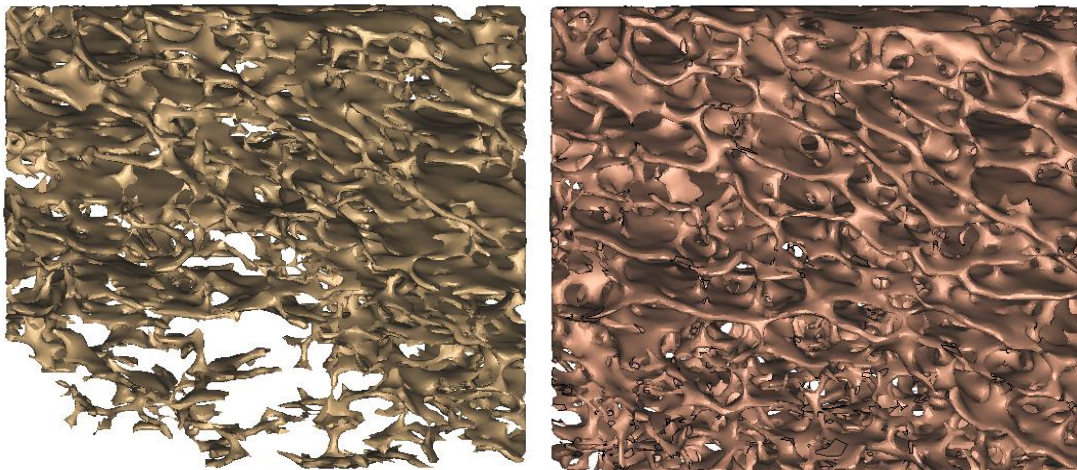
Figure 4-1: Two Bone densities from the same piece of bone, left image shows the eroded model and the right shows the original density

Table 4-1: Trabecular Thickness, Spacing and Bone Volume Density Data for the eroded model (all dimensions in mm.).

Region	Tb.Th Mean	Tb.Th S.D.	Tb.Th Max	Tb.Sp Mean	Tb.Sp S.D.	Tb.Sp Max	BV/TV
Bottom Third	0.126	0.044	0.352	1.053	0.336	1.863	5.8%
Middle Third	0.143	0.050	0.381	1.026	0.372	2.176	8.5%
Top Third	0.154	0.061	0.419	0.917	0.304	1.816	10.6%
Total	0.142	0.054	0.419	1.009	0.320	1.903	8.3%

Table 4-2: Trabecular Thickness, Spacing and Bone Volume Density Data for the smoothed model (all dimensions in mm.).

Region	Tb.Th Mean	Tb.Th S.D.	Tb.Th Max	Tb.Sp Mean	Tb.Sp S.D.	Tb.Sp Max	BV/TV
Bottom Third	0.173	0.052	0.385	0.855	0.306	1.513	14.1%
Middle Third	0.192	0.062	0.468	0.762	0.336	1.850	17.7%
Top Third	0.203	0.072	0.528	0.670	0.269	1.556	20.7%
Total	0.190	0.063	0.480	0.756	0.298	1.650	17.5%

Figure 4-2: Image showing the trabecular thickness of the 17.5%BV/TV bone piece using a thermal spectrum-white is thick, purple is thin. Produced with ImageJ and BoneJ software

Where appropriate a cortical shell was artificially created using CAD software, and therefore is an idealised body i.e. there is no graduated change in apparent density between the upper surface of the cancellous bone and the cortical layer (Figure 4-3). This was to ensure a controlled thickness of cortical shell could be used with the two cancellous bone BV/TV ratios.

Using CT manipulation software it is possible to create a high resolution 3-D model and this is currently the most accurate method of simulating bone, and therefore often produces the most relevant and interesting results. Meshing was carried out using 3matic® (Materialise 3-matic version 6.1) software. Due to its inherent architecture and the presence of many spicules of bone, the limitations of the currently available software mean that the surface mesh has to be completed by inserting missing surface elements manually (i.e. the software does not give a fully automated process). It is time-consuming and demanding to set-up and run each analytical model, and as models become more refined the need for the manual surface element insertion process increases dramatically.
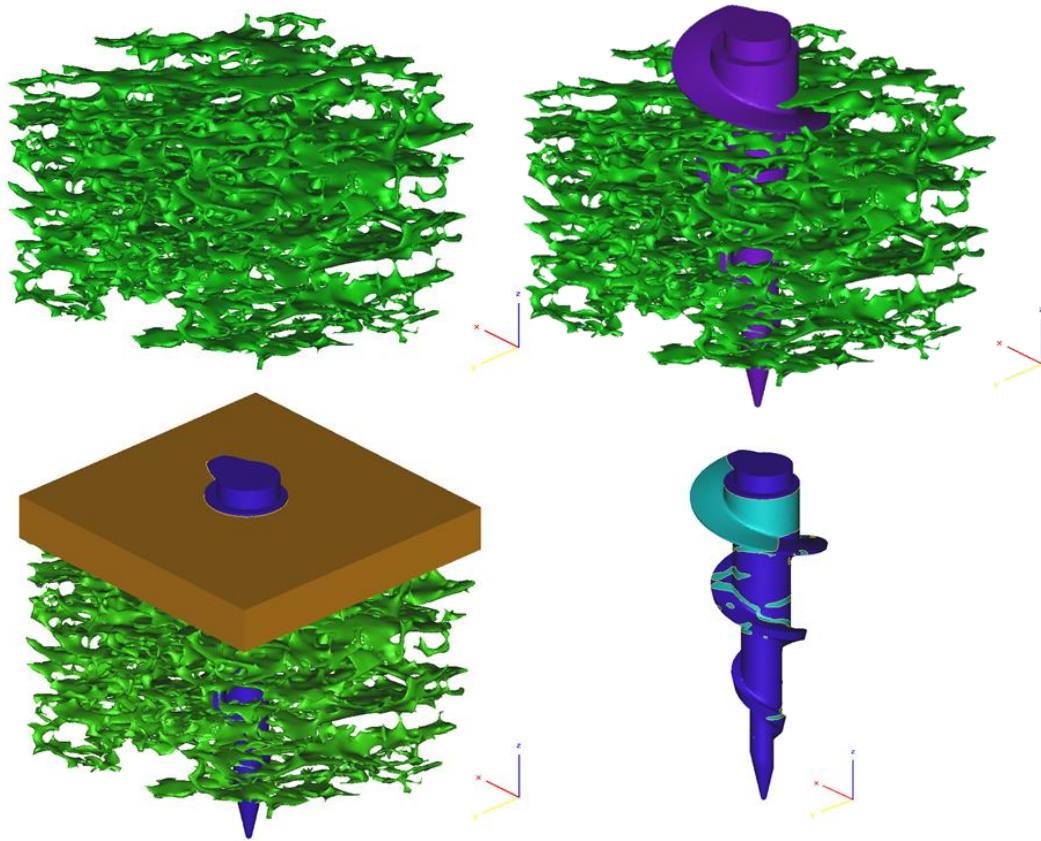
Figure 4-3: The assembly process and the contact area for the model

4.2.2 Assembly

The spiral anchor used had a maximum external thread diameter of 5.36 mm and is shown in Figure 4-4. Once the cancellous bone had been meshed, the anchor was placed into the two models using Boolean operations. The anchor was inserted vertically in the centre of the bone, and had the same position and orientation for each subsequent analysis. The key dimensions of the anchor used are: maximum diameter of 5.36mm, thread length of 12.88 mm, thread pitch of 3.4 mm, and a taper of 12°. The anchor's dimensions are based on a Stryker® Titanium Wedge anchor[1] but it is similar in design essentials to other industry anchors such as the AthroCare® ParaFix Anchor[2].
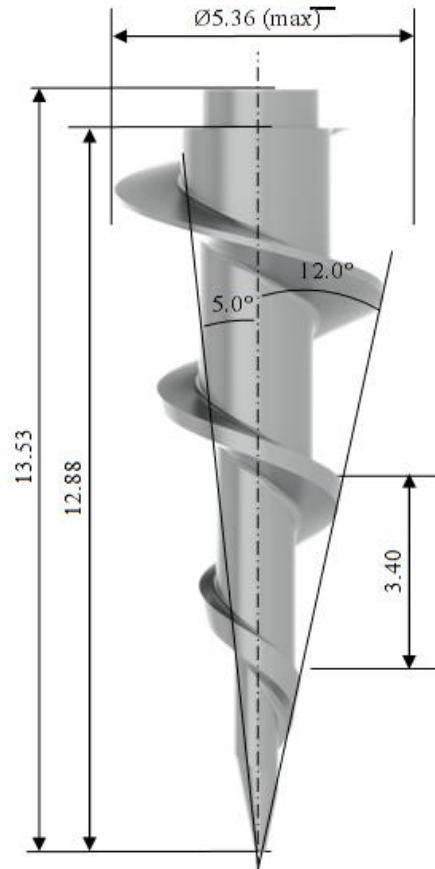
Figure 4-4: Anchor Dimensions (all in mm)

[1]   http://www.stryker.com/enus/products/Orthopaedics/SportsMedicine/Upp
        erExtremity/Anchors/Titanium/TitaniumWedgeAnchor/index.htm
        (1/11/2012)
[2]   http://international.arthrocaresportsmedicine.com/files/technique_guides/
        A50_4001D.pdf (1/11/2012)

Anecdotally, anchors generate increased pull-out resistance as they produce a radial stress field in the bone during the insertion process. This has not been modelled through the process used here. In weak bone, the radial stress field is very low, and while the ensuing results may be conservative it is felt this is justified.

In total, 8 different geometries were explored for each apparent density resulting in a total of 16 meshes. The geometries for each cancellous bone apparent density were: one with no cortical layer, one with a non-engaged cortical layer with five cortical thicknesses of 0.25, 0.5, 1.0, 1.5 and 2.0 mm respectively, and two with anchors fully engaged with a cortical layer of 0.5 mm and 1.5 mm respectively. The term "fully engaged" indicates whether the thread of the anchor is embedded in the cortical shell. If not, the shell may be present and important (Seebeack *et al.*, 2005) and so a cylinder of cortical bone thickness has been "removed" to allow the anchor to pass through.

4.2.3 Material Properties

In this preliminary study the elastic and strength properties used for bone elements (Ashman at el., 1984; Turner *et al.*, 1999) and titanium alloy are assumed to be the same in tension and compression. The bone elements have Young's Modulus=17GPa, Poisson's Ratio=0.3, yield strength=100MPa, and ultimate strength 120MPa. The values chosen fall within a range of measured values given in the literature for "normal" bone (Jee, 2001). The material properties used for titanium alloy (ANSYS, 2012) are Young's Modulus = 96GPa, Poisson's Ratio = 0.3, yield strength = 930MPa, and ultimate strength = 1070MPa.

4.2.4 Contact

The interface between the bone and anchor is a frictional contact. Previous experience (Brown *et al.*, 2013) has shown the results to be more appropriate to physical studies when compared to the alternative bonded model. This is because under bonded contact no contact shear stress or sliding occurs between

the surfaces, resulting in a significantly stiffer structure. A frictional coefficient of 0.6 (Brown *et al.*, 2013) was initially used – a more detailed comment on the variation of pull-out force with frictional contact is given below. A bonded contact was used between the cancellous bone and the idealised cortical layer.

4.2.5 Loading

The elements of cancellous bone were fully restrained on the four vertical sides (i.e. those outer surfaces lying in the z-x and z-y planes – the cortical layer lies in the x-y plane). For every simulation a linear ramped displacement in the appropriate direction of 0.2mm was applied to the cylinder at the top of the anchor (eyelet strength was not a point of interest for this study and so was replaced with a cylinder to simplify the F.E mesh and consequently reduce solver time). In clinical practice the loading on the eyelet varies in direction depending on tendon attachment location. Therefore the four different angles of loading in the positive z-y plane only are: vertical (0 degrees), 45 degrees, 72.5 degrees and horizontal (90 degrees). This latter is not a practical case but provides a limit analysis. The forces given as "pull-out" forces are in fact the reaction forces at the directional displacement of 0.2mm.

4.3   Results

Contact area between the anchor and the bone will vary for the same anchor in different apparent densities of bone with the same structure and topography. Figure 4-5 shows the contact area for the implant, the right image shows the same plot of the area in contact using a computer-eroded bone model, with the outline of the original contact area given in the same figure. In some cases the contact area of a particular trabecular strut slightly decreased, while in others it has been removed entirely. The higher apparent density model had a contact area of 16.28 mm², and this decreased to 10.13 mm² for the lower apparent density model. Contact area does not appear to relate directly to pull-out force, although Yakacki *et al.* (2009) suggest otherwise. However, greater contact area is likely to be associated with bone of higher apparent density, for which there is strong evidence of increased pull-out force (Asnis & Kyle, 1996)

High density
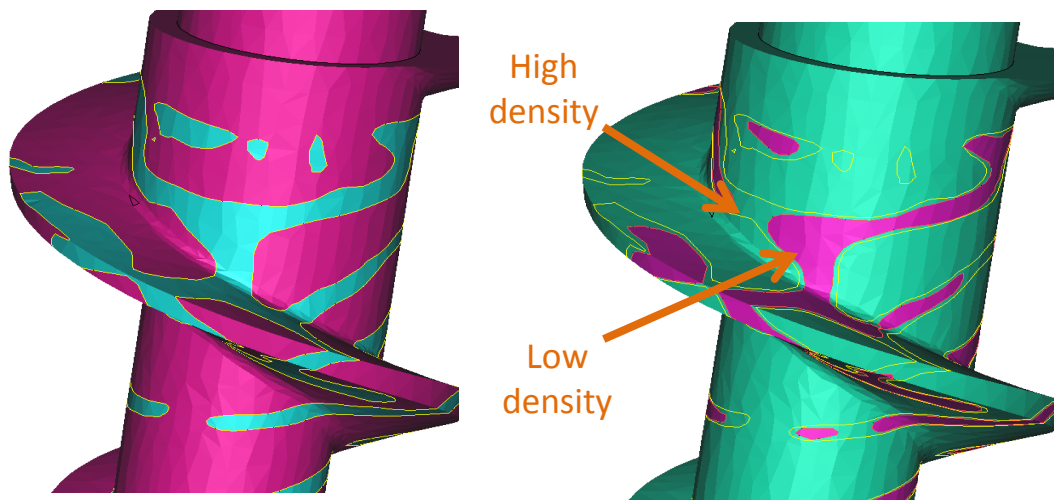
Low density

Figure 4-5: Contact area differences, High density shown on left, low density with high density outline shown right

Figure 4-6 shows the position of the upper surface of the anchor for the modelled configuration. On the left, the friction coefficient is low, and an un-screwing phenomenon can be observed through the rotation of the top of the screw. On the right with higher friction, there is no screw rotation and the upper surface of the bone is moved as a rigid body, even though sliding between surfaces in the model is still allowed. That this phenomenon can be observed in the model is somewhat surprising. In previous work on screw fixation (Brown *et al.*, 2013) the importance of friction coefficient has been examined and deduced it might not be a critical factor, but approximate models, including those that use continua for cancellous bone, are unlikely to exhibit this unscrewing behaviour. There is little change in pull-out force for a range of friction coefficients between 0.35 and 0.6. *In vivo*, friction coefficients may change with time as surfaces are lubricated to a greater or lesser degree.
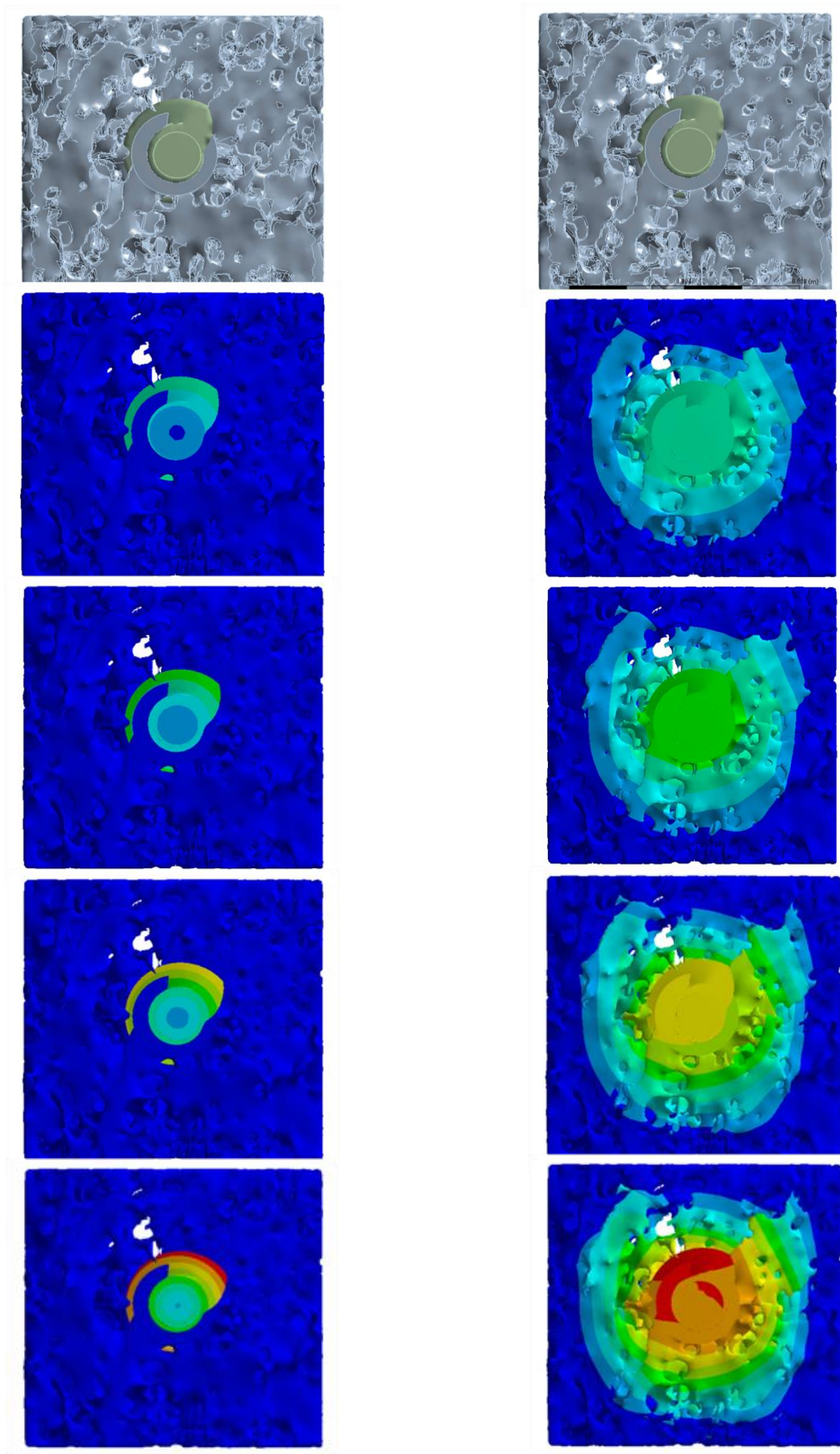
Figure 4-6: Comparison of lower and higher friction contact coefficients

The pull-out force output (Figure 4-6), is given as the peak reaction force at a vector displacement of 0.2 mm (i.e. in the direction of the pull). A value of 0.2 mm was used as this was the largest mean trabecular thickness of either bone model; values beyond 0.2 mm would be likely to indicate large deflections in the trabecular struts beyond the scope of the present analysis. Figure 4-7a is for vertical pull-out, while Figure 4-7b is for loading inclined at 45^0, Figure 4-7c is for 72.5^0, and Figure 4-7d is for 90^0. Two bone apparent densities each with two cases are given – when the anchor is engaged with the cortical layer and when it is not engaged. As expected, the pull-out force is greater if there is a cortical shell present (Chen, Lin & Chang, 2003) even if the anchor is not engaged with the cortex. However, this effect diminishes for non-engaged anchors as the cortex becomes thicker, and from 0.5mm to 2mm there is a negligible increase in force for both bone densities. Nevertheless the importance of maintaining even a minimal cortical layer is evident (Seebeck *et al.*, 2005).

For pull-out angles of zero, up to about 45^0 the importance of connecting to a cortical layer – even of limited thickness – can be remarkable. In the bone of higher apparent density there is little effect for thin cortical layers because the cancellous bone is relatively stiff, but for a cortical layer of about 1.5 mm the pull-out force is roughly trebled. In the bone of lower apparent density the cortical layer has an immediate effect, and even the 0.5mm layer will increase pull-out force for low angles of inclination.

Figure 4-7: Sequence of graphs comparing reaction force at the angles loaded

Figure 4-7a: Reaction Force Vs. Cortical Thickness for Two Apparent Densities with Engaged and Non-engaged Anchors (Vertical)

Figure 4-7b: Reaction Force Vs. Cortical Thickness for Two Apparent Densities with Engaged and Non-engaged Anchors (45°)

Figure 4-7c: Reaction Force Vs. Cortical Thickness for Two Apparent Densities with Engaged and Non-engaged Anchors (72.5°)

Figure 4-7d: Reaction Force Vs. Cortical Thickness for Two Apparent Densities with Engaged and Non-engaged Anchors (Horizontal)

The patterns of displacement on a slice through the centre of the construct under vertical pull-out, (Figure 4-8) and lateral pull-out respectively (Figure 4-9) show that the mechanism changes. Instead of a direct pull-out through failure at the bone anchor interface, the anchor is also engaged in cut-out as it tries to move through the bone so that at 90^0 the mechanism is almost entirely cut-out. For vertical pull-out, the deformation is almost the same at any position around the anchor, while for the lateral load it is evident that significant deformation is happening in the cancellous bone adjacent to the top of the anchor.

The developing number of elements in contact (Figure 4-10 – zero point not shown) while increasing the loading shows quite marked differences between pull-out and cut-out for the same anchor in the same piece of bone. In Figure 4-10 - Top, the data are given for vertical pull-out, while the contacts developed for horizontal pull-out are shown in Figure 4-10 - Bottom. In the early stages of loading, the number of contacts increases as the gaps between the anchor surface and adjacent bone elements are closed. More contacts are generated under lateral loading than under vertical loading.
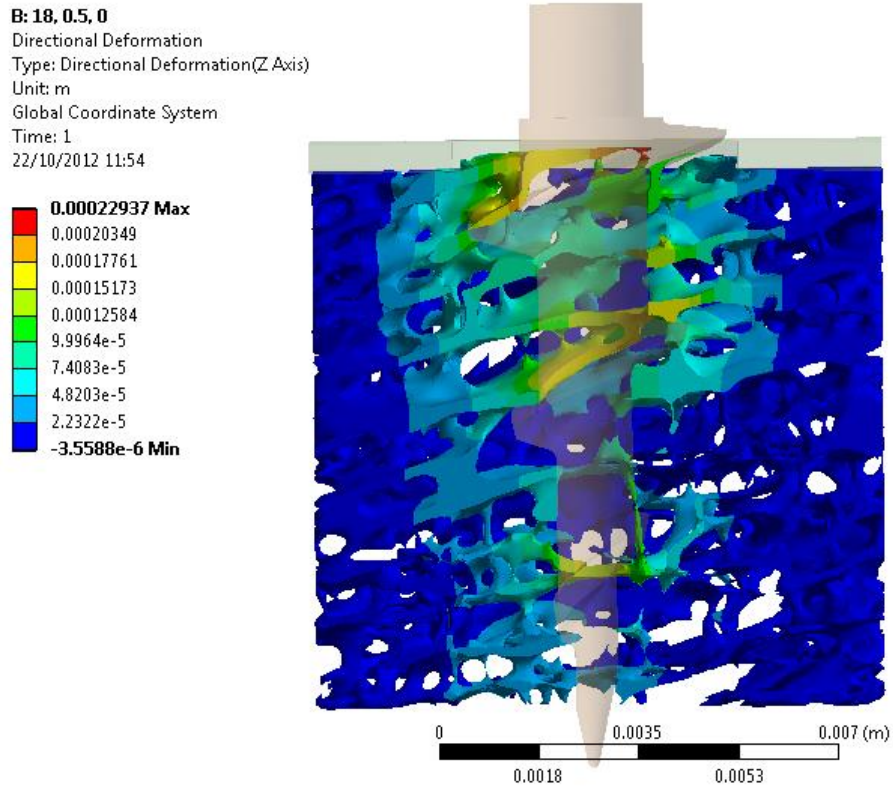
Figure 4-8: Deformation of the bone under vertical loading
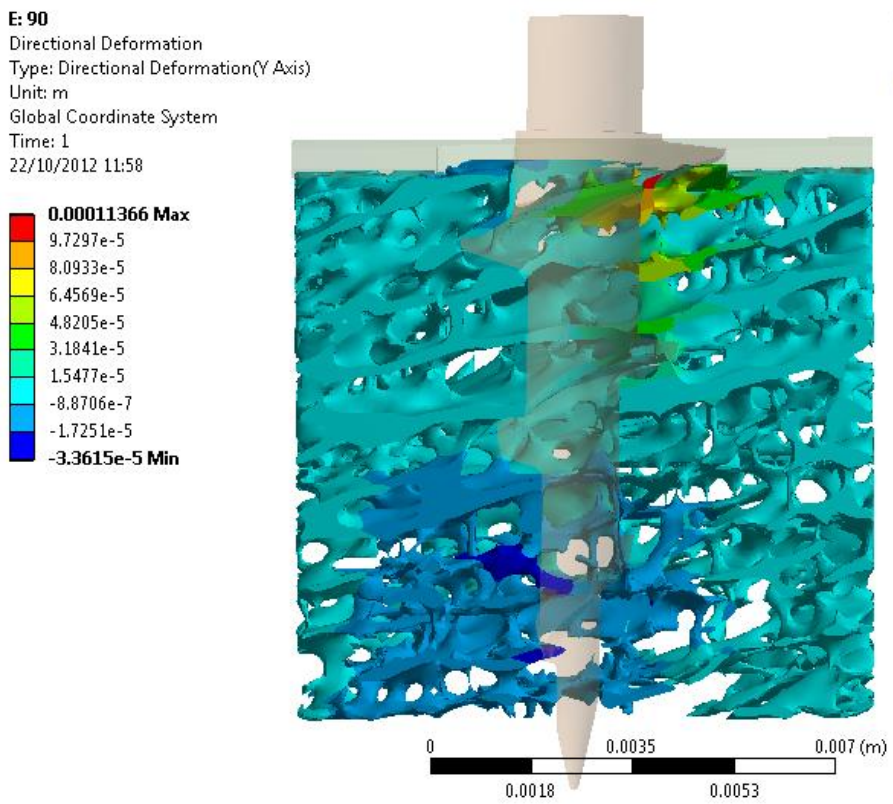
Figure 4-9: Deformation of the bone under horizontal loading
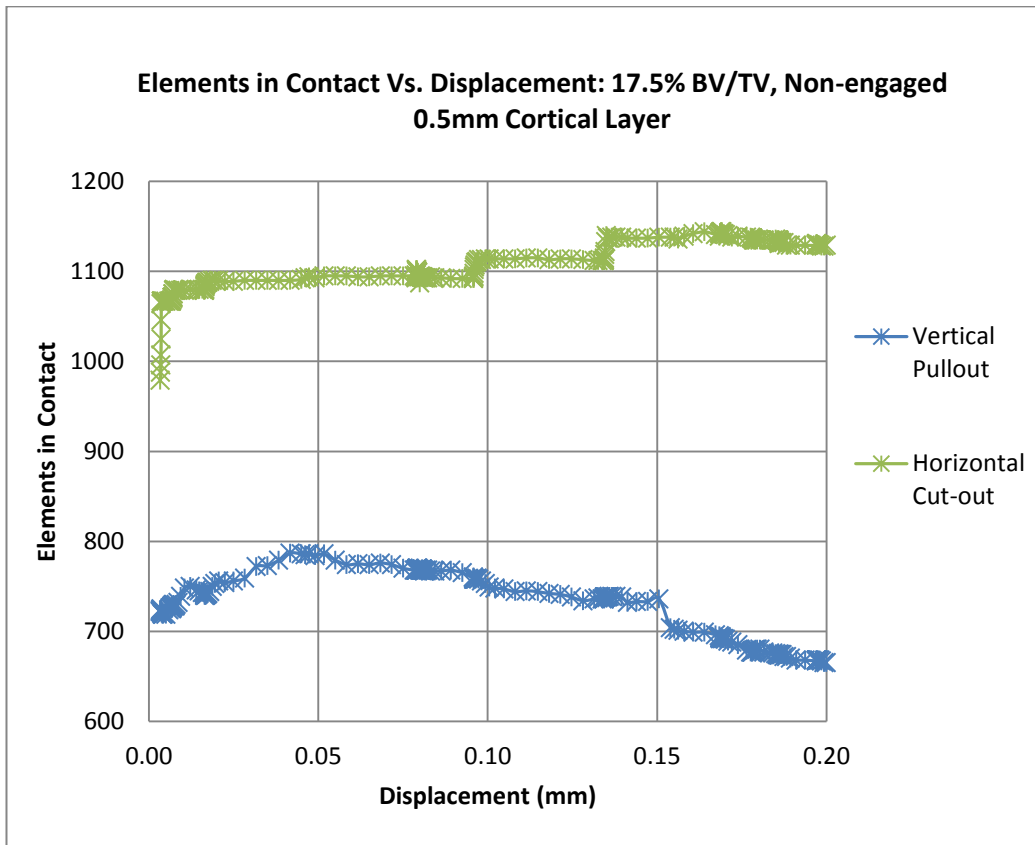
Figure 4-10: Elements in contact

4.4   Discussion

The results show the relative magnitudes of pull-out force for different anchor/bone configurations. Validation of implant pull-out force is difficult in real bone because of its variability, while substitute materials produce unrepresentative loads.   Nevertheless, the results from the FE model for equivalent non-engaged anchors are consistent with those data presented in the literature (Barber, 2006) for the pull-out of suture anchors from porcine bone where mean pull-out values of between 220N and 710N are given.

Combined vertical and horizontal loading has been examined in one arbitrarily selected plane (Figure 4-7). However an additional study has been carried out that observes the effect of load direction. This effect can be quite dramatic. In this test, the direction of the lateral load is changed by 45° on the x-y plane to give seven other directions (eight in total). The reaction load can change quite markedly. In the lower apparent density bone, the mean pull-out force for loads on the horizontal plane is 344N (CV = Coefficient of Variation = Standard deviation/mean =28.9%) but the minimum value is 223N, and the maximum 489N – a ratio of 2.19:1. As might be expected, the variation is less when the pull-out is at 45° to the plane, with a mean of 255N (CV=13.7%), a minimum of 200N, and a maximum of 314N – a ratio of 1.57:1. As the angle to the horizontal plane increases this ratio should decrease, so that at 90° to the horizontal plane the ratio must be unity. In the bone of higher apparent density the variation is not as great. The CV values are both 14%, and the mean values show much less divergence. Nevertheless, such variation could never be detected in any models that use a continuum representation of cancellous bone, and this small study again shows the sensitivity of pull-out force to local bone structure and the importance of models that include this feature.

4.5   Conclusions

This study has shown the importance of friction coefficient in models of anchor pull-out from a porous structure, and suggests that very low coefficients might

lead to quite different mechanisms than those where friction is high. Any change in friction in vivo could lead to a marked change in performance.

The study has also re-confirmed the importance of a cortical layer. At the angles and apparent densities simulated, engagement with the cortical layer increases pull-out force dramatically. Engaging the anchor even with a thin cortical layer can produce a significant advantage to pull-out strength.

Finally, it has been shown the critical nature of modelling the microstructure of bone. Changing the direction of loading in the model leads to significant changes in the response of the construct, and this cannot be represented in continuum models, or in physical models using artificial cancellous bone. These results demonstrate that the fundamental variability in real bone can lead to large changes in behaviour over quite a small volume.

5 The orientation effect on pull-out of a spiralled anchor and additional studies

5.1 Introduction

This chapter continues to explore the variability in anchor pull-out. The same two models of "normal" and "weaker" cancellous bone were used to investigate the change in reaction force for a single anchor under a set displacement in different directions on the horizontal plane and at an angle of 45°. The objective of this study was to observe the variation of reaction forces within the structure of bone from a single location, and how it may change with a decrease in bone quality.

5.2 Materials and Methods

The same methods and parameters were used to assemble the model as seen in the previous chapter. The same two pieces of cancellous bone have been used, again with bone orientated so the higher "local" apparent density is parallel and near to where the cortical shell would be. The smoothed bone model (Figure 4-1 – right) had an overall apparent bone density of 17.5%, and this might represent normal or healthy cancellous bone, while the eroded model had an overall apparent bone density of 8.3% (Figure 4-1 – left), and this might be more appropriately described as weak or osteopenic bone. The same anchor dimensions were used - based on a Stryker® Titanium Wedge anchor.

After looking at variability in reaction force in the vertical plane, it was logical expand the study and look at change in reaction force in the horizontal plane; this also led to looking at the reaction force radially at a 45° angle. To see how the thread factor affected pull-out, a continuum model was created.

The elements of cancellous bone were fully restrained on the four vertical sides (i.e. those outer surfaces lying in the z-x and z-y planes – the cortical layer lies in the x-y plane). As before, for every simulation a linear ramped displacement in the appropriate direction of 0.2mm was applied to the top of the anchor.

Figure 5-1 shows the side view of the loading cases, with the red arrow showing the 0.2 mm displacement applied in the horizontal loading case and the blue arrow the 45° case. In the case of 45° a displacement of 0.1414 mm was applied in the vertical and horizontal direction, to produce a final vector of 0.2 mm. The forces given as "pull-out" forces are in fact the reaction forces at the directional displacement of 0.2 mm.
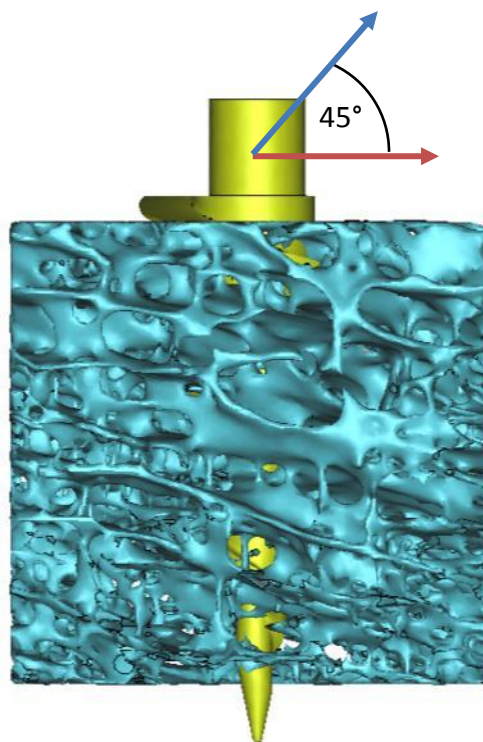
Figure 5-1: Loading applied to the anchor
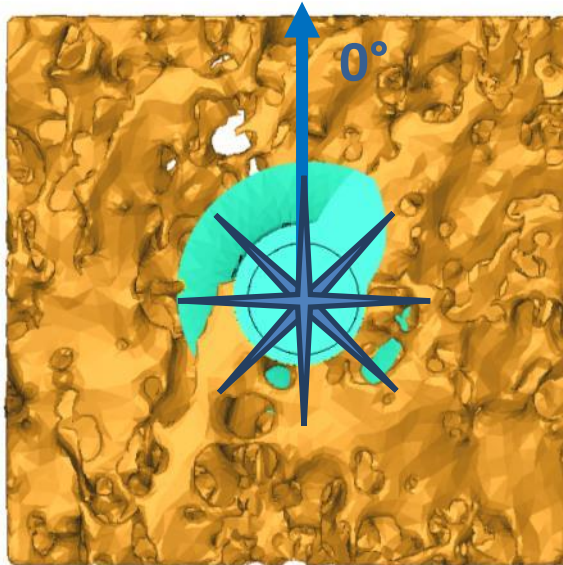
Figure 5-2: Orientation of the bone and anchor in the original study

Figure 5-2 gives the orientation of the bone to the anchor from above, to maintain consistency this will always be the orientation of the bone, the arrow pointing in 0° will refer to this direction in the result plots (Figure 5-4, Figure 5-5, Figure 5-8 &Figure 5-9). For the continuum model 0° refers to the same direction as the anchor shown in this figure. The model shown here is the lower apparent density bone, a hole can be seen above and to the left of the anchor, giving a clear marker to check the alignment of the model when setting-up. In the higher apparent density there is no line-of-sight hole so the orientation was checked by lining up the orientation of the trabecular plates – looking at Figure 5-2 it can be seen that the trabecular plates have a diagonal grain to them. In total 8 results were taken for each data set, points were 45° apart as shown by the blue points in Figure 5-2.

5.2.1 Material Properties and Contact

As reasoned and used in the previous simulation, the bone elements have Young's Modulus=17GPa, Poisson's Ratio=0.3, yield strength=100MPa, and ultimate strength 120MPa.

The material properties used for titanium alloy (ANSYS, 2012) are Young's Modulus = 96GPa, Poisson's Ratio = 0.3, yield strength = 930MPa, and ultimate strength = 1070MPa.

The contact settings were the same as used previously.

5.3 Results

Figure 5-3 shows the continuum model and its results. It can be seen that there is some variation in the reaction force (245-290N), showing the thread design factor does have some influence, the standard deviation is 20.6N for a mean of 265.3N on the horizontal plane. A complete result set for continuum was considered unnecessary so only the cardinal points of the compass were simulated.
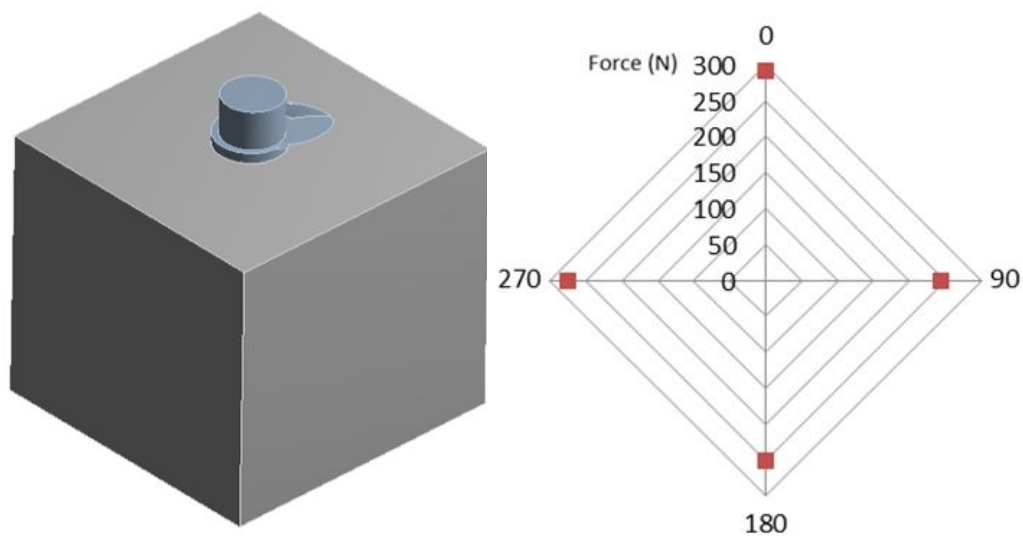
Figure 5-3: Left shows the continuum Model, right shows the Radar plot of the results

Figure 5-4 and Figure 5-5 show the final result set; Figure 5-4 shows the values for the 8.3% BV/TV model and Figure 5-5 shows the values for the 17.5% BV/TV model. Comparing the figures it can clearly be seen that there is a much larger deviation for the horizontal plane. In the low apparent density model the largest reaction force is 489 N at 180° and the smallest reaction force is 223 N at 315°, a

ratio of 2.2:1. For the higher apparent density model on the horizontal plane the largest reaction force is 617 N at 180° and the smallest reaction force is 286 N at 90°. At 45° loading (labelled in blue on the charts) in lower BV/TV bone the standard deviation and mean force drops (Table 5-1). For the higher BV/TV model the mean force and standard deviation increases.

Figure 5-4: Radar Plot showing the reaction force of anchor in lower apparent density bone in the original orientation
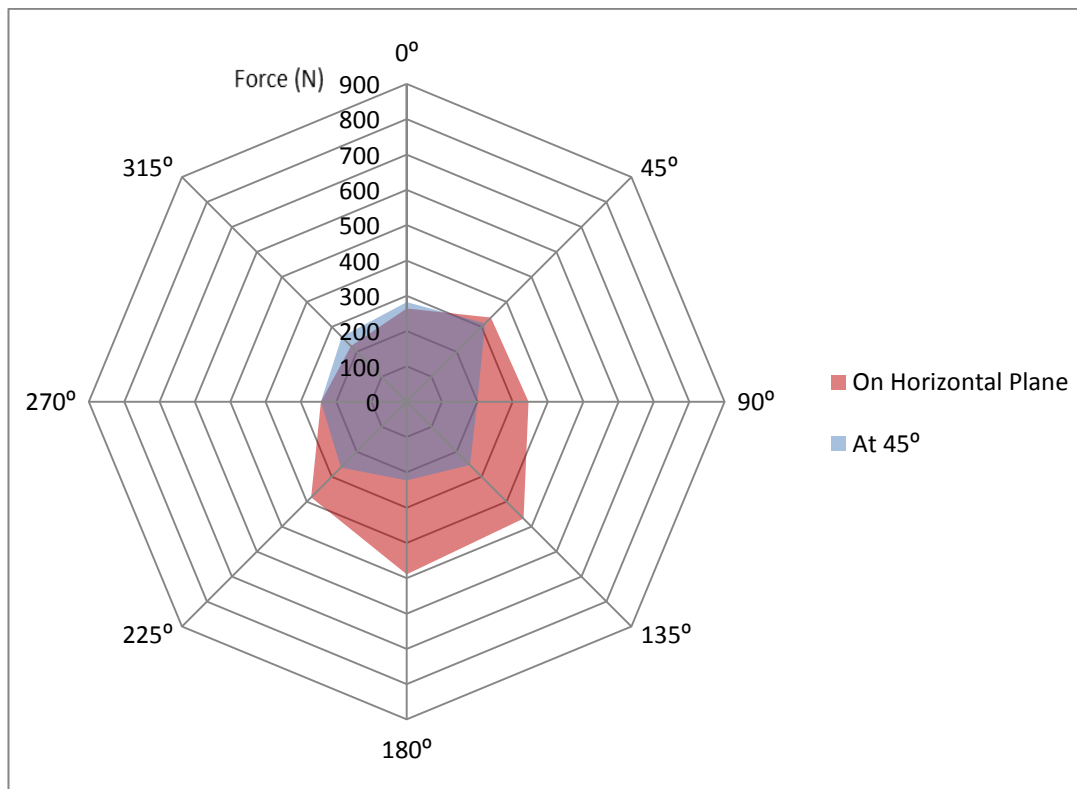
Figure 5-5: Radar Plot showing the reaction force of anchor in higher apparent density bone in the original orientation
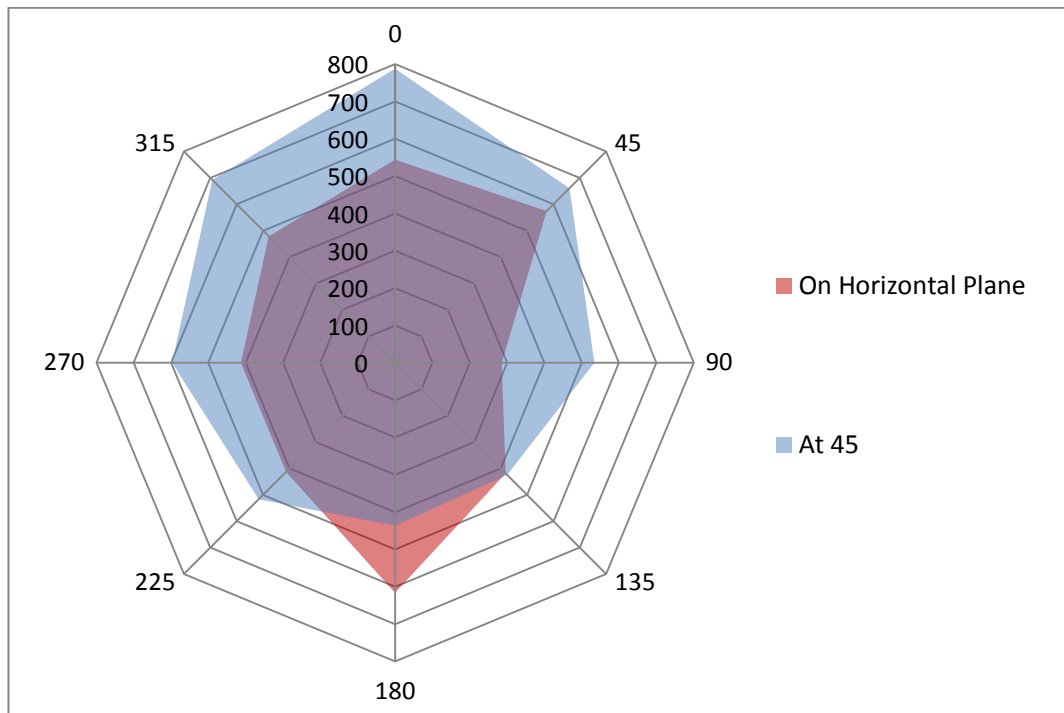
To further check the observed effects were not due to the thread position and the bone structure, an anchor was inserted at the same depth but rotated around its thread axis 180° i.e. it was not physically rotated in. This can be seen in Figure 5-6, notice the orientation of the bone remains the same but the anchor has rotated 180°. For the radar plots the 0° angle is the same and its direction is shown in Figure 5-6.
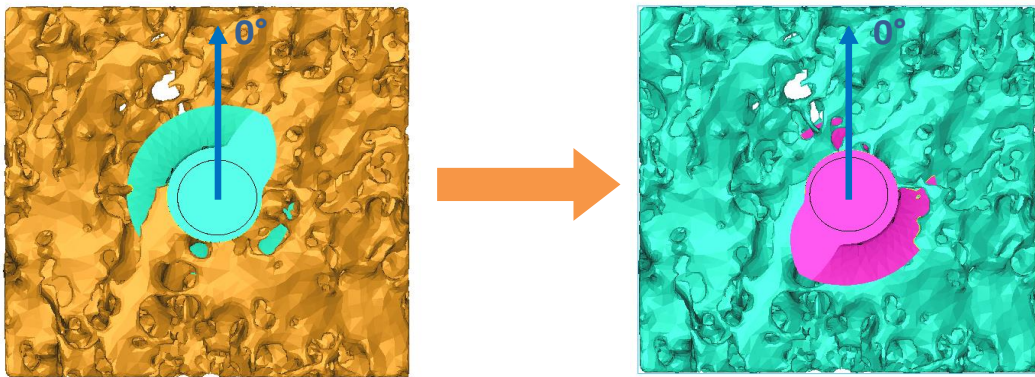
Figure 5-6: Showing the change in orientation of the anchor, this is the lower apparent density bone

Original Study	Rotated Study
Lower BV/TV: 10.1 mm²	Lower BV/TV: 9.7 mm²
Higher BV/TV: 16.3 mm²	Higher BV/TV: 17.2 mm²
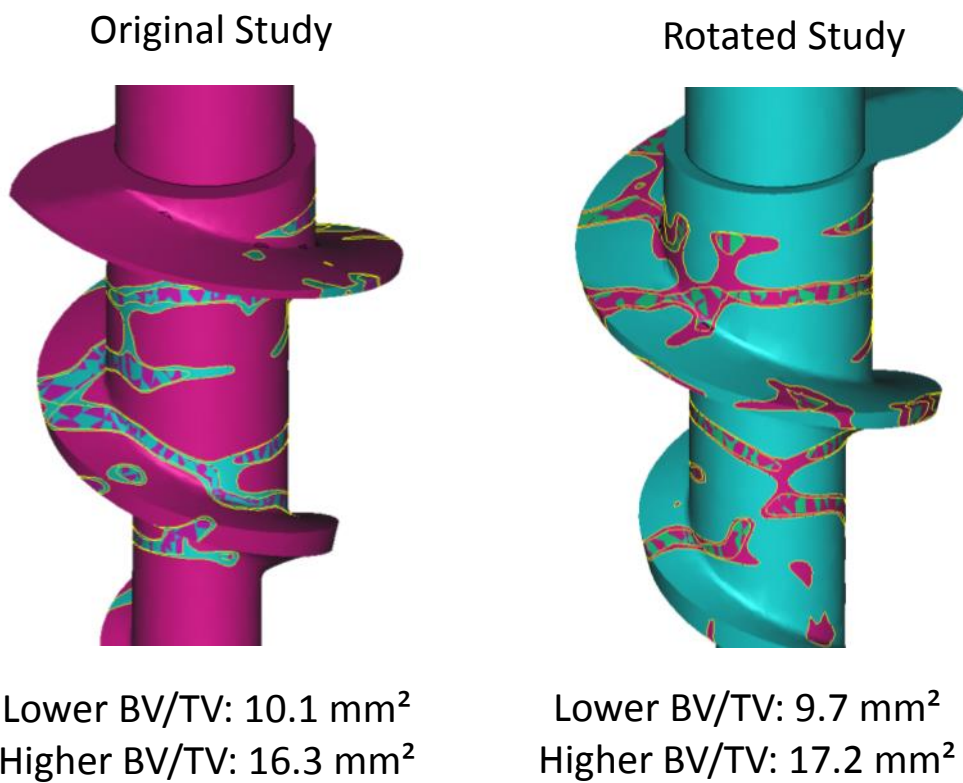
Figure 5-7: Contact area for both sets of results for both lower and higher apparent densities

Figure 5-7 shows the difference in contact area between anchors taken from the same viewpoint. There is considered to be a small correlation (Yakacki *et al.,*

2009) between contact area and stiffness, but it is interesting to see the variability that exists for the same implant in the same piece of bone in the same position. Figure 5-8 and Figure 5-9 show the final result set for the rotated anchor; Figure 5-8 shows the values for the 8.3% BV/TV model and Figure 5-9 shows the values for the 17.5% BV/TV model.

Figure 5-8: Radar Plot showing the reaction force of anchor in lower apparent density bone in the rotated orientation
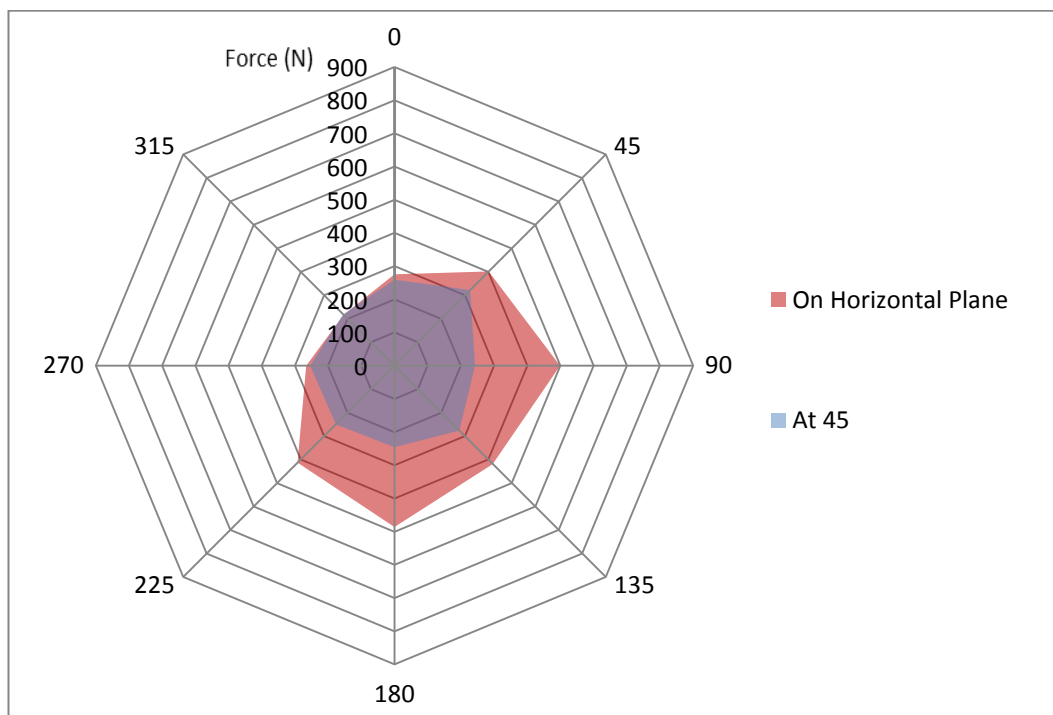
Figure 5-9: Radar Plot showing the reaction force of anchor in higher apparent density bone in the rotated orientation
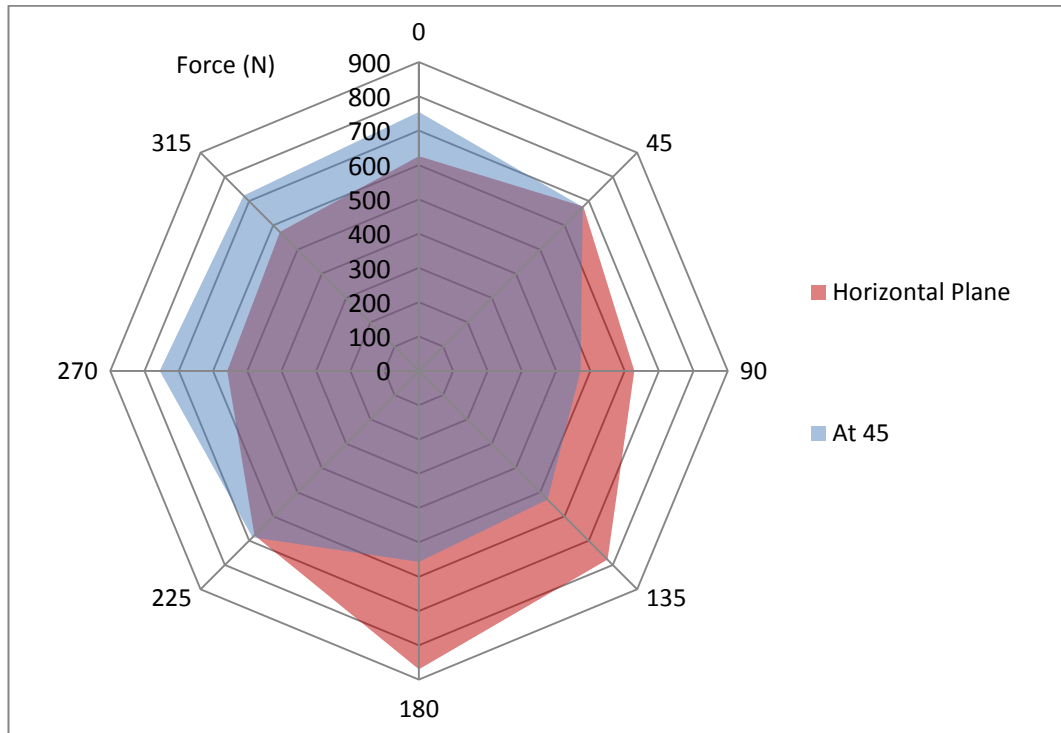
Table 5-1 gives the means pull-out forces and standard deviation for each result set. It can be seen that the mean forces and standard deviation are very close for the lower apparent density model, with an 8% difference for the horizontal study and only a 1.5% for the 45° study.

For the higher bone apparent density the results on the horizontal plane do not align so closely. Although, generally the pull-out forces are lower, the point at 90° in the original study does noticeably lower the mean value. The 45° results however do align more consistently

Table 5-1: Mean Pull-out Forces for each result set with standard deviation

Study	Original Study				Rotated Study			
Bone Type	17.5% BV/TV		8.3% BV/TV		17.5% BV/TV		8.3% BV/TV	
Orientation	Horizontal	45°	Horizontal	45°	Horizontal	45°	Horizontal	45°
Mean Force (N)	468	581	344	255	674	644	372	259
Std. Dev.	108	127	99	35	105	110	106	30

5.4   Discussion
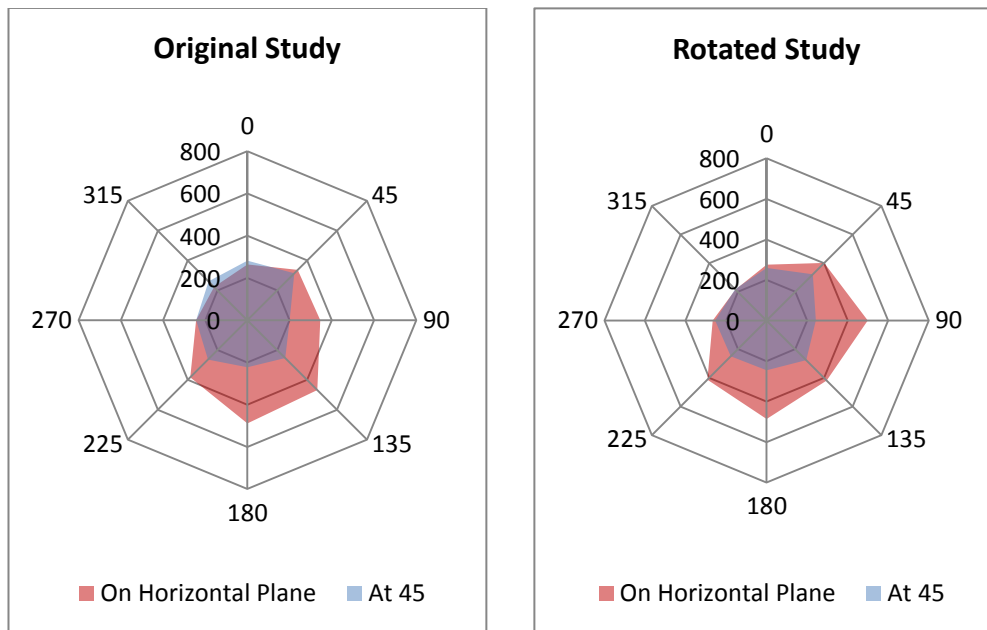
Figure 5-10: Lower BV/TV values compared.

Figure 5-10 compares the results from the lower apparent density bone. It can be seen there is similar mean stress and standard deviation for both planar loading and 45° loading. The reaction force footprint in the planar direction is not identical but does have clear similarities, i.e. the lowest reaction force for both is at the 315° point, while the highest reaction force area is the 90-180° region. For the 45° results the radar plot footprint is also similar, both peaking in the 45° direction.

Horizontal loading provides greater mean pull-out force for both models in this case. Indicating in lower apparent density bone it could be better to load it in this manner. This is further backed up by the results for vertical loading (Table 5-2), in this direction the force drops to 160 N for the original study and 126 N for the rotated anchor study. Horizontal loading does have much larger standard deviation, circa 100 N for both models compared to circa 30 N for 45°. This can be explained due to the fact that as the loading moves towards the vertical it is moving towards a single load point.
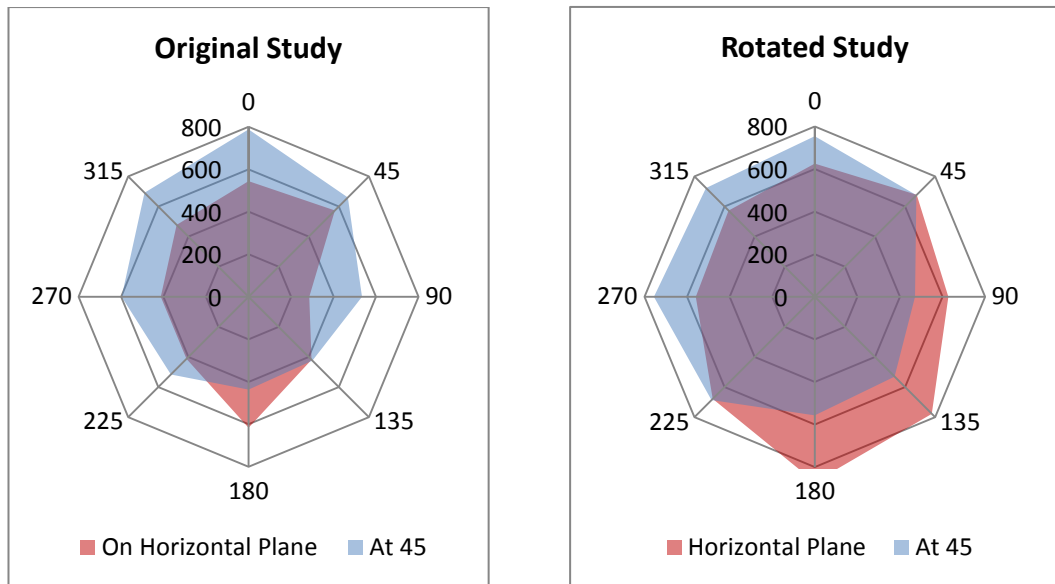
Figure 5-11: Higher BV/TV values compared

Figure 5-11 compares the higher apparent density bone. In the horizontal plane an unusual footprint arises for the original orientation, specifically the result at 90°. However similarities can be seen between both on the left-hand side (clockwise from 180° to 0°). At 45° the results are similar, with the maximum and minimum forces occurring in the same positions.

It is clear that the previous chapter did not tell the complete story when observing pull-out forces. In some directions a horizontal application gives a better holding power and for other directions 45° gives a higher force - Showing that a reliable relationship between reaction force and angle applied cannot be established for cancellous bone. Interestingly the standard deviation for horizontal and 45° is very similar for higher density bone, unlike the results for lower apparent density bone, indicating weaker bone behaves in a different way to healthy bone, this indicates weaker bone behaves diffferently. This is further demonstrated in the vertical force results which behave in the opposite way to the lower apparent density model – with force increasing rather than decreasing.

Table 5-2: Contact Area compared to Pull-out Forces

Contact Area (mm^2)	Horizontal Mean Force	45° Mean Force	Vertical Force
9.7 (Rotated Study)	372 N	259 N	126 N
10.1 (Original Study)	344 N	255 N	160 N
16.3 (Original Study)	468 N	581 N	643 N
17.2 (Rotated Study)	674 N	644 N	677 N

Table 5-2 compares the contact areas to the mean forces observed. From these results it can be said that there is obviously an increase in pull-out force as contact force increase but where there is a small increase in contact force there can be said to be no relationship between the two properties. Although contact area has some relationship with pull-out force, it is debatable whether it is a worthwhile property to look at. Apparent density gives a good indication for pull-out force and is relatively easily to measure ex-vivo and in-vivo. However outside of simulations contact areas are very difficult to measure and even-more difficult to predict, meaning outside of computer modelling it is not a practical value to explore.
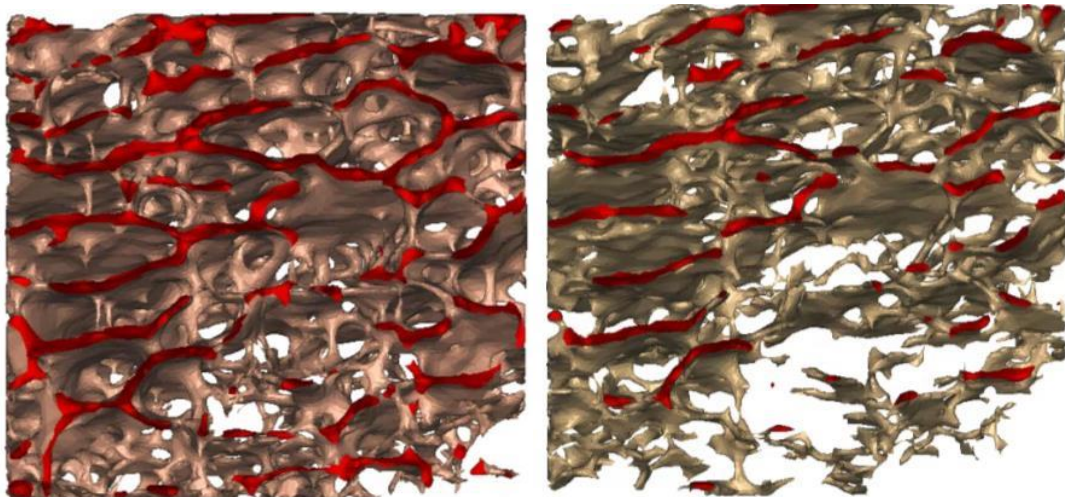
Figure 5-12: Cross-section of bone, 17.5% BV/TV Bone on the left, 8.3% on the right

A possible explanation for the difference in behaviour between the two bone types can be seen it Figure 5-12. It shows the cross-section of the bone where the anchor lies i.e. a central axis. It can be seen in the right image that there is

hardly any vertical struts left in the eroded bone – in fact none at all in the plane of the cross-section. This lack of vertical struts could account for why the pull-out force is so low in the vertical direction in the weaker bone but approximately three times greater in the horizontal direction. In the "healthy" bone (left) there are clearly more vertical struts, meaning that a greater load can be supported in the vertical direction. There is evidence (Snyder *et al.*, 1993) that trabeculae do re-model in this way, vertical trabecular are resorbed at twice the rate as horizontal.

5.5   Conclusions

This chapter has further demonstrated the importance of models using architecture taken from CT scans over continuum models. A clear variation of pull-out force has been observed, with a 2.2:1 ratio between highest and lowest pull-out forces being observed in the horizontal plane for both models in the lower apparent density bone. In the higher apparent density there is also a significantly large standard deviation in reaction forces. This highlights how difficult it is to make predictions for pull-out forces, particularly in weak bone.

An explanation has been offered for the difference observed in behaviour for the "healthy" bone and the osteopenic bone. Displaying that as bone ages (or this case is eroded) the structural properties of bone will not weaken uniformly in all directions – raising the issue that it could be especially important to observe the "grain" of the structure in osteopenic bone before an implant is inserted.

The study has shown the need for a substrate in lower apparent density models, with very low pull-out forces observed in the vertical direction and although horizontal pull-out forces are higher they possess a large standard deviation. Use of cement or other substrate would likely increase the pull-out force and decrease the standard deviation.

5.6   Additional Side Studies

Carrying out these studies always generated further questions and points of interest to look out. Presented here are two of the side studies that produced interesting results.

5.6.1   Rotated Bone

For the previous studies the cancellous bone has always had its trabecular plates orientated horizontally as this generally the way an anchor would be inserted in - as the cortical bone would be located at the top of bone. Out of interest a model was created in the lower apparent density bone in which the anchor's thread axis ran near parallel with the trabecular plates rather than perpendicular. This model is shown left in Figure 5-13 and the original bone orientation as used previously is shown on the right.
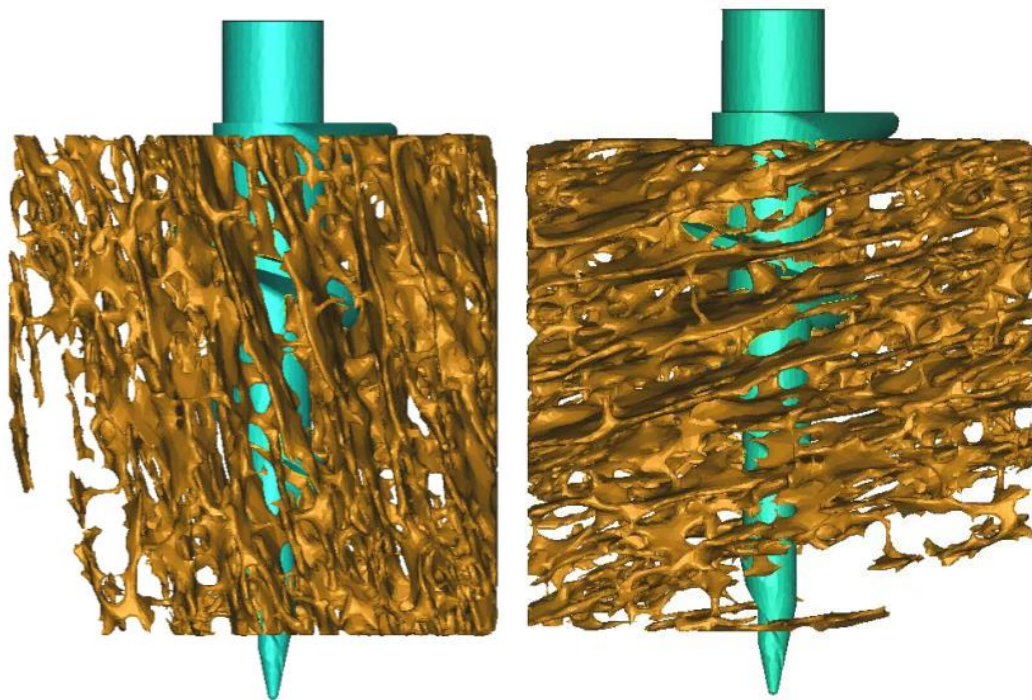
Figure 5-13: Left image shows new orientation, right image shows original orientation.

The exact same parameters and settings were applied to the model in the FEA simulation as has been previously given but now the orientation had been

The orientation effect on pull-out of a spiralled anchor and additional studies rotated 90°. The anchors orientation now lies near parallel to that of principal loading direction. Cancellous bone adaptively remodels along the loading lines as laid out in Wolff's theorem. Due to this it was expected that the reaction force would increase as the thread axis is now orientated with the direction of loading the bone as adaptively remodelled to.

The reaction force for a 0.2 mm displacement is 427.6 N, compared to 126 N (original) and 160 N (rotated) for the reaction force in the lower apparent density bone where the trabecular plates are orientated horizontally. This is approximately a threefold increase in reaction force, showing again the large affect anchor orientation and placement can have on the reaction force. Figure 5-14 shows the total deformation plot of the bone.
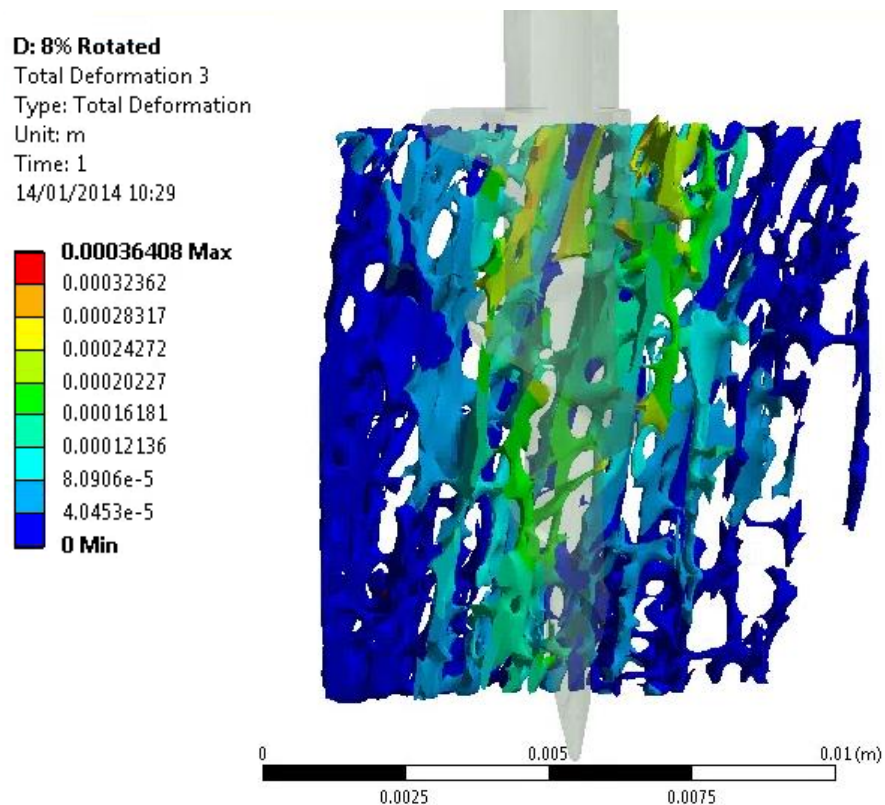
Figure 5-14: Deformation Plot of the rotated study in the lower apparent density bone

5.6.2 External Taper Angle

In this case the anchor geometry was adjusted; the external taper was decreased to maintain thread depth lower down the anchor. Figure 5-15 shows the three

anchors; left is the original anchor with 12° of external taper, middle has 8° of taper, and right shows the anchor with 4° of external taper. An anchor is tapered as it allows for easier insertion into the bone but it can be observed that the thread down the bottom on the original anchor (12°) will have little holding power. Therefore it was of interest to see what would happen if the overall thread depth was increased without completely disregarding the taper.
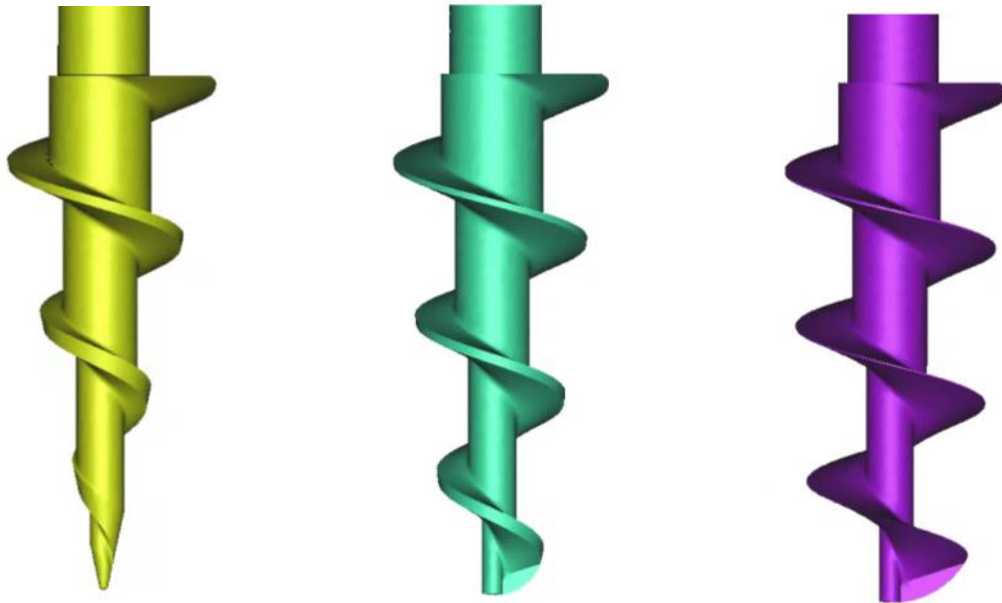
Figure 5-15: Shows the three anchors with decreasing external taper - left to right: 12°, 8°, and 4°

Again the study had the exact same parameters and settings as mentioned and applied previously. It was carried out in both lower and higher apparent density bone types. The results from the vertical simulations can be seen in Table 5-3.

Table 5-3: External taper of the anchor compared against reaction force

Taper (Degrees)	Vertical Reaction Force (N)
8.3% BV/TV Cancellous Bone	
12°	126 N
8°	166 N
4°	184 N
17.5% BV/TV Cancellous Bone	
12°	643 N
8°	862 N
4°	965 N

For the 8.3% BV/TV cancellous bone there was a small increase in reaction force for the decreased taper. The small increase is likely due to the very low BV/TV value (5.8%) in the bottom third of the bone. This results in the increased thread depth having little extra bone to engage with.

For the 17.5% BV/TV cancellous bone there is a greater increase, even though the BV/TV volume is at its lowest in bottom third (14.1%) there is still sufficient bone to engage with. This results in a 200 N increase from 12° to 8° then a 100 N increase from 8° to 4°. These results are dependent on the bone geometry but they do indicate that there is an argument for increasing the thread depth on anchors and it should be examined why these dimensions are used.

6 Modelling Sonic Fusion

6.1 Introduction

This chapter covers the application of sonic fusion as a suture anchor. Sonic fusion was developed to minimise the destruction of bone during surgery, although a hole must still be drilled to insert the implant. Instead of a threaded anchor a resorbable polymer pin is inserted, and then melted under shear forces induced ultrasonically into the pores of cancellous bone. After 3 months to two years (time is primarily size dependant) complete resorption takes place leaving minimal evidence of an implant. It also has the advantage of reducing the time needed for the operation procedure (Müller-Richter *et al.*, 2011).

After successfully modelling a threaded anchor the opportunity arose to simulate the newer sonic fusion technology. The sponsor company (Stryker®) provided access to technical information on technique and specifications, which allowed a sonic fusion model to be conceived. The objective was again to establish a working model of this technology, and eventually compare the sonic fusion anchoring system to conventional anchors.

As this was an original study there was no clear path to set up a simulation, which meant considerable ground work had to be done to produce a model with acceptable parameters. Two investigation methods were explored for studying the pin. They were simplified geometry models and CT scanned models of the pin in bone. The simplified models involved simulation in a human bone sample whilst the CT scanned model was imaged in ovine bone. This chapter is therefore split into two separate parts, one covering a complete CT model and the other covering the simplified models.

Using simplified pin models proved to be a less complex task than a complete CT model although still more difficult than a threaded anchor. This was due to the much larger contact area and the fact that the contact was always parallel to the bone. The difference in contact area compared to a threaded implant meant an

increase in the number of calculations per iteration and therefore increased the total number of iterations required.

6.2   Sonic Fusion Re-cap

The Sonic Fusion process (sometimes known under one if its trade names: Bone Welding® or Spine Welding®) uses ultrasonic energy to liquefy a polymer implant. The ultrasound vibrations rapidly melt the polymer at the bone interface (due to heat developed through friction (Langhoff *et al.*, 2009)) and with a downward force applied to the implant it forces the melted polymer into the pores of the cancellous bone.

The current sonic fusion surgical procedure follows these steps:

1) The surgeon firsts taps a hole with a small clearance of approximately 0.05mm diametrically

2) The pin is attached to an end of a sonotrode (a tool that creates ultrasonic vibrations), and while applying minimal downward force (approximately 10 N), an active ultrasound signal allows the pin to be driven into the cancellous bone

3) Contact between the pin and bone creates shearing forces under ultrasonic vibrations (Langhoff *et al.*, 2009), causing the pin to liquefy (reaching temperatures up to 180°C) and infiltrate into the voids of the cancellous bone, forcing out the marrow in the pore space

4) The thermoplastic cools within a few seconds, solidifying and creating a steady fix that can be immediately loaded.

6.3   Simulating a complete CT model

The first approach to model a sonic fusion device was to scan an implant within a piece of bone. To simulate the complete CT model, with both the geometry of the bone and the pin being derived from a single scan an implant was inserted using the standard method in the laboratory before being scanned. The bone used was a piece of ovine tibia from the proximal end; the bone was washed out

with an ultrasonic bath to remove any marrow. It was necessary to remove the marrow as it added complexity when trying to distinguish between it and the polymer in the CT scan. This is because the polymer and marrow have a similar density range, making it hard to distinguish between them. As it was a feasibility study, animal bone was used instead of human to simplify the process. PU foam would have been another option. It is frequently used in labs to test pins but it would be difficult to distinguish from the implant in the CT images, and for open pore foam the pore size is too large.
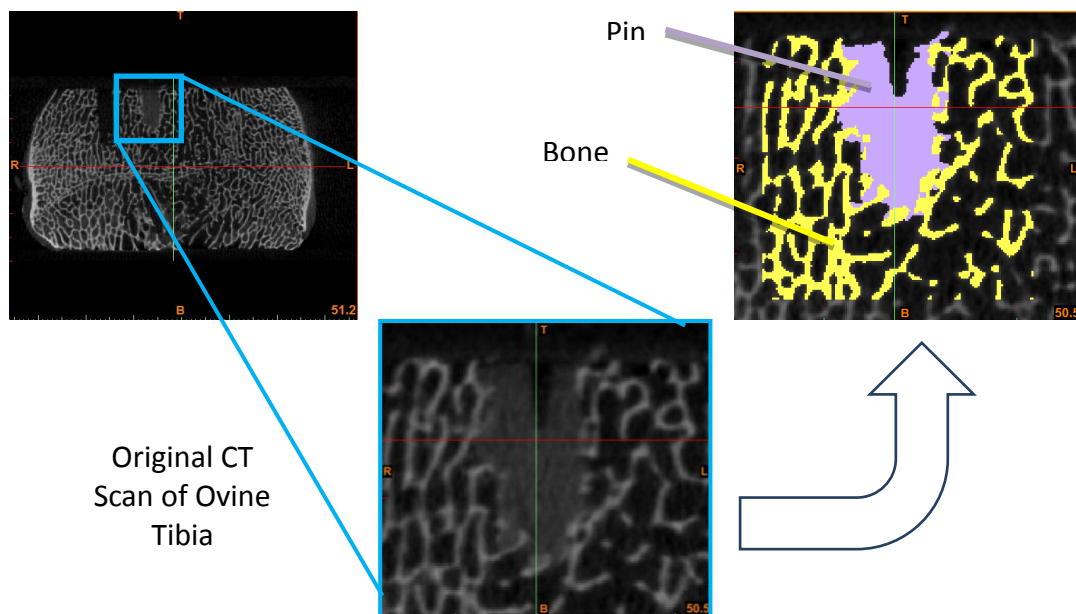
Figure 6-1: Thresholding operation to determine pin and bone geometry

Figure 6-1 shows the thresholding process, the top-left image is a slice through on the sagittal plane, the bottom imaged is a zoomed in area showing the melted polymer pin. The pin can be distinguished from the bone in the bottom image but the actual pixels used are highlighted in the top-right image. The indent at the top of the pin is left from the sonotrode tip. Thresholding the bone was straight forward due to its relatively high and known density but thresholding the pin required more finesse. The range of densities for polymers varies and there was no set standard to use. Therefore the thresholding process had to be done visually rather than with known Hounsfield units.
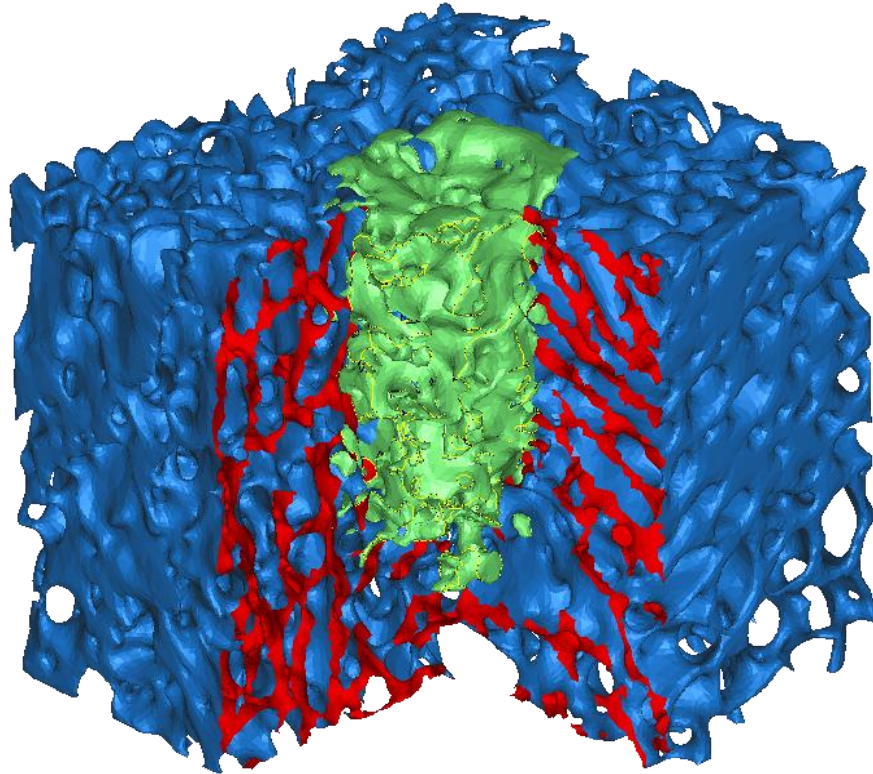
Figure 6-2: Final 3D surface model of pixels used in the final model (approximate size of bone is 10mm x 10mm x 10mm)

The BV/TV value for this animal bone is 27% which is above the value of interest for osteopenic studies, as it is of sufficient apparent density to produce a reliably good holding power. This is the highest apparent density bone which was studied throughout the project. Clearly there was no opportunity to simulate erosion of the bone as this would remove the contact between the pin and the bone.

Figure 6-2 shows the completed 3d model with a quarter cut-out, the melted pin is shown in green and the bone in blue (the red is the internal bone surface on display where it has been sectioned to show the pin). From the shape of the pin, it can clearly be seen that it moulded around and into the bone.

As this piece of bone contained no marrow it is thought that there is slightly deeper penetration of polymer into the bone compared to living bone. An

argument could be made to wash out the marrow post implantation. However it was feared that this may affect the geometry of the implant as the lavage process involved the bone being placed in a heated water bath and ultrasonically cleaned.

6.4 Material Testing

The material used for this particular sonic fusion is Poly(L-lactide-co-D,L-lactide), also known by its trade name Resomer LR706S and under the acronym PLDLLA but more commonly by the shorter umbrella acronym PLA. Limited mechanical data was available on the polymer so it had to be mechanically tested. At first testing showed the material to be more brittle than expected, with failure occurring at low displacement. It was then realised that it needed to be heated to see the similar properties observed post-melt.
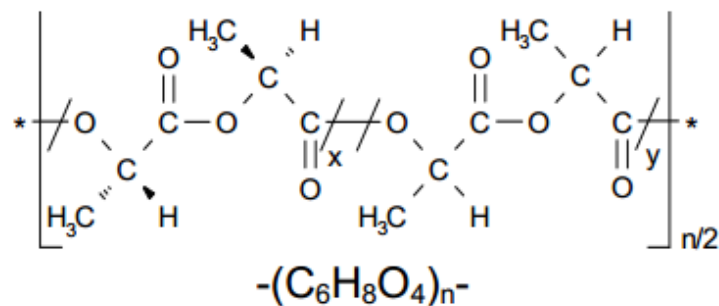
Figure 6-3: Chemical formula for a unit of Poly(L-lactide-co-D,L-lactide)

Under *in vitro* conditions temperatures of approximately 180°C have been reached. Although these temperatures are high, due to rapid cooling of the material only a 7-8°C transient rise is observed (Langhoff *et al.*, 2009) which is on the 45°C threshold for bone tissue injury (Li *et al.*, 1999). 180°C can be considered the peak temperature reached, and in reality most of the polymer does not reach above 100°C. Therefore, the PLA pins were heated to between 65-70°C and then cooled to obtain the material properties observed post melt. The PLA pins were wrapped in a polymer sheet with a much higher melting point to ensure it kept a similar geometric shape. They were then placed in an oven for two minutes at 65-70°C. Figure 6-4 shows the difference between testing the

samples as received and testing once they had been heated and then cooled. The bottom pin is as received, second from bottom was tested as received and the top two samples have been heated then tested. The top sample was tested until failure.
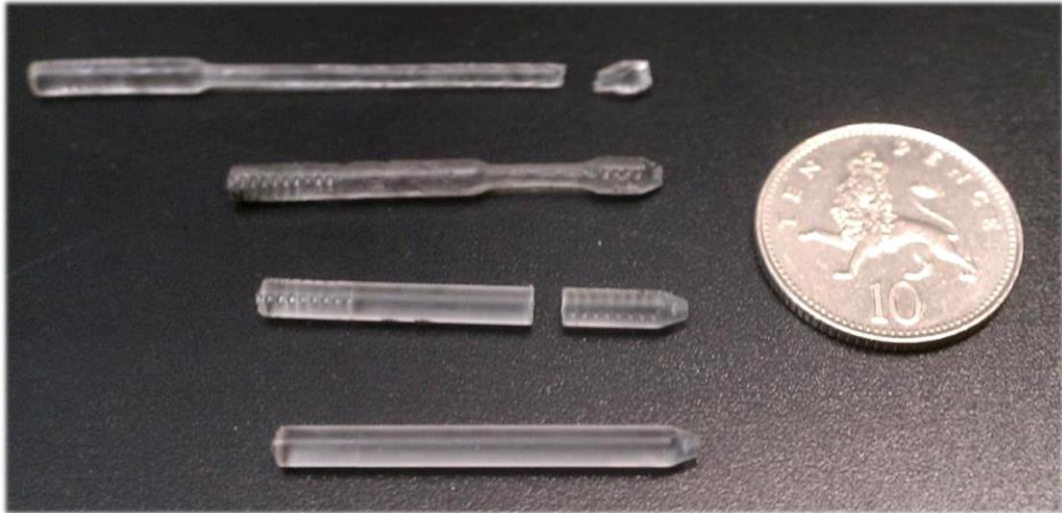
Figure 6-4: Top two samples heated to 65-70°C and then cooled, bottom two samples were tested as received (coin diameter is 24.5mm)

Figure 6-5 shows a sample being tested in the jaws of a hydraulic Instron® machine. This was a uni-axial tensile test carried out at a slow rate of 1mm/min. Figure 6-4 shows the untreated pin behaved in a brittle manner, whilst the heated samples exhibited very plastic behaviour. The heated samples had similar maximum loads and similar elastic moduli, but much higher maximum tensile strain: 1 mm/mm vs. 30 mm/mm.

Figure 6-5: Material test on the polymer used, the sample being tested has been heated then cooled

Once the data-logger had recorded (Figure 6-6) the stress/strain plot for the test, the mechanical results from the testing could then be input into Ansys. This provided a more realistic material model for the pin. This test was repeated three times.

Figure 6-6: Stress vs. Strain plot of the Polymer

Stress vs. Strain Plot of PLA Test
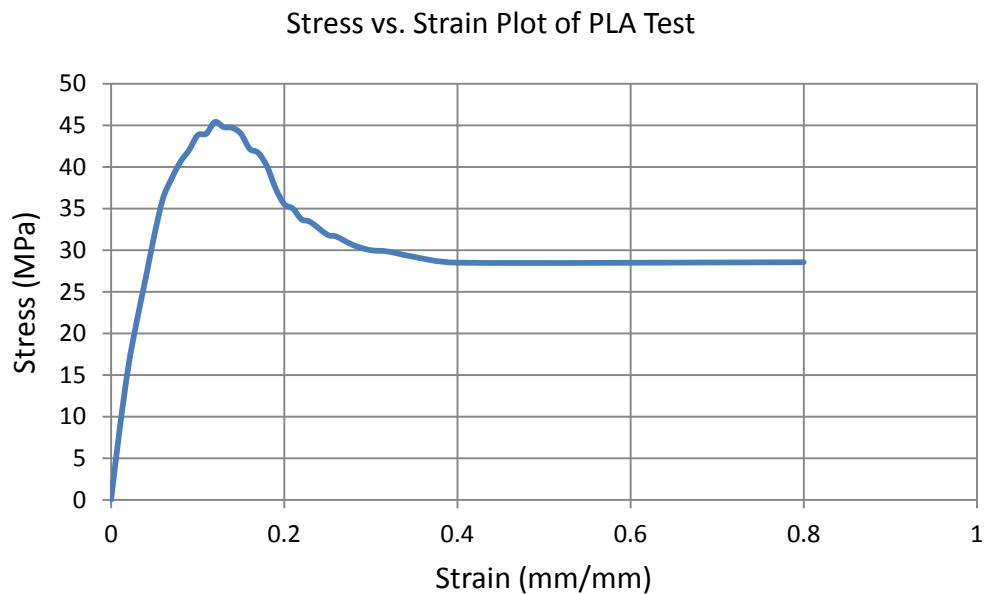
The above plot does not take into account the reduction in cross sectional area (necking) as can be seen in Figure 6-4. If it was adjusted to show true stress (instantaneous load acting on the instantaneous cross-sectional area), then the value of true stress would increase further as the reduction in cross-sectional area would be taken into account.

6.5 Simulation

6.5.1 Material Properties

The bone elements have the following material properties: Young's Modulus = 17GPa, Poisson's Ratio = 0.3, yield strength = 100MPa, and ultimate strength = 120MPa. The values chosen fall within a range of measured values given in the literature for "normal" bone (Rincon Kohli, 2003). The mechanical test data in Figure 6-6 was used for the PLDLLA elements

6.5.2 Contact

The interface between the bone and anchor is a frictional contact. Previous experience (Brown *et al.*, 2013) has shown the results to be more appropriate to physical studies when compared to the alternative bonded model. This is because under bonded contact no contact shear stress or sliding occurs between the surfaces, resulting in a significantly stiffer structure. Although bonded contact has been observed with this material and process this is under dry conditions. Under conditions with moisture present there will be minimal bonding.

6.5.3 Loading

The constraints applied were similar to the spiral anchor model, with the four vertical sides of the bone restrained. In this denser bone there is an argument to also restrain the base of the model as converse to the lower density human bone there is sufficient cancellous bone to select as a restraint. However, for consistency only the four vertical sides were restrained in this case. In practice a suture loop would be placed round the top of the pin, to simulate this, the top 0.5 mm of the pin's nodes was selected and a 0.2 mm displacement was applied vertically upwards. Again a frictional contact of 0.6 (Grant *et al.*, 2007) and pure penalty formulation was used.

6.5.4 Results

Figure 6-7 shows the deformation of the bone, looking at the scale it can be seen that this is generally less than observed for a titanium anchor. Additionally it can

be seen there is a uniform deformation which decreases evenly from the centre, this can be observed to some extent with a threaded anchor but there is frequently concentrated deformation to a trabecular or in cancellous bone some "peeling". This lower deformation is of benefit of the patient as it implies lower peak stresses will occur.

D: f2
Total Deformation 2
Type: Total Deformation
Unit: mm
Time: 1
06/12/2013 16:17

0.031699 Max
0.028177
0.024655
0.021133
0.017611
0.014088
0.010566
0.0070442
0.0035221
0 Min

0.000   3.000   6.000 (mm)
    1.500   4.500
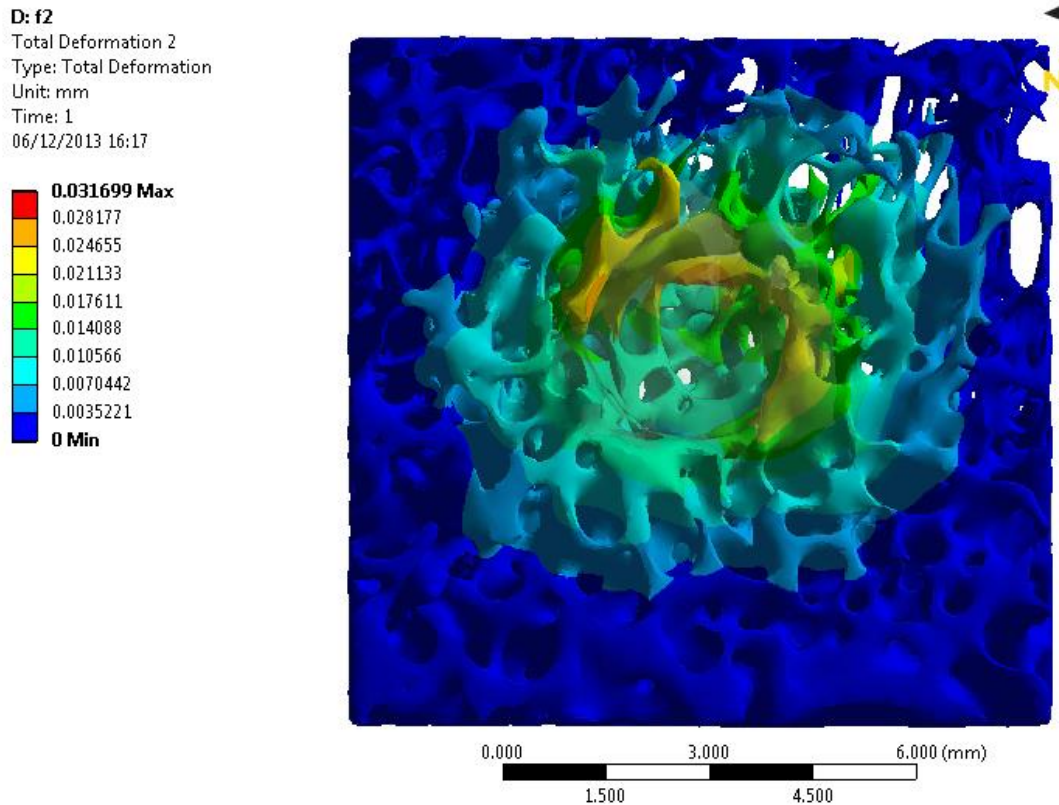
Figure 6-7: Total Deformation of the cancellous bone

Figure 6-8 shows the total deformation of the pin, there is large deformation at the top which decreases further down the material. This is different to what is observed in a titanium anchor which has a uniform deformation due to its higher stiffness. The pin's maximum deformation is larger than the bone's deformation; this is expected due to the difference in stiffness of the two materials.

D: f2
Total Deformation
Type: Total Deformation
Unit: mm
Time: 1
06/12/2013 16:20

0.20518 Max
0.18238
0.15959
0.13679
0.11399
0.091191
0.068394
0.045596
0.022798
0 Min

0.000   2.500   5.000 (mm)
     1.250   3.750
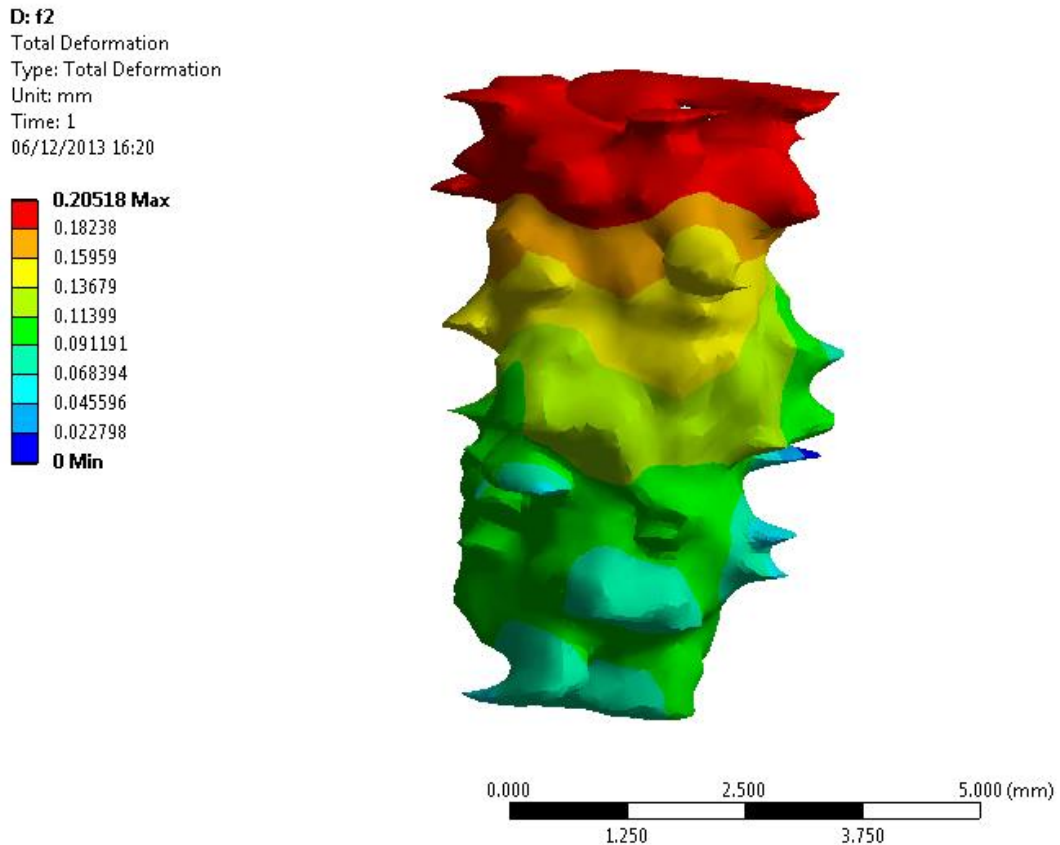
Figure 6-8: Total deformation of the CT model polymer pin

The reaction force for this test was 254 N, which is in the order of what is expected in the laboratory - As this is a new technology there is no current literature on pull-out on this particular pin but preliminary tests at Stryker (the project sponsors) have be carried out and generally produce results within a 200-350 N range.

6.5.5 Discussion

As has been described this is an intricate process involving specialist equipment, making it not readily accessible for many researchers. It was an exploration of what was possible to achieve the most accurate model of sonic fusion - with the resources available. It has produced interesting results and given insight into the sonic fusion and modelling processes, revealing the many considerations that must be taken into account. It has shown that in sonic fusion the pin is under greater deformation than the bone, whereas with a titanium implant the bone

and implant are under similar deformation and therefore the bone is under greater stress. This is of benefit to patients with weaker bone as it is less likely damage will occur to bone if high loads are applied.

6.6 Additional Studies Considered: Use of Fluid Dynamics

After researching into a full CT scan model and deciding it was an excessively time intensive process to pursue for the project, the next simulation option was to look into simulating the melt stage using computational fluid dynamics (CFD). CFD is a numerical method used to analyse the flow of fluid under certain boundary conditions. If the direction of flow of the pin as it melts could be determined then this would be incredibly useful not to just to model stress and displacement but also to determine the resultant geometry that will be produced. Observing the change in the final pin shape after looking at bone, pin and drill geometry could prove extremely useful and provide answers to questions that are very difficult to observe in the laboratory. Factors such as the effect of changing the suture position, pin geometry, or even the force applied to the pin could be considered. If an ideal distribution of polymer could be found, it would be possible to work backwards and find the mechanism best to distribute the polymer to an ideal shape. Exploring distribution possibilities with simulation is often more efficient and less limited in many aspects. In this case for example distributions could be imagined that would not be physically possibly to create with a current design process.

The first step towards this process was producing a simplified model of the process. Figure 6-9 shows the geometry used. The view shown is cross-sectional and the model is three dimensional. The pin is shown in purple and is a cylinder with a 0.2mm diameter. The porous region of the "bone" is shown in yellow with a central horizontal cylinder acting as the drilled hole, with three vertical cylinders either side acting as pores. A suitable dynamic viscosity (1.0 Pa·s) was applied to the polymer with just gravity acting as a force. The pores were set as

air with the end of each of the six horizontal cylinders having an outlet to provide minimal resistance to the polymer flow.

The software used for this process was COMSOL®, which allows simulation of multi-physics models. This meant the changing properties could be observed during flow and then a load could be applied to the post melt geometry to observe the stresses and strains of loading.
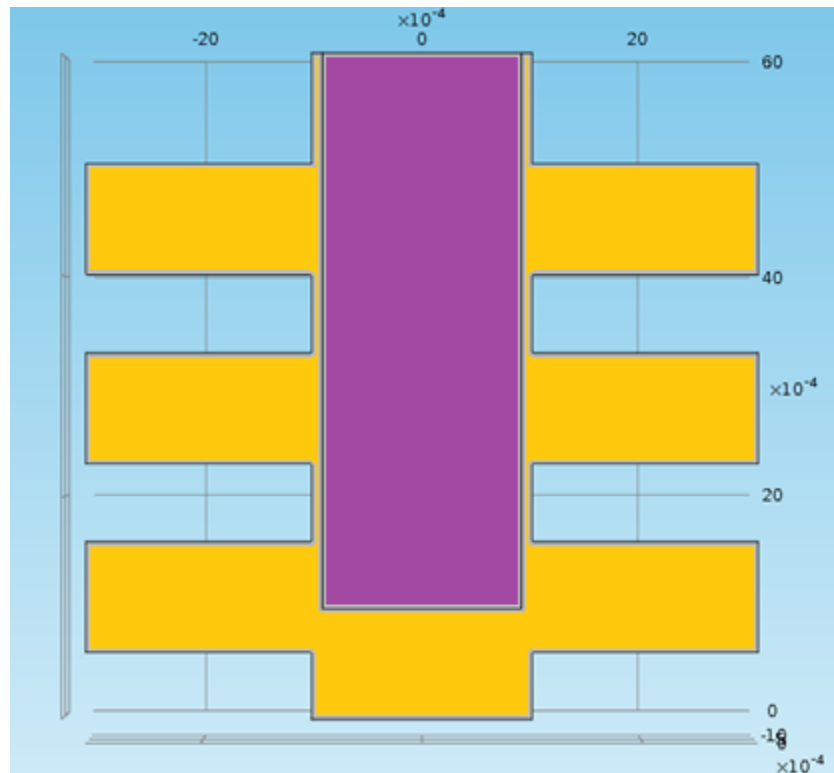
Figure 6-9: A cross-sectional view of the simplified model to simulate pin melt, the pin is shown in purple and the pores of the bone are in yellow. Dimensions are in meters

Unfortunately this process proved impossible with the computing power available. Simplified simulations were solved but required significant processing power and time to solve – meaning that complex solutions with CT bone geometry would not be possible to solve. Hopefully in the future as hardware and software improves this option will become viable and lead to a greater understanding of how the polymer flows into the bone. The same software could also be used to determine how cement or other types of augmentation can be

inserted. For example, how cement flows through different needle heads and its final distribution.

After investigating flow simulation and concluding with current accessible technology it was not feasible, the use of computer-created pin models was used to investigate sonic fusion. This was done by changing the geometry and location of the pin.

6.7   Computer Generated Pin Models

After exploring the paths described, the next option is to simplify the geometry of the pin. This approach retains all the bone geometry but allows the user to define the pin shape. Figure 6-10 shows three views of a concept model.
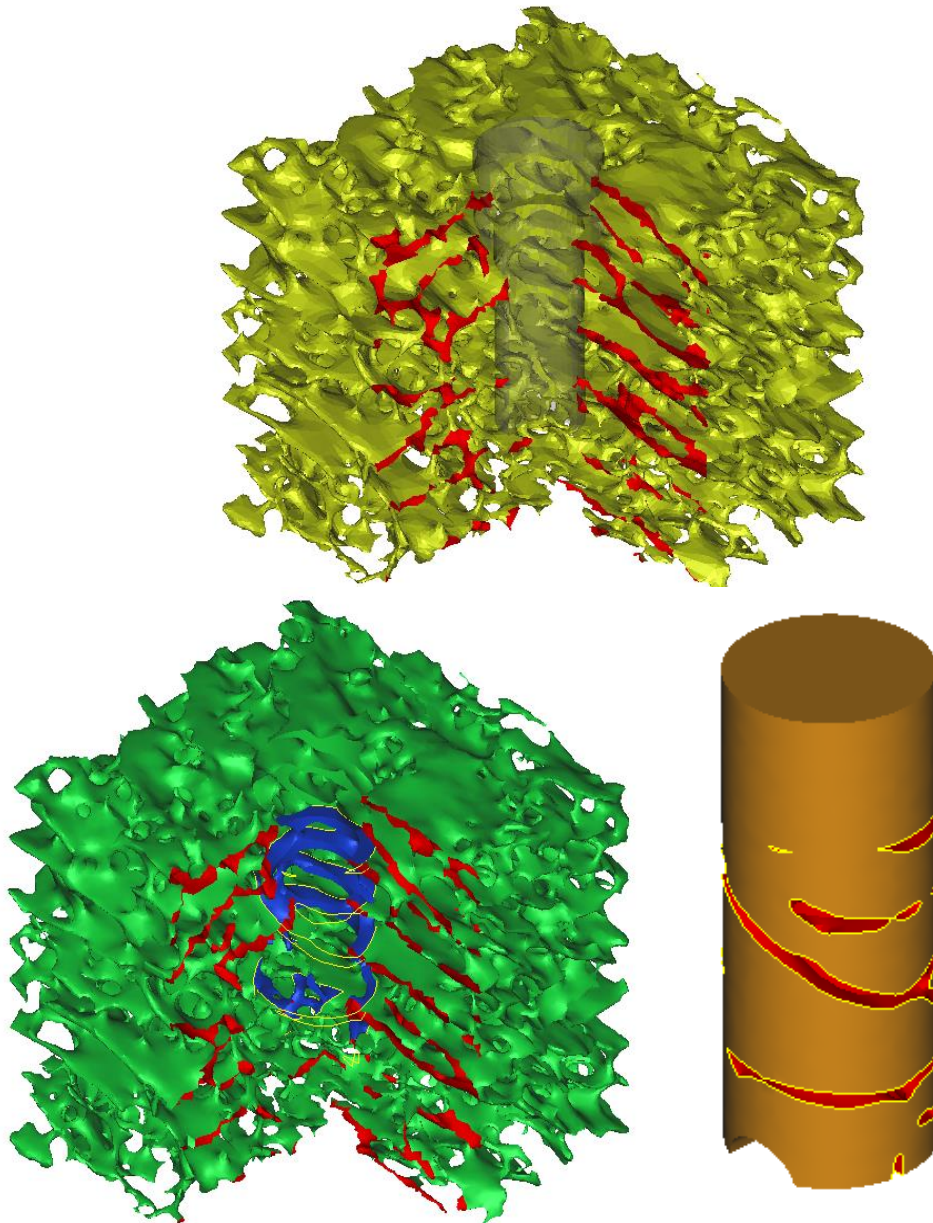
Figure 6-10: 3 views of a concept model: Top shows the drill cut out of the bone; bottom left is the final bone with the surface in contact shown in blue; bottom right is the pin, with the red surface showing the surface in contact. The red area in the bone is simply the internal surface.

Although the term simplified here is used, it does not mean it was a simple process. It was in fact more complex to model than threaded anchor models. It required an additional stage and more intensive manual meshing.

For normal threaded anchor models once the bone had been tessellated to a desired standard there was only one modelling stage left – to insert the anchor into the bone with a Boolean operation. However, in sonically melted models a pre-drill volume had to be removed from the bone (Figure 6-10 – Top), although in practice a hole is often drilled or tapped for anchors/screws it was not necessary to model this as the anchor would always end up overlapping the pre-insertion volume. However with the sonic-fusion the bone had to be removed first as the sonic-fusion process does not eradicate any bone – although may remove some marrow. The next stage of modelling is to insert the pin and perform a negative Boolean operation on it to remove the volume which the bone intersects - rather than remove the bone, which is the case for threaded implants. Figure 6-10 – Bottom Right shows the final "melted" pin geometry with bone volume removed.
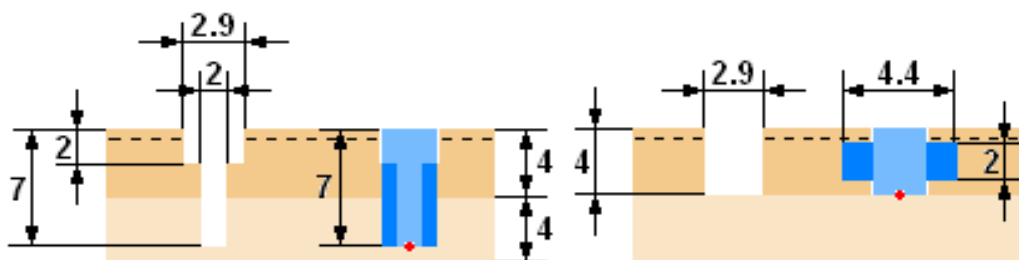
Figure 6-11: Comparing two different polymer distributions .The light blue area is the pre-drill volume, whilst the entire blue area is the volume that the polymer fills. All dimensions are in mm.

Figure 6-11 shows two pin geometries to be compared, the light blue area is the pre-drill volume and the entire blue area is the pin volume. Penetration of the polymer is primarily dependent on the bone geometry. Its final shape can be

manipulated by changing the bone geometry via drilling but it may also be adjusted from the ultrasound energy applied. The final melted geometry will also depend on the initial pin design. Features such as a taper or split may alter the flow of the melt. Figure 6-11 – Left shows Concept A with deep vertical penetration into the bone but less horizontal, whilst Figure 6-11 – Right shows Concept B with deep horizontal penetration into the bone with no vertical penetration. Figure 6-11 – Left shows the dimensions used for the model in Figure 6-10. Concepts were created, depending on how high the possibility of them actually being formed was. Barrel shaped concepts were also modelled initially but it was decided that this would be too difficult to consistently reproduce in a laboratory, let alone in a surgical procedure. Therefore only concepts with clear geometrical distinctions were modelled as shown in Figure 6-11.
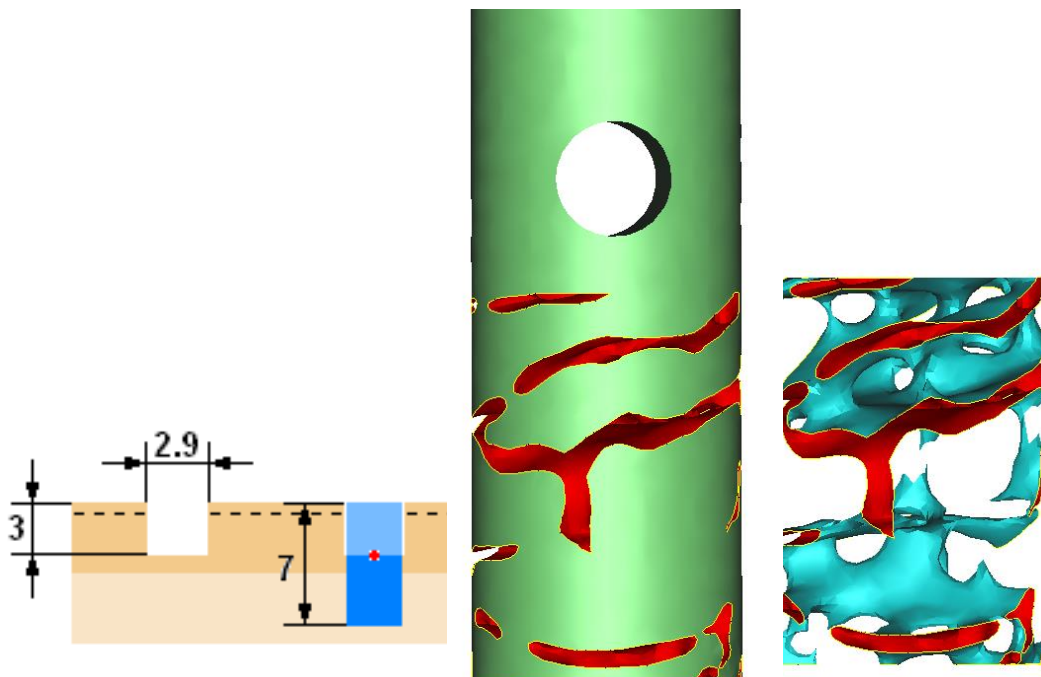
Figure 6-12: An unused concept, left shows the dimensions to be used for the drill and melted model, middle shows the modelled "melted" pin and right shows the contact surface. All dimensions are in mm.

Other concepts were also created and modelled but were discounted once evalutaed. Figure 6-12 shows a concept which has a shallow drill depth but a deep vertical penetration of the polymer. This was not simulated in FEA due to its unrealstic "melted" geomtry. The left image shows the dimensions for the drill and pin, the drill depth is shallow but there is an aim for deep penetration for the pin. The middle image shows the final pin geometry once melted, and the right image shows the surface in contact with the bone. In the right image it can be seen that towards the top there is a large trabecular plate which would inhibit the polymer flowing through to the concept depth. Therefore this and other concepts which were not believable were discounted and only concepts with suffcent pre-drilling could be used.

6.7.1 Study Parameters

The purpose of this study was to initially check if the concept procedure worked and additionally to compare concepts. If successful this process could then be used for further studies.

6.7.1.1 Material Properties

In this study the elastic and strength properties used for bone elements (Turner *et al.*, 1999) and PLDLLA are assumed to be the same in tension and compression. The bone elements have Young's Modulus = 17GPa, Poisson's Ratio = 0.3, yield strength = 100MPa, and ultimate strength 120MPa. The material properties used for PLDLLA are Young's Modulus = 3 GPa and Poisson's Ratio = 0.3 (Black, 1992).

6.7.1.2 Loading

The elements of cancellous bone were fully restrained on the four vertical sides as with other studies.

For the pin a linear ramped displacement in the vertical upward direction of 0.2mm was applied to the base. Figure 6-11 shows the suture position in red, in this case it is located at the base for both. A semi-circular cut-out has been

applied to the base of each to simulate the suture bearing area, as can be seen in Figure 6-13.

6.7.1.3 Contact

The same contact settings were used as before. A bonded contact was considered but after trialling bonded contact first, it was decided to retain a frictional model. Bonded contact pulled additional trabeculae upwards, particularly any attached to the base of the pin. This was not considered realistic, as well as not being consistent with other models.

6.7.2 Results: Comparison of Two Concepts

The pin models – Concept A and Concept B from Figure 6-11 were simulated and compared.

Figure 6-13 shows the total deformation in Concept A. It can be seen that most of the deformation occurs around the suture point and it decreases further away from this suture point. This same pattern of deformation around the suture point can also be seen in Figure 6-14; the total deformation of Concept B.
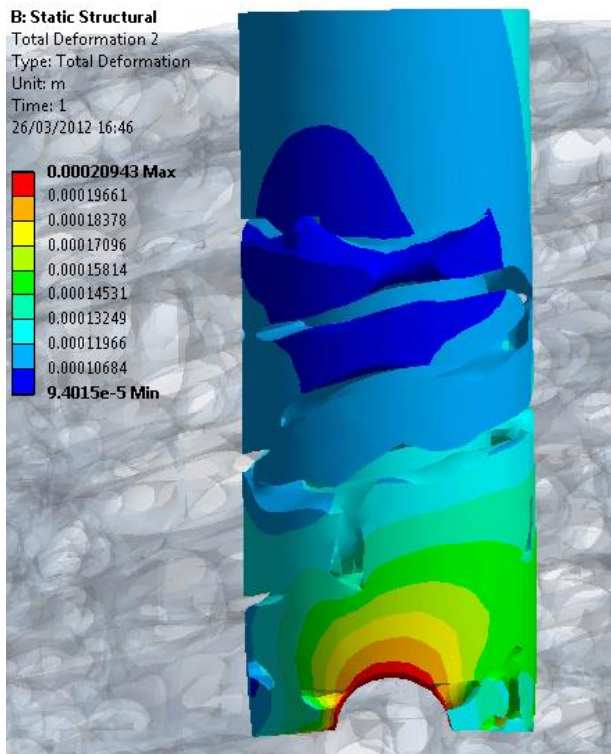
The deformation in Concept A is as generally expected, with the least deformation occurring where there is a secure contact with the bone.

Figure 6-13: Total Deformation of Concept A

Observing the deformation in Concept B reveals good engagement with the bone where it is engaged around the central flange. However, it also reveals the material's lack of stiffness compared to a metal anchor. It can be seen that the central cylinder begins to extrude through the outer flange which is being held securely by the bone. This could be a possible weakness, especially if plastic deformation begins to occur.
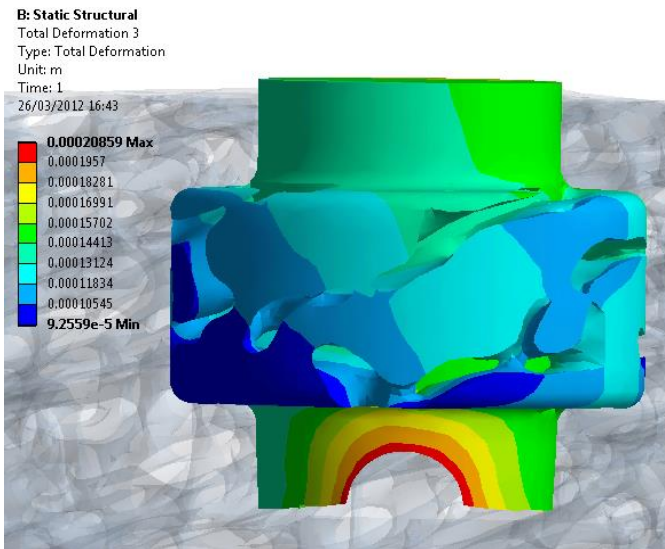
Figure 6-14: Total Deformation of Concept B
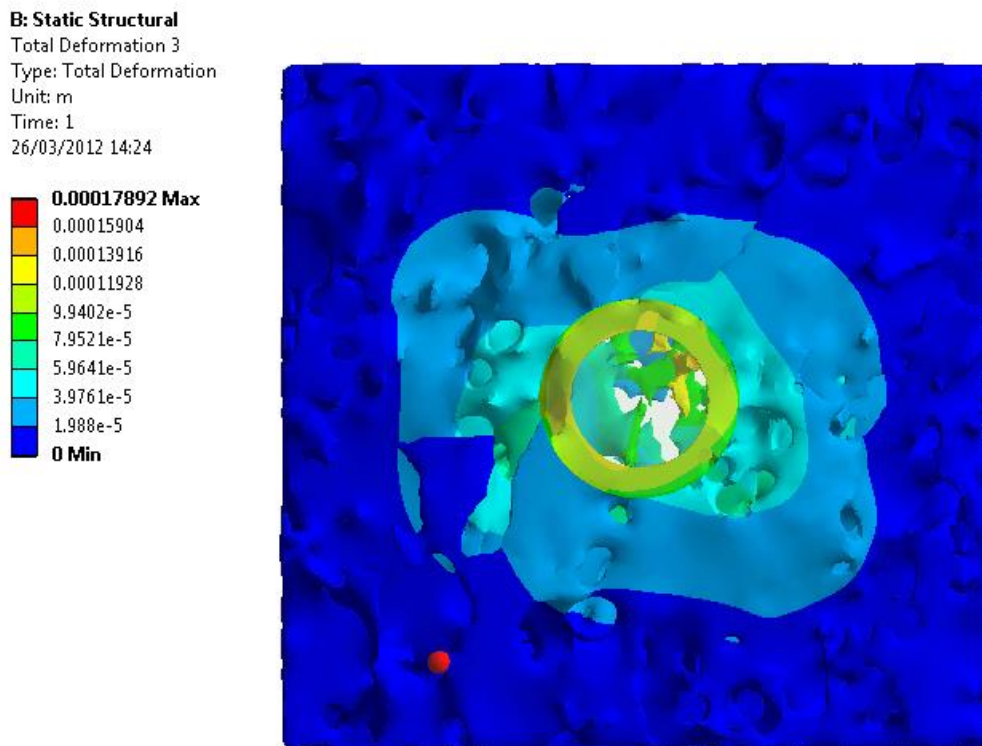
Figure 6-15: Total Deformation of the cancellous bone for Concept A, Top View

B: Static Structural
Total Deformation 2
Type: Total Deformation
Unit: m
Time: 1
26/03/2012 14:25

0.00017186 Max
0.00015276
0.00013367
0.00011457
9.5478e-5
7.6382e-5
5.7287e-5
3.8191e-5
1.9096e-5
0 Min
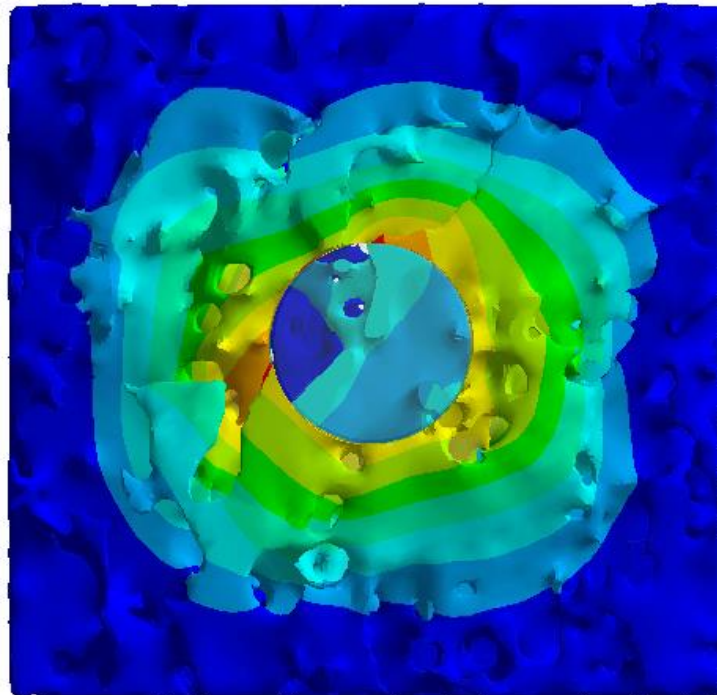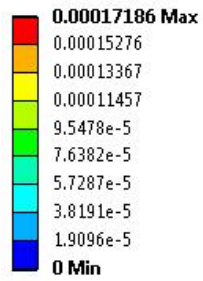
Figure 6-16: Total Deformation of the cancellous bone for Concept B, Top View

B: Static Structural
Total Deformation 3
Type: Total Deformation
Unit: m
Time: 1
26/03/2012 14:32

0.00017892 Max
0.00015904
0.00013916
0.00011928
9.9402e-5
7.9521e-5
5.9641e-5
3.9761e-5
1.988e-5
0 Min
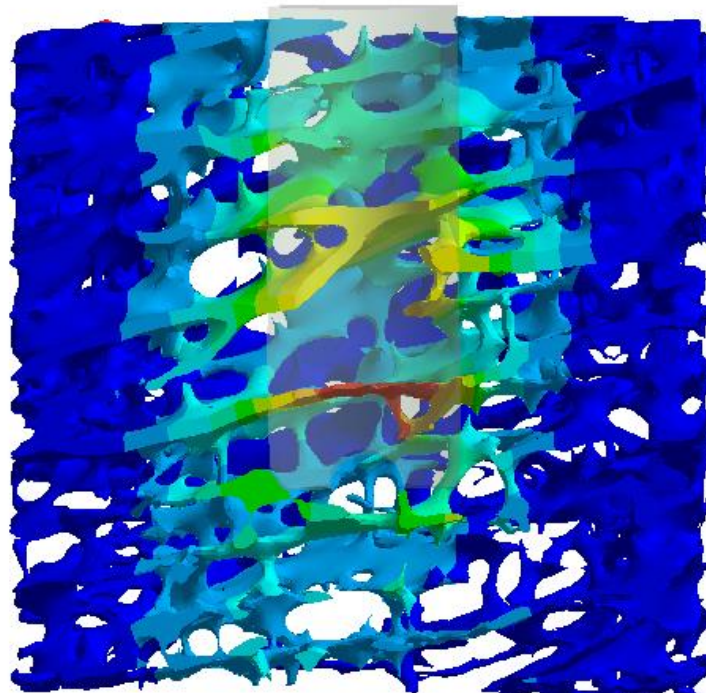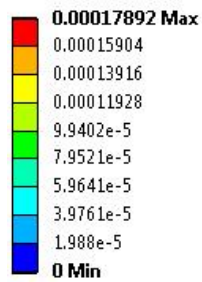
Figure 6-17: Total Deformation of the cancellous bone for Concept A, Side Cross Section View
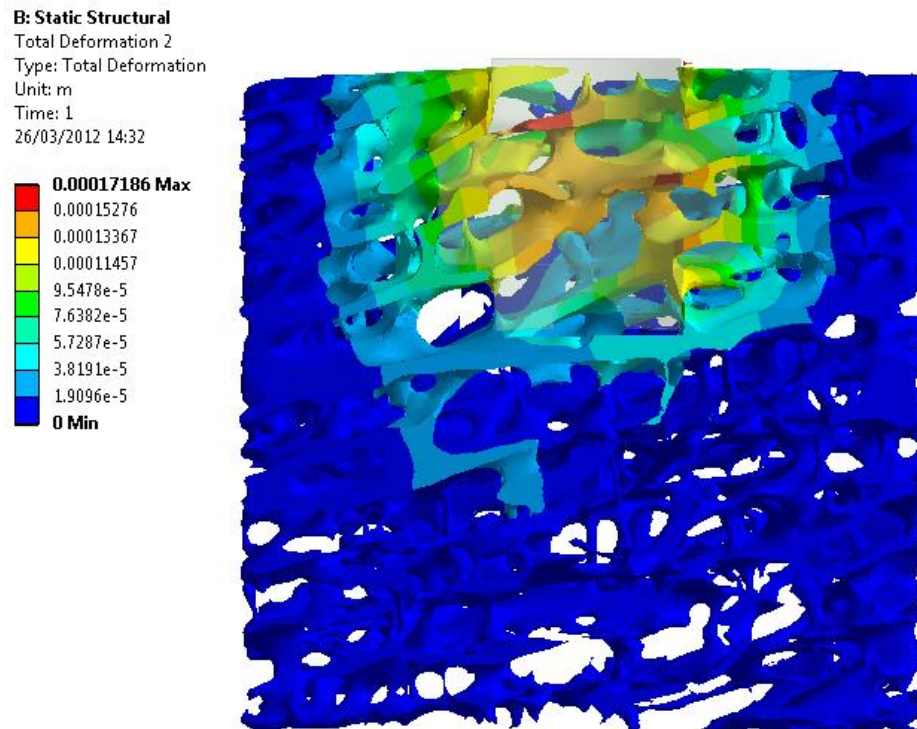
Figure 6-18: Total Deformation of the cancellous bone for Concept B, Side Cross Section View

Figure 6-15 and Figure 6-16 compare the deformation of the bone from above, whilst Figure 6-17 and Figure 6-18 compare the deformation of the bone in the central cross section. It can be seen that Concept A is loaded through the full depth of the bone (Figure 6-17) and in Concept B only the upper, higher apparent density half of the bone is under load. Comparing reaction forces, Concept B has a slightly higher reaction force of 629 N over Concept A's 610 N reaction force. It can be said that neither design has a clear advantage over the other in this case, although the slight extrusion of the central cylinder of concept B seen in Figure 6-14 is an undesirable quality.

6.7.3 Comparison to Threaded Anchors

After comparing concepts it was of interest to compare the method of pin loading to anchor loading. Figure 6-19 shows the maximum principal stress of the cancellous bone under loading from Concept B, and Figure 6-20 shows the maximum principal stress of the cancellous bone under a titanium anchor. It can be observed that the trabecular struts are under tensile loading when the

polymer is used as an anchor, with minimal stress-loading to the trabecular plates.
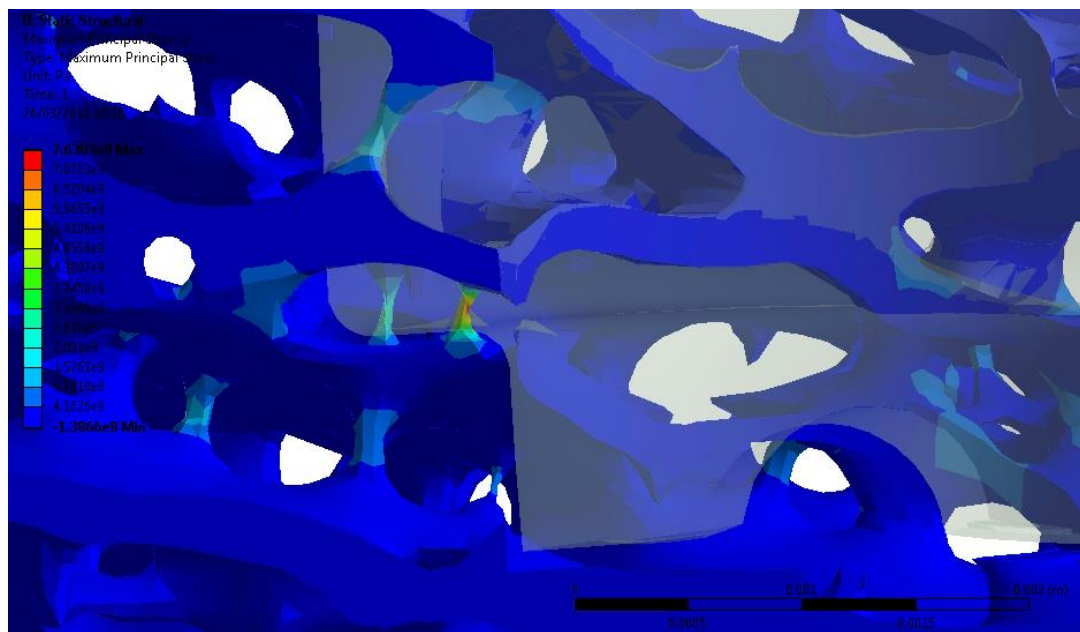
Figure 6-19: Maximum Principal Stress in the cancellous bone under load with a polymer pin

The stress distribution under a metal thread is very different to the stress seen under polymer; here the thread is causing stress (maximum principal stress observed) wherever it is contact with the bone (Figure 6-20), resulting in bone being under a higher total stress than with a polymer pin. The bone also deforms less for the same displacement when attached to the pin, this is likely due to the softer and less rigid properties of PLA.

Figure 6-20: Maximum Principal Stress in the cancellous bone under load with a titanium anchor

Comparing the vertical reaction force for the same displacement, the value for the anchor is 643 N and for the rotated anchor study the value is 677 N compared to 610 N and 629 N for the two concept pins. Although less than the threaded anchor, it is of comparable strength, meaning that with a good engagement with the bone this technology is of suitable stiffness.

6.8   Discussion

Currently the most suitable method to do was to use computer generated geometry to investigate the various designs and approaches. By industrialising the CT process the time between pin insertion and simulation could be greatly reduced, although there would still be the bottle-neck of thresholding and meshing by hand. However, although important to model behaviour of the physical world, in reality this process is of interest but is of less practical use, as the whole physical testing procedure must be carried out in any case to create a computer model. Creating computer models of the pin is still labour intensive but it has produced the most useful and interesting results.

As software and hardware becomes more powerful the application of CFD would certainly be useful in this area of polymer study and other areas such as cement or even drug distribution from implant coatings. If it could be made to work efficiently it would greatly reduce the time and intricacy involved in the laboratory to test and measure these properties.

6.9   Conclusions

Different methods of modelling sonic fusion geometries and their results have been explored, discussed and evaluated. The study has revealed the difficulty of modelling sonic fusion geometry over threaded implants but has shown it is possible. It can be concluded that using computer generated models is the most efficient way to currently model and evaluate the geometries, although there is naturally some difference between a model produced from a CT scan and a computer generated model. This difference arises because a better engagement or deeper penetration can be modelled using CAD. The CT generated model aligns with what has been found with preliminary laboratory results, indicating that the FEA model has been accurately produced.

The study has shown that if good engagement is made with bone, as in the case of both concepts then sonic fusion can produce a good holding power comparable with the holding power of a threaded anchor. Although less stiff than a threaded metal anchor, it is of sufficient strength and with the additional benefit of undergoing resorption.

This chapter has also presented a brief insight into the future of modelling this technology and explained how CFD could be of fundamental use to this technology and others.

7 Sonic Fusion Comparison with a Predicate Device

7.1 Introduction

This chapter continues examines the efficacy of sonic fusion by comparing it to a predicate device. A predicate device is used in the medical industry when a new device is to be introduced into the market. A new device must have the same intended use as the predicate as well as having either the same technological aspects, or different technological aspects which do not raise new questions of safety and effectiveness (FDA online, 2014). A predicate device is used to obtain a 510K Premarket Notification from the Federal Drug Administration (FDA), which is a key document for proving the device is safe and effective. Therefore comparing a device with a predicate is often a priority for research and development divisions of biomedical companies.

This chapter presents a study comparing a computer modelled sonic-fusion device against a device chosen as a predicate, a PLA threaded anchor. It also compares the sonic-fusion device against a threaded anchor of the equivalent thread length of the sonic-fusion pin.

7.2 Predicate Device

The predicate chosen in this case was the Bio Mini-Revo manufactured by CONMED (Figure 7-1). This device was selected as it has a similar volume compared to the sonic-fusion prototype model. It has a 3.1 mm diameter and a 5.0 mm thread length, it is also manufactured from PLA, and consequently has comparable material properties, i.e. similar strength and it is resorbable. It requires a 2.1 mm diameter tap before insertion, which is comparable to the sonic fusion model.

Figure 7-2 shows the dimensions for the sonic-fusion pin. It has 3.1 mm external diameter and a 2.1 pre-drill diameter, these dimensions were chosen as it is the same depth engagement as the predicate anchor. It has an engagement length of 2.5 mm, this is half of the thread length of the predicate anchor. Therefore an

additional anchor (Right, Figure 7-2) was modelled with the same 2.5 mm engagement/thread length as the sonic-fusion pin to see how this would compare. All models were created using the methods as described in the previous chapters.
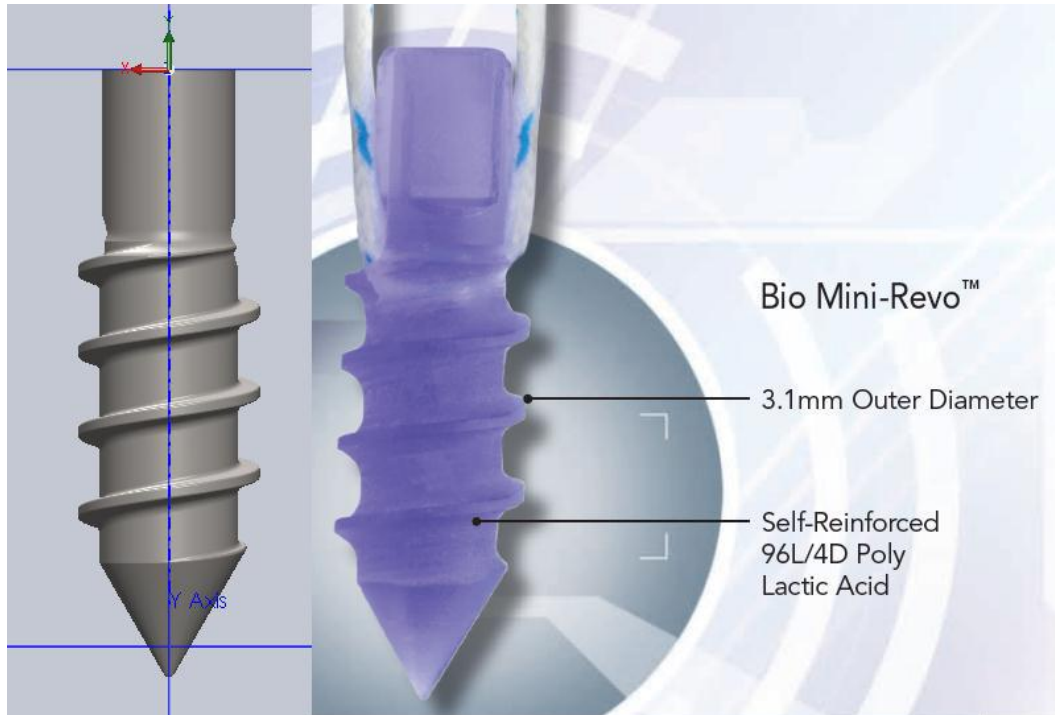
Figure 7-1: Image of the Bio Mini-Revo Device compared to the CAD model (CONMED)
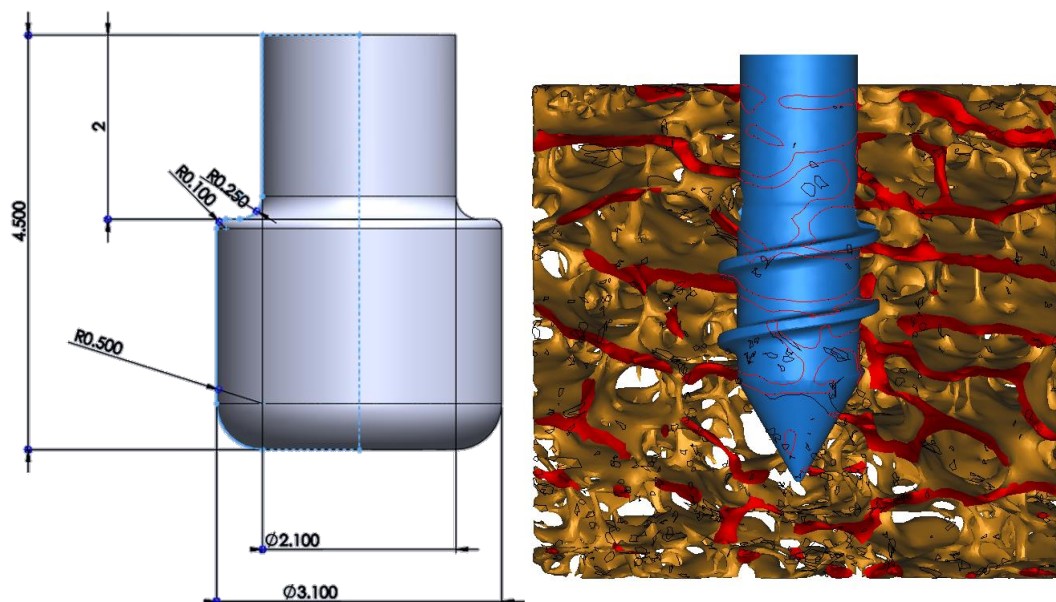
Figure 7-2: Left image shows the dimensions of the sonic pin, Right image shows the equivalent length predicate

7.3   Study

Rather than apply a displacement at different angles the method for this test was to compare a vertical test at nine different locations in the bone. These locations were: central, +/- 0.5 mm from the centre in the x and y directions, and +/- 1.0 mm from the centre in the x and y directions as shown in Figure 7-3 (each circle represents a device location).
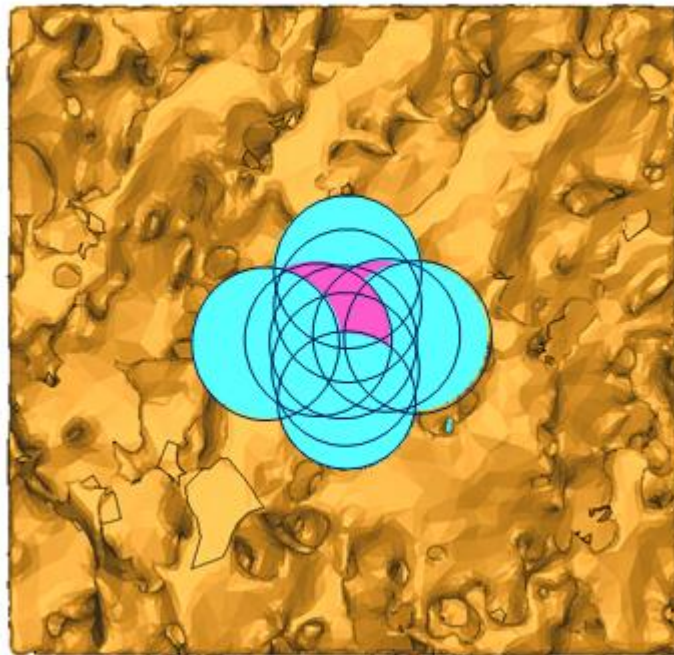
Figure 7-3: Top view of simulation showing the 9 locations

All three different test devices were placed in the same nine locations, and as they had the same engagement diameters they were effectively attached to the same trabecular plates and struts in each location, the only differences being the engagement depth and type of engagement. This made it a comparative study, and importantly something which could not be achieved testing in the labrotary in real or substitute bone.

Nine locations were originally conceived to give an idea of the mean pull-out of each device. It also gives an idea on the relationship with contact area and the change in reaction force at each position.

7.3.1 Material Properties and Contact

The bone used for the study was the same used as before. In this study the elastic and strength properties used for bone elements (Turner *et al.*, 1999) and PLDLLA are assumed to be the same in tension and compression. The bone elements have Young's Modulus = 17GPa, Poisson's Ratio = 0.3, yield strength = 100MPa, and ultimate strength 120MPa (Rincon Kohli, 2003). The material properties used for PLDLLA are Young's Modulus = 3GPa and Poisson's Ratio = 0.3 (Black, 1992). Only the higher apparent density bone was modelled for this simulation, as most devices are not certified for use in osteopenic bone.

The same contacts settings were used as previously given.

7.3.2 Loading

The elements of cancellous bone were fully restrained on the four vertical sides as with other studies. For all the devices a linear ramped displacement in the vertical upward direction of 0.2mm was applied to the top.

7.4 Results

The following plots compare the reaction force to contact area of the sonic fusion pin and the Bio Mini-revo predicate device (Table 7-1 & Table 7-2). They compare the contact area at each of the 9 locations for both devices and the equivalent length predicate device (Table 7-3).

Figure 7-4: Plot of Sonic Fusion Reaction Forces (N) vs Contact Area (mm^2)
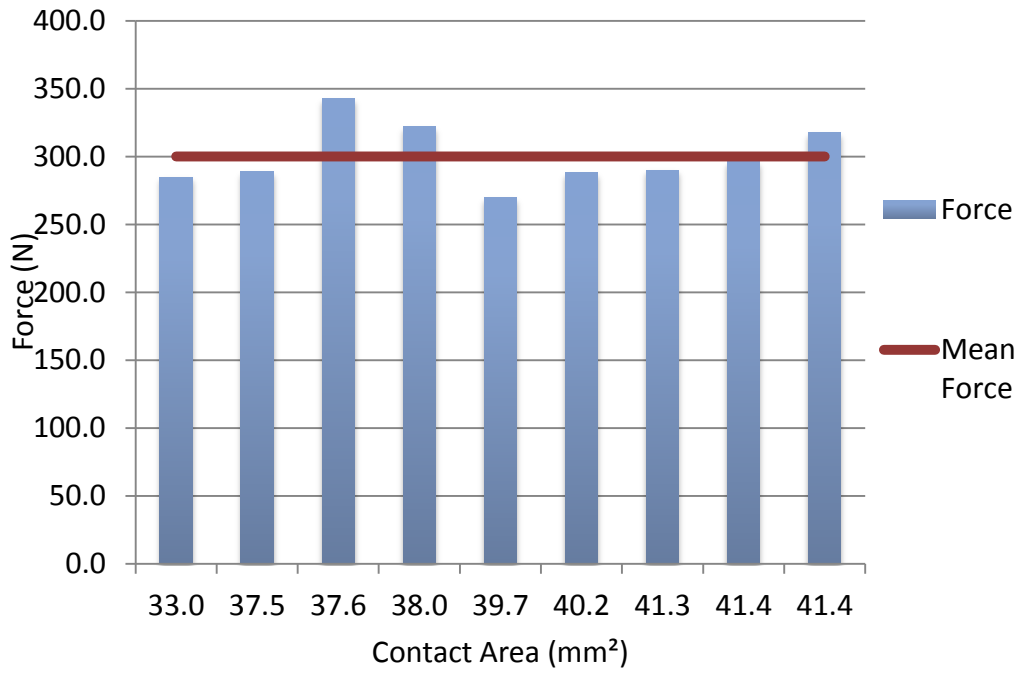
Figure 7-5: Plot of the Bio Mini-revo device Reaction Forces (N) vs Contact Area (mm^2)
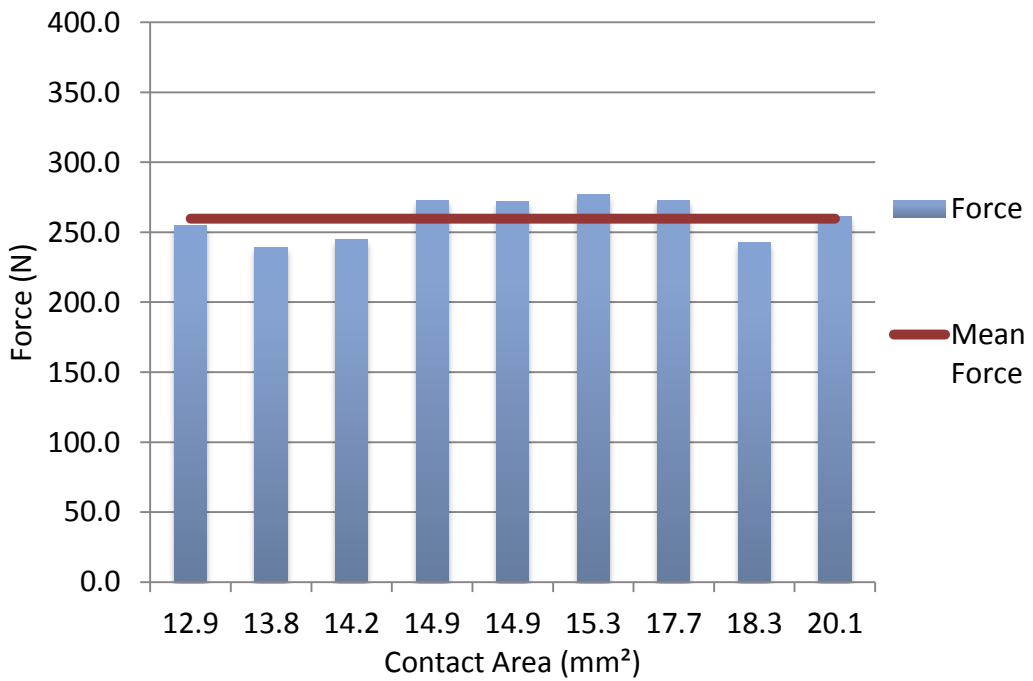
Table 7-1: Sonic-fusion reaction forces (N), positions, and contact areas (mm^2)

X Position (mm)	Y Position (mm)	Force (N)	Contact Area (mm²)
0	0	270.08	39.71
- 1	0	284.93	33.01
- 0.5	0	288.84	37.52
0.5	0	296.30	41.43
1	0	317.85	41.43
0	- 1	342.54	37.61
0	- 0.5	322.19	37.95
0	0.5	288.09	40.24
0	1	290.13	41.26
Mean		300.11	38.91
Standard Deviation		22.69	2.74

Table 7-2: Bio Mini-revo reaction forces (N), positions, and contact areas (mm^2)

X Position (mm)	Y Position (mm)	Force (N)	Contact Area (mm²)
0	0	254.84	14.93
- 1	0	239.27	14.94
- 0.5	0	244.83	13.83
0.5	0	272.70	18.33
1	0	272.18	20.10
0	- 1	277.30	17.70
0	- 0.5	272.40	15.31
0	0.5	242.70	14.20
0	1	261.16	12.94
Mean		259.71	15.81
Standard Deviation		14.79	2.37

Table 7-3: Equivalent length Bio Mini-revo reaction forces (N), positions, and contact areas (mm²)

X Position (mm)	Y Position (mm)	Force (N)	Contact Area (mm²)
0	0	47.7	12.82
- 1	0	25.0	10.54
- 0.5	0	Non-Compute	11.63
0.5	0	Non-Compute	14.92
1	0	10.7	15.36
0	- 1	Non-Compute	14.00
0	- 0.5	6.4	12.27
0	0.5	9.3	11.68
0	1	8.9	10.64
Mean		(17.96)	12.65
Standard Deviation		(15.98)	1.77

7.5 Discussion

From the results it can be seen the sonic fusion device has a greater mean pull-out force than the predicate device but interestingly it also has a larger standard deviation figure. The higher standard deviation in force was unexpected. It was hypothesised that the sonic fusion would produce a lower standard deviation due to encasing the cancellous bone rather having point contacts with it. Instead it appears that the idealised pin models may be more dependent on the local geometry. However, it should be reiterated that these are idealised geometry models and the complex shear force interactions (under ultrasonic melting) between the bone and polymer will result in different localised geometry.

It can be seen that the sonic-fusion pin has a contact area approximately twice that of the mini-revo device (Table 7-1 & Table 7-2). In this case there is no obvious relationship between reaction force and contact area. This is generally accepted for screws but it indicates there is no clear relationship between sonic fusion devices and contact area either.

For the equivalent length predicate the results (Table 7-3) show a significantly lower reaction force. This is unexpected, as a linear relationship is accepted for thread length vs. shear failure force (Chapman *et al.*, 1996). In all except two

cases the shortened predicate device did not produce any mentionable holding power. Even though the models did not have significantly less contact area, they produced a small fraction of the threaded anchor with twice the thread length. Although some of the contact area is not providing any holding power e.g. the tip of the anchor.

In the results it appears as if there is a required connection length for a thread in a spicular structure. If the device is too short, it will just fall out. This may not be true for all threads. This thread has a relatively low thread depth (distance between inner and outer thread radius), and an anchor with a greater thread depth may produce a linear relationship as expected. However, it shows for these thread dimensions a longer thread requiring further penetration into the bone is required. Sonic fusion could prove beneficial in bones were there is little bone to engage into such as osteoporotic bone or in flat/small bones.

7.6   Conclusions

This study has shown that sonic fusion may produce a holding power equivalent to that of a polymer threaded anchor, and in some cases produce a higher holding force. It has shown that sonic-fusion requires less drill penetration into the bone, meaning less of the bone structure is removed – vital for patients with poor bone quality.

It has indicated that for a spicular structure, the well accepted linear relationship between thread length and pull-out force for screws (Chapman *et al.,* 1996) may well not apply. That there is likely a required length in a porous structure before a holding force can be achieved. The results have indicated that sonic fusion would not be as prohibited by length and could prove beneficial in bone with little cortical or cancellous bone.

8 Towards Validation

8.1 Introduction

All FEA should have some form of validation, and the objective of the work presented in this chapter is to show that the virtual models created match with physical testing. Validating with human bone was considered at first but on further investigation there proved to be too many drawbacks: a greater number of bone samples would have to be sourced, the samples would have to undergo CT scanning and modelling, and any computer eroded models could not be tested. Therefore it was decided to use 3d printed models to help physically validate the models. The main benefit of using Rapid Prototype (RP) models is that any shape can be produced, meaning that computer eroded, scaled and structurally supported models can be manufactured. Rapid prototype models were produced using Selective Laser Sintering (SLS) and physically tested; the results were then compared against FEA results and analysed.

This chapter provides validation for the FEA studies. It continues to explore the variability in anchor pull-out. The same two models of "normal" and "weaker" cancellous bone are used to investigate the change in reaction force for a single anchor under a set displacement in different directions on the horizontal plane and at an angle of 45°. The sonic-fusion pin model presented in the previous chapter (section 7.2) will also be used to validate the FEA in the "normal" cancellous bone model. In this case the addition of the cortical shell was not examined.

8.2 Rapid Prototyping

The 3d printing process used was Selective Laser Sintering (SLS). Previously stereo-lithography (SLA) manufacturing was trialled but this was found to produce a structure which was too anisotropic (Bennani-Kamane, 2013). SLS also utilises additive layer manufacturing but the layers are not as clearly pronounced as they are with SLA manufacturing, leading to a less anisotropic structure. The

price of SLS has dropped significantly over the last three years (in 2014 it is approximately less than a sixth of what it what was in 2010) increasing accessibility.

The polymer used to manufacture the models was Polyamide PA-12, a form of nylon which is commonly used in 3d printing. The resolution of print was 0.2mm, the model had to be scaled up by a ratio of 1:5 partly because of resolution size, but it also meant the model was easier to handle as well as the pull out forces being of a similar magnitude to the FEA (rather than an order greater or less). PA-12 has a Tensile Modulus of 1500 – 1800 MPa and an Ultimate Tensile Strength of 40 – 45 MPa. Both these values are dependent on laser strength and to some extent on build orientation – there still may be some anisotropy.

Lower apparent and higher apparent density models were produced to compare both sets of threaded anchor results. For the sonic-fusion pin model (Figure 8-1), only the higher apparent density model was compared. The anchor model was a two piece construction, i.e. the anchor could be inserted and removed from the bone. It was inserted to the same depth as the FEA model by checking the rotational position of the anchor (the anchor cut out was included in the printed model). The pin model could not be made into a two piece model, so was a single piece construction. The scale of 1:5 was used across all models, i.e. the size of the bone in model was 50 mm x 50 mm x 50 mm – original size approximately: 10 mm x 10 mm x 10 mm. The bone was encased in 5mm thick polymer on four sides to act as a similar restraint to those used in the FEA simulations.
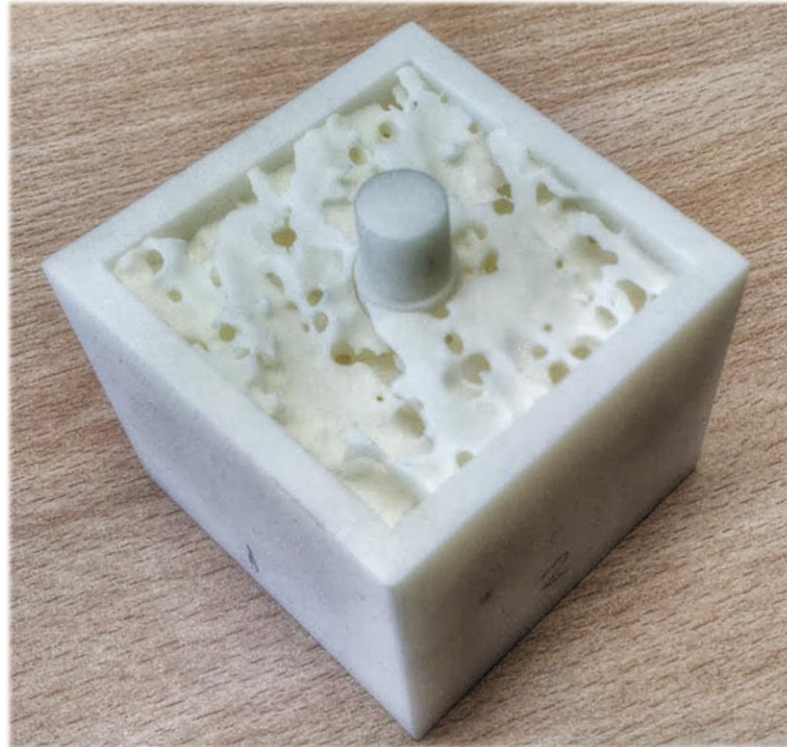
Figure 8-1: RP model of the sonic fusion pin in 17.5% apparent density bone – Total width of model is 60mm and total depth of model is also 60 mm, height is 50 mm

8.3   FEA Materials and Methods Re-Cap

Two pieces of cancellous bone have been used, with bone orientated so the higher "local" apparent density is parallel and near to where the cortical shell would be. The smoothed bone model (Figure 8-2 – right) had an overall apparent bone density of 17.5%, and this might represent normal or healthy cancellous bone, while the eroded model had an overall apparent bone density of 8.3% (Figure 8-2 – left), and this might be more appropriately described as weak or osteopenic bone. The same anchor dimensions were used - based on a Stryker® Titanium Wedge anchor.
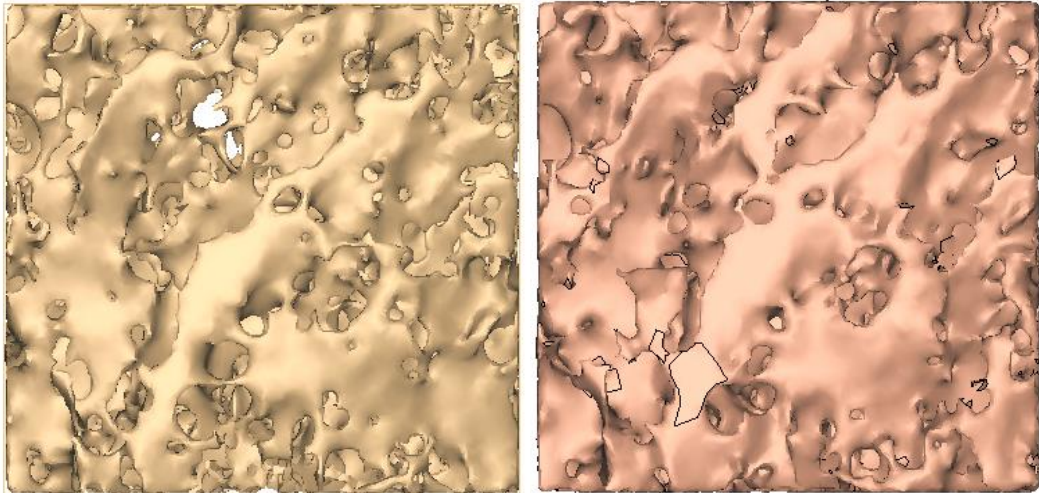
Figure 8-2: Two Bone densities from the same piece of bone, left image shows the eroded model and the right shows the original density – shown from above

The elements of cancellous bone were fully restrained on the four vertical sides. For every simulation a linear ramped displacement in the appropriate direction of 0.2mm was applied to the cylinder at the top of the anchor

Figure 8-3 shows the side view of the loading cases, with the red arrow showing the 0.2 mm displacement applied in the horizontal loading case and the blue arrow the 45° case. In the case of 45° a displacement of 0.1414 mm was applied in the vertical and horizontal direction, to produce a final vector of 0.2 mm. The forces given as "pull-out" forces are the reaction forces at the directional displacement of 0.2 mm.
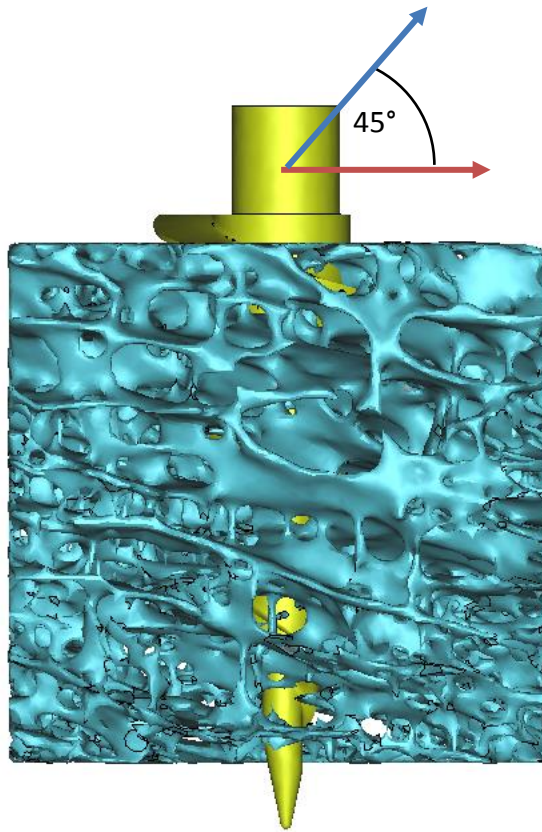
Figure 8-3: Loading applied to the anchor
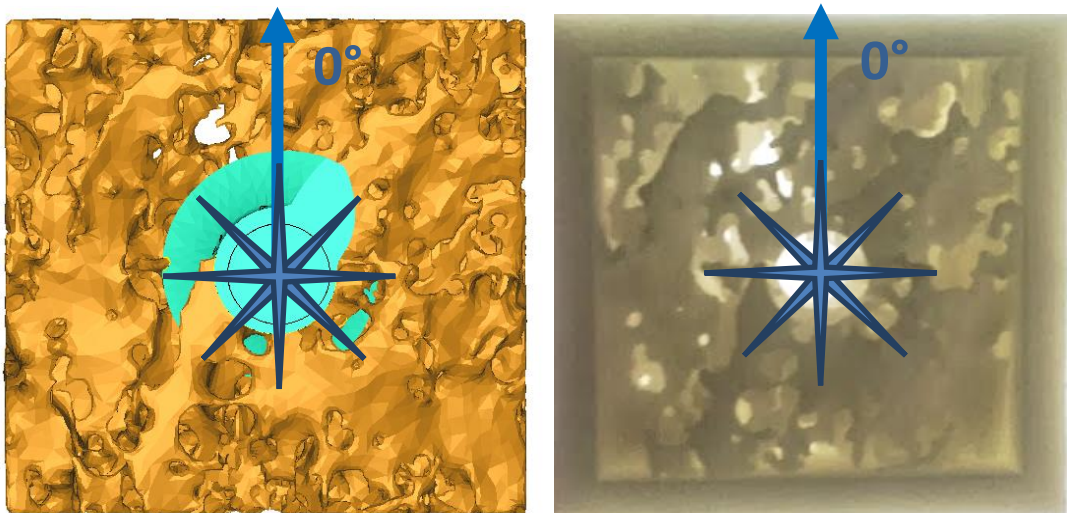
Figure 8-4: Orientation of the bone and anchor compared to the RP model – shown in the original low density study from above.

Figure 8-4 shows the CT scanned model next to the RP model (without anchor). The photograph of the RP was taken with a light-box behind to highlight any line of sight holes through the bone. The figure also gives the orientation of the bone to the anchor from above, to maintain consistency this will always be the orientation of the bone, the arrow pointing in 0° will refer to this direction in the result plots (Figure 5-4, Figure 5-5 & Figure 8-14). The model shown in Figure 8-4 is the lower apparent density bone, in both the virtual model and RP model a hole can be seen above and to the left of the anchor, giving a clear marker to check the alignment of the model when testing. In the higher apparent density (Figure 8-2 – right) there is no line-of-sight hole so the orientation was checked by lining up the orientation of the trabecular plates – looking at Figure 8-2 and Figure 5-4 it can be seen that the trabecular plates have a diagonal grain to them.

In total 8 results were taken for each data set, points were 45° apart as shown by the blue points in Figure 8-4.

8.3.1 Material Properties and Contact

As before, the bone elements have Young's Modulus = 17GPa, Poisson's Ratio = 0.3, yield strength = 100MPa, and ultimate strength 120MPa.

The material properties used for titanium alloy (ANSYS, 2012) are Young's Modulus = 96GPa, Poisson's Ratio = 0.3, yield strength = 930MPa, and ultimate strength = 1070MPa.

The material properties used for PLDLLA are Young's Modulus = 3GPa and Poisson's Ratio = 0.3

Contact settings are as previously stated.

8.4 Anchor FEA Results Re-Cap

Figure 5-4 and Figure 5-5 show the final result set; Figure 5-4 shows the values for the 8.3% BV/TV model and Figure 5-5 shows the values for the 17.5% BV/TV model. Comparing these figures it can clearly be seen that there is a larger deviation for the horizontal plane (labelled in red on the charts). On the horizontal plane in the low apparent density model (Figure 5-4) the largest reaction force is 489 N at 180° and the smallest reaction force is 223 N at 315°, a ratio of 2.2:1. For the higher apparent density model (Figure 5-5) on the horizontal plane the largest reaction force is 617 N at 180° and the smallest reaction force is 286 N at 90°. This deviation was interesting as it stood out as anomaly when plotting the FEA (Figure 5-5). To investigate this point further, loading was applied either side of the point on the horizontal plane at 80°, 100°, and 110° (with reference to Figure 8-4). The results can be found below in Table 8-1.

Table 8-1: Shows further reaction forces the original orientation in the higher BV/TV bone (found in Figure 5-5)

Angle (°)	Reaction Force (N)
80	342.4
90	266.3
100	223.0
110	379.2

Table 8-1 shows that rather than the 90° point being a random drop there is a small area of low strength with the reaction force increasing by approximately 50% either side of it - further showing the varying mechanical nature of cancellous bone. This shows that the point at 90° is unusual but verified in the FEA, the second lowest reaction force was 413 N at 225° and 270°.

At 45° loading (labelled in blue on the charts) in lower BV/TV bone the standard deviation and mean force drops (Table 5-1). For the higher BV/TV model the mean force and standard deviation increases. This increase in reaction force at 45° is due to the increased number of vertical struts providing support in the

higher BV/TV bone. The standard deviation rises due to the average reaction force also increasing. This was discussed further in section 5.4.

Figure 8-5: Radar Plot showing the reaction force of anchor in lower apparent density (8.3% BV/TV) bone in the original orientation
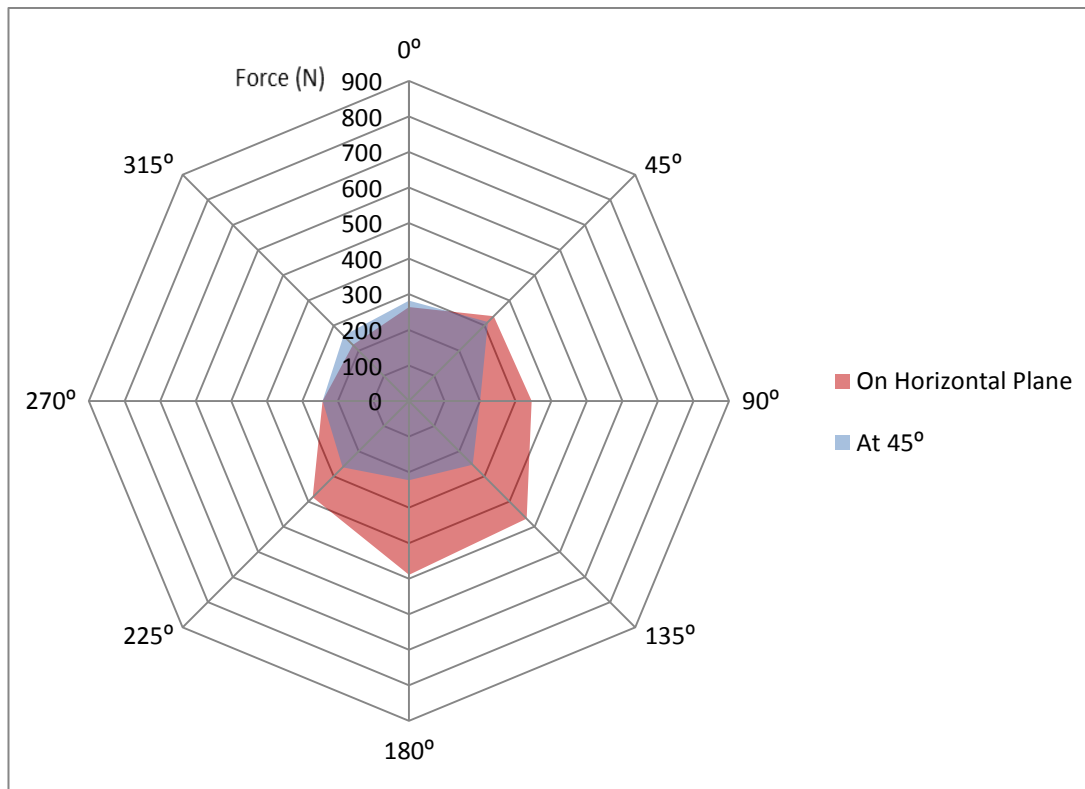
The above figure is a duplicate of Figure 5-8, it is shown here again for ease of comparison, the same is true of Figure 5-9 on the next page.

Figure 8-6: Radar Plot showing the reaction force of anchor in higher apparent density (17.5% BV/TV) bone in the original orientation
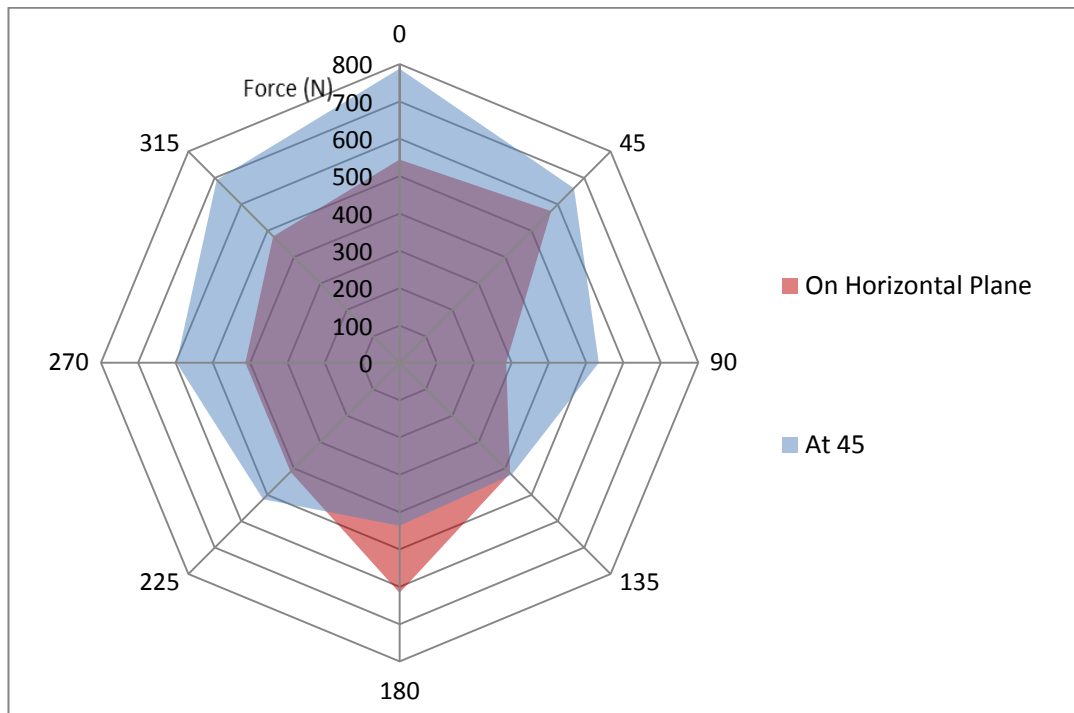
Table 8-2: Mean Pull-out Forces for each result set with standard deviation

Study	Original Study			
Bone Type	17.5% BV/TV		8.3% BV/TV	
Orientation	Horizontal	45°	Horizontal	45°
Mean Force (N)	468	581	344	255
Std. Dev.	108	127	99	35

8.5   Testing

Three different mechanical test set-ups were used; one test horizontally (Figure 8-7), one at 45° (Figure 8-8), and one vertical pull-out test (Figure 8-9). For the horizontal and 45° tests the same 1mm total displacement at a slow rate of 0.5mm/min was used. A displacement of 1mm was used as once scaled (1:5) this was equal to the 0.2mm applied in FEA. A slow rate was chosen so the test could be paused or halted if cracking or failure was observed and were non-destructive. For the vertical destructive pull-out test the same rate of extension was used but it ran until 10mm was applied, this was to ensure failure occurred.

Figure 8-7 shows the test set-up for horizontal testing. The bone was placed on its side and clamped to the base of the machine with two toolmaker's clamps. The displacement in this case was applied downward via a steel bar.
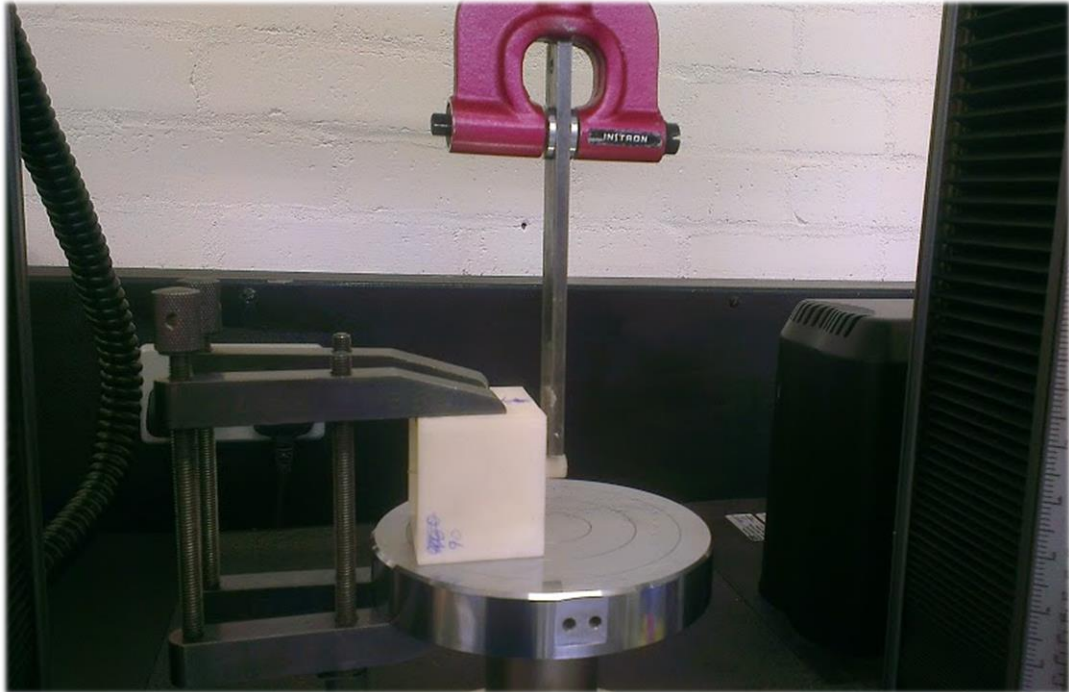
Figure 8-7: Horizontal Testing

Figure 8-8 shows the test set-up for 45° testing. Here the bone is placed in a 45° V-block to apply the correct angle; it is then clamped down with a specific rig to hold the bone in place. An aluminium alloy head was manufactured and bonded to the top of the anchor, this allowed a collar with a rod attached at 45° to be placed over the anchor. The collar was held in place with a grub screw. A displacement could then be applied upwards.
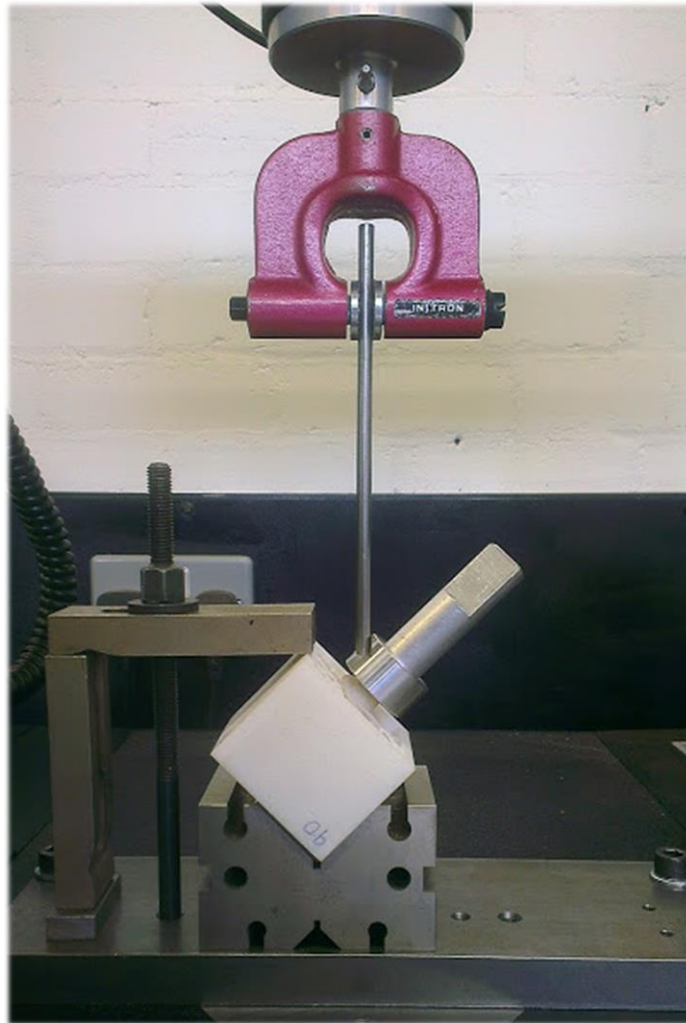
Figure 8-8: 45° Testing

Figure 8-9 shows vertical testing. The bone was placed upright on two bars, and clamped down with four toolmaker's clamps. The bars were necessary as they raised the bone-anchor assembly up so the anchor protruded as in the FEA model. The machine's load cell clamp was then directly secured on to the aluminium alloy head bonded to the anchor. Although the loads observed were high in this test (due to it running to a 10 mm displacement), at no point did the head become detached, polyamide is slightly porous and provided a good bond with the alloy.

Figure 8-9: Vertical testing

8.6   Anchor Results

The following tables and plots give the results for all three testing set-ups in both bone types. The non-destructive tests were performed three times, this produced a mean result to be compared against the FEA results. The vertical test was a destructive pull-out test and was only performed once due to cost issues of destroying a printed model.

8.6.1 Horizontal Results

Table 8-3: Lower Apparent Density Results on the Horizontal Plane

Direction (°)	Reaction Force (N) at 1mm			(N)	
	Test 1	Test 2	Test 3	Mean	Range
0	89.1	85.5	75.4	83.3	75.4-89.1
90	103.5	90.6	87.8	94.0	87.8-103.5
180	155.5	144.3	139.8	146.5	139.8-155.5
270	79.5	80.4	77.7	79.2	77.7-80.4

Table 8-4: Higher Apparent Density Results on the Horizontal Plane

Direction (°)	Reaction Force (N) at 1mm			(N)	
	Test 1	Test 2	Test 3	Mean	Range
0	207.1	243.6	241.9	230.9	207.1-243.6
90	308.6	269.2	283.8	287.2	269.2-308.6
180	306.0	284.5	332.2	307.6	284.5-332.2
270	177.3	209.6	221.6	202.8	177.3-221.6

Table 8-5: Results for both models compared to FEA results in the Horizontal Plane

Direction (°)	17.8% Apparent Density (N)			8.3% Apparent Density (N)		
	Lab (mean)	FEA	Ratio	Lab (mean)	FEA	Ratio
0	230.9	544.2	2.4	83.3	264.0	3.2
90	287.2	285.7*	1.0	94.0	345.0	3.7
180	307.6	616.2	2.0	146.5	489.0	3.3
270	202.8	413.0	2.0	79.2	243.0	3.1

8.6.2 45° Results

Table 8-6: Results for both models compared to FEA results in the 45° direction

Direction (°)	17.8% Apparent Density (N)			8.3% Apparent Density (N)		
	Lab (mean)	FEA	Ratio	Lab (mean)	FEA	Ratio
0	400	787.8	2.0	145	282.0	1.9
90	365	533.8	1.5	103	200.0	2.0
180	355	436.5	1.2	113	223.1	2.0
270	318	597.2	1.9	118	242.9	2.1

8.6.3 Vertical (Pull-out) Results

Figure 8-10 shows the load vs. extension plot of the pull-out test in the higher BV/TV bone model. Figure 8-11 shows the same plot with the same load values but with the scaled down extension i.e. 10 mm in the 3d printed model is 2 mm in the FEA due to the 1:5 ratio. It can be seen there is good correspondence between the models. In this simulation a displacement on 0.2 mm was used as the maximum value. This is because above 0.2 mm was the mean trabecular strut thickness and anything above this would be considered to be failure.

Figure 8-10: Instron Plot of Load (N) vs. Extension (mm) for a pull-out test in higher density bone
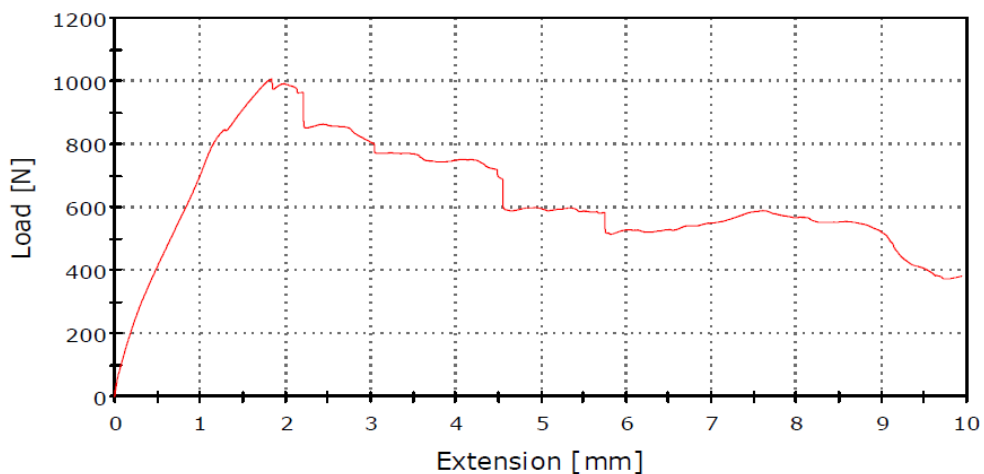
Figure 8-11: Instron Plot of Load (N) vs. Extension (mm) for a pull-out test in higher density bone with an overlay of the FEA results shown in blue.
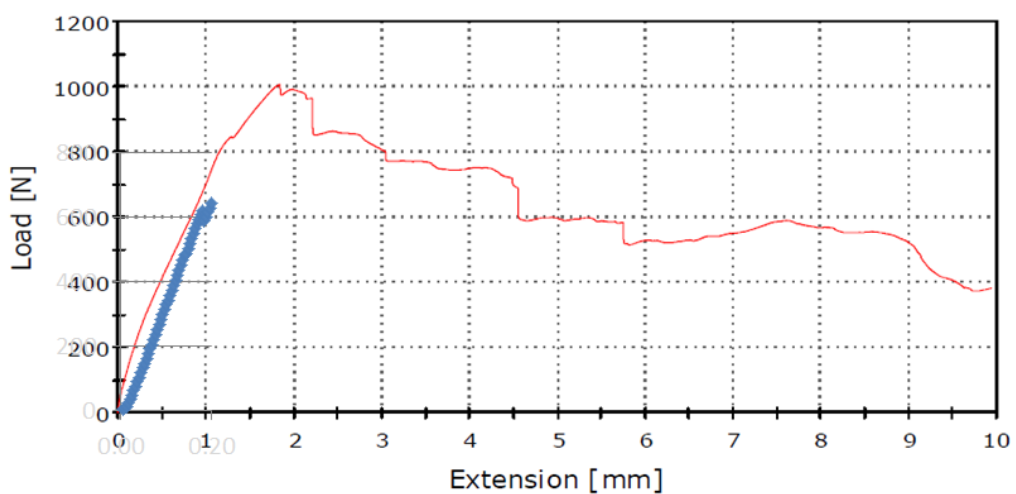
Figure 8-12 shows the deformation of the bone under pull-out. By comparing this with the displacement plot in Figure 8-13 it can be seen that the same trabeculae are moving, particularly in the trabecular circled in both figures. This gives further alignment between the physical and virtual models.

Figure 8-12: Photograph of pull-out test showing movement of trabecular
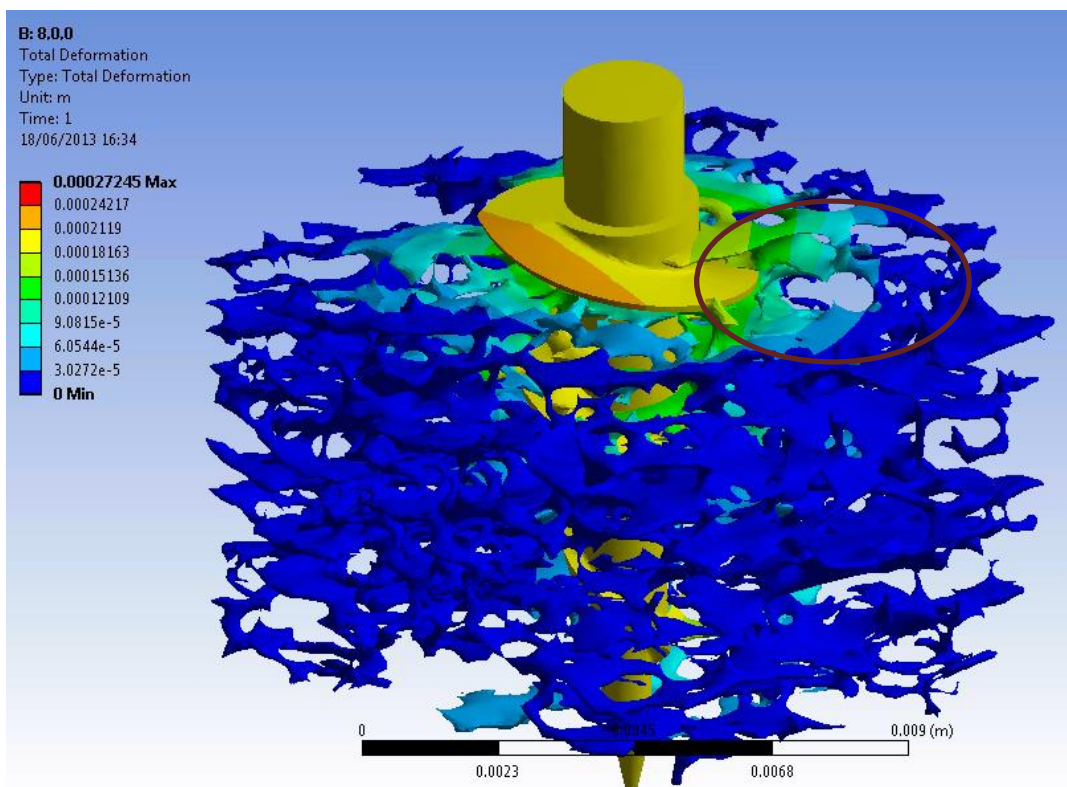
Figure 8-13: FEA Displacement Plot of Higher Apparent Density Bone

8.7 Anchor Discussion

Observing the mean reaction forces in the results (Table 8-5 and Table 8-6) it can be seen that there is a clear variation in the reaction force and the ratios of laboratory to FEA are generally consistent, but there are some interesting points. Looking at horizontal results first (Table 8-5) it can be seen that overall the lower apparent density results align well with a ratio (LAB: FEA) between 3.1 and 3.7, importantly the order of reaction force from lowest to highest matches.

For the higher apparent density bone the ratios are around 2.0 with a consistent order except for the 90° point (as discussed in section 8.4). One reason for the variance between the physical and FEA results could lie in the difference between loading methods. The FEA always begins loading at a defined zero point, however in the physical laboratory tests, the anchor was loaded until a small (10N) reaction force was observed. Therefore the anchor under load may only move with a small reaction force for the initial displacement and then begin to escalate after it has engaged with the bone.

The 45° study also saw a clear variation in the reaction force. The lower apparent density had very consistent results with the FEA, a ratio of 1.9 to 2.1 was observed, which importantly had the same order of reaction force from lowest to highest.

The higher apparent density model did not provide such a clear answer but did correlate with three out of the four points.

The vertical results indicate the FEA has a good match with physical results, with a near 1:1 ratio being plotted in Figure 8-11.

8.8 Sonic-Fusion Pin Study

As well as the threaded anchor models a sonic fusion model was also produced. These 3d printed models of the sonic fusion and bone used the same manufacturer, material (PA-12), and scale (1:5), but due to the nature of the sonic fusion process this was a one piece construction rather than two piece i.e. the pin and bone were one piece rather than two pieces as modelled. This was

believed to increase the reaction force of the tests. The models were only produced in the higher BV/TV bone as in the case presented in chapter 7 - the dimensions for the pin were the same as used in section 7.2 and was centrally located in the bone. The settings and properties for the simulation were the same as used above in section 8.3.1.

8.8.1 Sonic-Fusion Pin Results

Figure 8-14 shows the radar plot of the FEA results in the horizontal plane, the reaction forces are at 0.2 mm displacement. Table 8-7 shows the mean forces and compares the laboratory results with the FEA results.

Figure 8-14: Radar Plot showing the reaction force of the sonic fusion pin simulation in FEA in higher apparent density bone
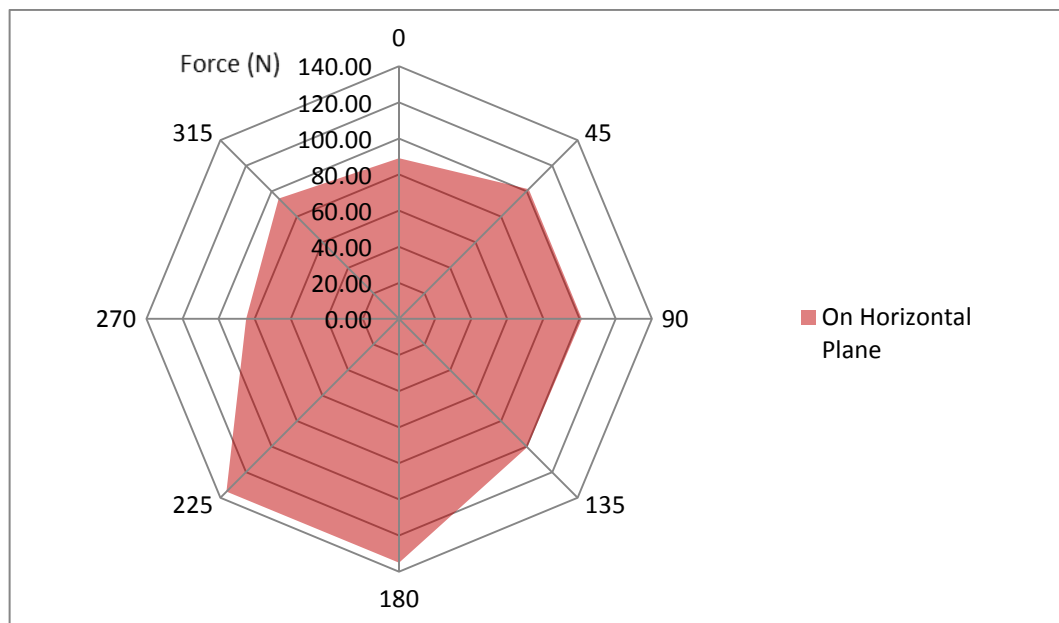
Table 8-7: Higher Apparent Density Results on the Horizontal Plane for the Sonic Fusion Pin

Direction (°)	Test 1 (N)	Test 2 (N)	Test 3 (N)	Mean (N)	Range (N)	FEA (N)	Ratio (Test : FEA)
0	728.6	637.7	719.2	695.2	637.7-728.6	89.0	7.8
90	738.9	782.5	683.7	735.0	683.7-782.5	101.3	7.3
180	925.9	1036.7	821.1	927.9	821.1-1036.7	135.1	6.9
270	477.3	559	632.9	556.4	477.3-632.9	84.7	6.6

Table 8-7 shows the values for mechanical testing were around 7 times greater than FEA, to give a better comparison between the mechanical test and FEA the mesh was scaled up five times to match the size of the 3d printed model. Contact was also set to bonded as the rapid prototype model was one model rather than two entities in contact. The material used for FEA was PLDLLA for the both the pin and bone, with the same values as given previously. Table 8-8 gives the results for this below:

Table 8-8: Comparing Scaled Results against Testing for the Sonic Fusion Pin

Direction (°)	Mechanical Test Mean (N)	Range (N)	FEA to Scale (N)	Ratio (Test : FEA)
0	695.2	637.7-728.6	674.8	1.03
90	735.0	683.7-782.5	740.5	0.99
180	927.9	821.1-1036.7	1114.4	0.83
270	556.4	477.3-632.9	1015.9	0.55

8.8.2 Sonic-Fusion Discussion

Figure 8-14 shows the radar plot for the sonic fusion pin. The mean reaction force was 105.2N and the standard deviation was 19.4N, compared to a mean of 466.5N and standard deviation 116.0N for the anchor in the same piece of bone. Part of the reason for a lower FEA mean compared to the anchor simulations is that the two models are not identical. Firstly, the sonic fusion pin is a smaller device and more comparable to a 3 mm anchor, secondly due to the nature of the geometry and mechanical properties the sonic fusion pin is not as stiff.

Table 8-7 compares the FEA with the laboratory; the ratios are higher than the threaded anchor models. This is down to two reasons: first, the titanium anchor is modelled with a higher Young's Modulus (approximately 35 times) and second, it is a one piece construction. Both these limitations were known so higher ratios were expected. Importantly, the results do correlate, with rankings from highest to lowest reaction force being consistent.

Table 8-8 gives the comparison of the scaled up model, it can be seen there is very good alignment at 0° and 90°, at 180° the FEA is 20% greater than the

mechanical test but both values are the highest in terms of order. At 270° the result for FEA is nearly twice as high as that for the mechanical test. This differs from the results in Table 8-7 for the original FEA, it could possibly be due to the fact that a bonded contact was used, resulting in a higher reaction force.

8.9   Validation Conclusions

This chapter has described methodology for validating the models. It has shown that there is alignment between the physical and virtual for both the threaded anchor and sonic-fusion pin models. Emerging technologies have been utilised to solve a problem that was previously very difficult to achieve. Rapid prototyping has confirmed the difference between modelling a continuum and modelling from a CT scan.

Again, it has been shown the critical nature of modelling the microstructure of bone. Changing the direction of loading in the model leads to significant changes in the reaction of the model, something which cannot be represented in continuum models, or in physical models using artificial cancellous bone. These results demonstrate that the fundamental variability in real bone can lead to large changes in behaviour over quite a small volume.

Finally, it has nurtured the idea that in the future, 3d printed models instead of PU foam could be used as a bone substitute. If a material with similar properties to bone was used in conjunction with the appropriate printing process, an excellent bone substitute could be used. If a material created from Hydroxyapatite (HA) and an organic compound was selected correctly then only the challenges of print resolution and cost would need to be overcome.

9 Cement Studies

9.1 Introduction

One method of improving any threaded fix is bone augmentation through the use of an adhesive or cement, especially in a weak and porous structure such as osteoporotic bone. Increased cancellous porosity has been shown to decrease screw stability where the cortical bone plays a critical role in screw holding power as demonstrated previously and shown by Seebeck *et al.* (2005). Currently Calcium Phosphate (CaP) cement is being increasingly used to augment bone due to its good bio-compatibility and strength. Cement is typically mixed by hand, a rapid process due to its fast setting time then delivered by a pre-injection or via cannulated screw.

The objectives of studying augmentation in FEA were to see if the addition of cement made a difference to anchor pull-out forces, and if varying geometries of cement led to further differences. This study takes the previously presented anchor models and adds simplified cement geometry. This produced a results for both higher and lower apparent density models demonstrating how cement can change the holding power of an anchor.

9.2 Study Method

This investigation looked at three different idealised cement geometries (Figure 9-4) and compared them to a model without cement in 8.3% and 17.5% BV/TV cancellous bone models. Figure 9-1 shows the three parts of the model, in reality the bone and cement structure was modelled first, then the anchor added in to create the final assembly.
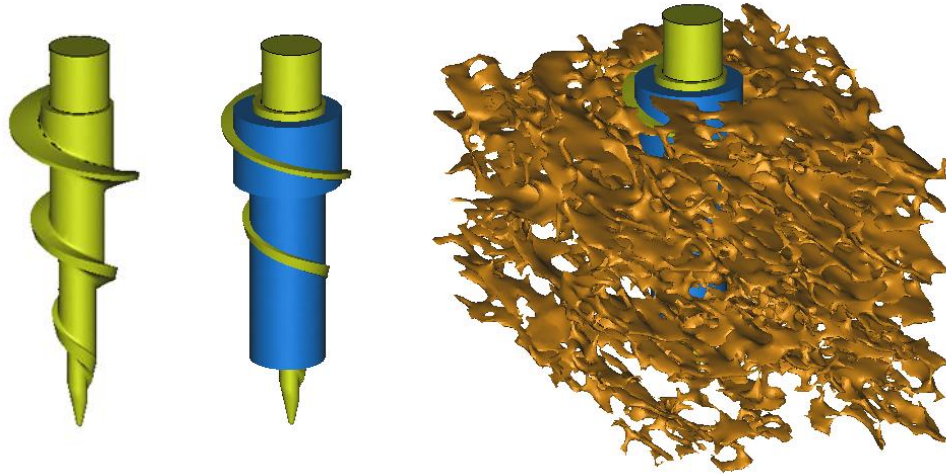
Figure 9-1: shows the model with addition of idealised cement geometry

Figure 9-2 shows an initial model concept in the lower apparent density bone. Figure 9-3 shows the difference in contact area between the two models. Although no correlation has been found between contact area and reaction force in this project, it is still interesting to see what little contact there is in low apparent density cancellous bone compared to a continuum.
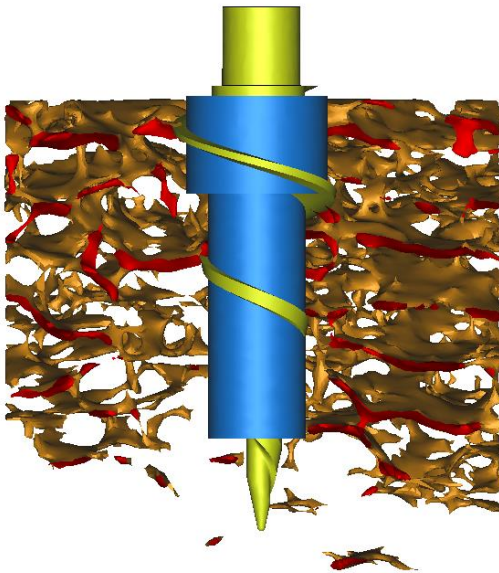
Figure 9-2: Cross section of cement and bone
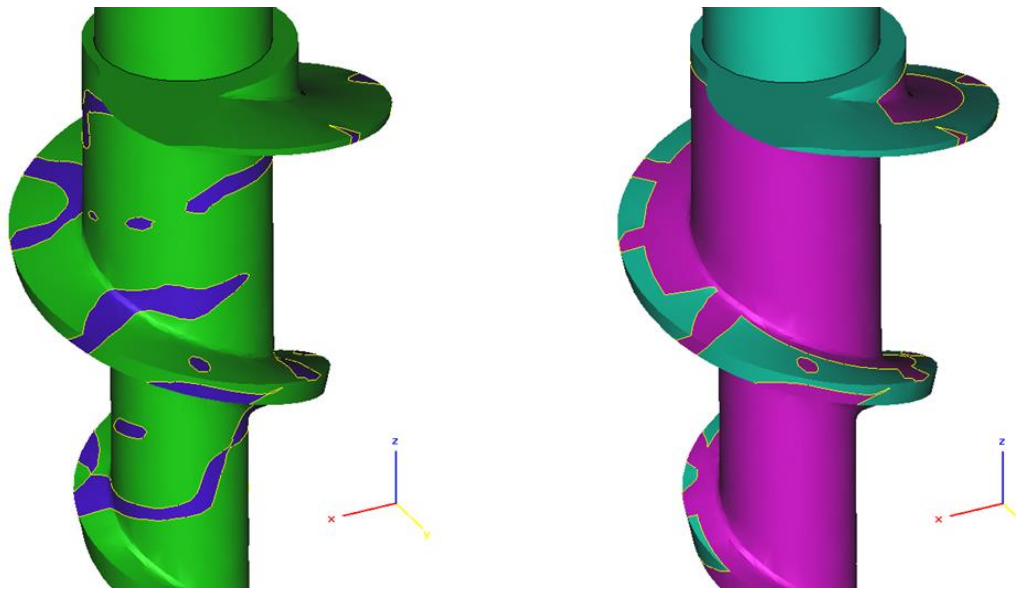
Figure 9-3: Showing the variation between contact areas

Figure 9-4 shows the three concepts. Concept A has a conical cement distribution following the external thread diameter, ensuring all threads are filled with cement. Concept B is a disc of cement which has a depth of 2/3rds the thread pitch (2.67 mm). Concept C is a cylinder of cement. The figure also shows that the bone and cement are modelled as one. This was due to limitations in the 3matic® mesh creation software. It produces errors when creating an assembly with 3 or more parts when faced with complex geometry such as cancellous bone.

A   B   C

Max. Ø5.0mm tapering   Ø7.1 mm x 2.667 mm   Ø3.6mm x 10mm
by 12° to Ø0mm   (2.667 =2/3 thread pitch)
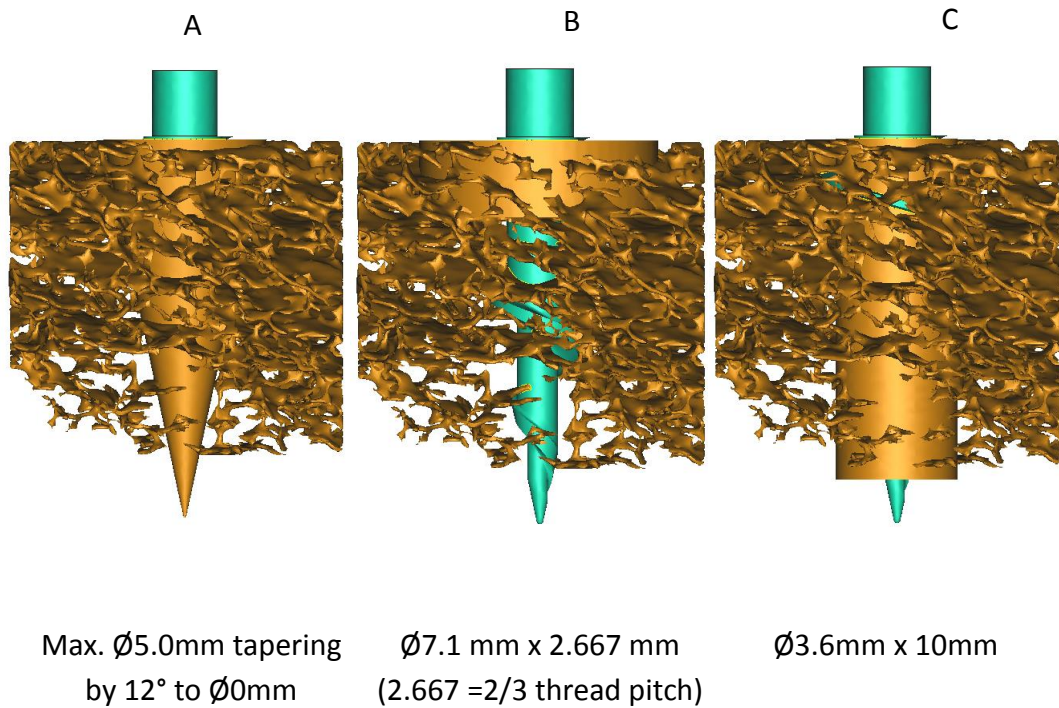
Figure 9-4: Showing the three concepts in lower BV/TV bone with their corresponding dimensions

Table 9-1 gives the cement volumes, each concept was modelled to give the similar CAD volumes. However, due to the anchor's geometry the volumes were slightly different. Concept A has the smallest final meshed volume and concept C has the largest meshed volume. The anchor has a constant volume of 34.9 mm^3.

Table 9-1: Volumes of Cement and Bone for each model, all measurements in mm^3

	Cement A	Cement B	Cement C	No Cement	Anchor
CAD Volume	77.0	74.2	74.3		34.9
Meshed Volume of Bone plus Cement (mm^3)					
8.3%	125.5	148.5	151.5	83.4	34.9
17.8%	216.0	236.0	240.6	178.3	34.9
Meshed Cement Volume (mm^3)					
8.3%	42.1	65.1	68.1		
17.8%	37.7	57.7	62.3		

9.2.1 Material Properties

The material properties for CaP cement and bone are similar. Burguera, Xu, & Sun (2008) give the relationship between Elastic Modulus and Porosity of Calcium Phosphate cement as:

$$E = 17\,(1 - P)^{1.7}\,GPa$$

$$Where\ E = Elastic\ Modulus\ and\ P = Porosity\ (between\ 0\ and\ 1)$$

Compared to the 17 GPa value used for cancellous bone in the FEA study it was considered acceptable to model cement and bone as one. However the material strength of CaP cement is given as 8-10 MPa (Moreau, Weir, & Xu, 2009), which is a magnitude lower than the value used in FEA for cancellous bone. This and the fact there were no contact parameters between the cement and bone were taken into account when evaluating at the results.

The bone used for the study was the same used as before. Table 9-2 shows the bone data for the imported CT cancellous model and Table 9-3 the bone data for the eroded model , the data was produced by BoneJ plugin (Doube *et al.*, 2010) for ImageJ.

Table 9-2: Trabecular Thickness, Spacing and Bone Volume Density Data for the smoothed model (all dimensions in mm)

Region	Tb.Th Mean	Tb.Th S.D.	Tb.Th Max	Tb.Sp Mean	Tb.Sp S.D.	Tb.Sp Max	BV/TV
Bottom Third	0.173	0.052	0.385	0.855	0.306	1.513	14.1%
Middle Third	0.192	0.062	0.468	0.762	0.336	1.850	17.7%
Top Third	0.203	0.072	0.528	0.670	0.269	1.556	20.7%
Total	0.190	0.063	0.480	0.756	0.298	1.650	17.5%

Table 9-3: Trabecular Thickness, Spacing and Bone Volume Density Data for the eroded model (all dimensions in mm.).

Region	Tb.Th Mean	Tb.Th S.D.	Tb.Th Max	Tb.Sp Mean	Tb.Sp S.D.	Tb.Sp Max	BV/TV
Bottom Third	0.126	0.044	0.352	1.053	0.336	1.863	5.8%
Middle Third	0.143	0.050	0.381	1.026	0.372	2.176	8.5%
Top Third	0.154	0.061	0.419	0.917	0.304	1.816	10.6%
Total	0.142	0.054	0.419	1.009	0.320	1.903	8.3%

In this study the elastic and strength properties used for bone elements (Turner *et al.*, 1999) are assumed to be the same in tension and compression. The bone elements have Young's Modulus = 17GPa, Poisson's Ratio = 0.3, yield strength = 100MPa, and ultimate strength 120MPa (Rincon Kohli, 2003). The material properties used for titanium alloy (ANSYS, 2012) are Young's Modulus = 96GPa, Poisson's Ratio = 0.3, yield strength = 930MPa, and ultimate strength = 1070MPa.

9.2.2 Loading

The elements of cancellous bone were fully restrained on the four vertical sides as with other studies. For all the devices a linear ramped displacement in the vertical upward direction of 0.2mm was applied to the top of the anchor.

9.2.3 Contact

The same contact settings were used as before, Table 9-4 summarises these below:

Table 9-4: Summary of Contact Parameters

Parameter	Value/Setting
Friction Coefficient	0.6
Behaviour	Auto Asymmetric
Formulation	Pure Penalty
Normal Stiffness Factor	0.01
Update Stiffness	Each Iteration
Pinball Region	Auto Detection Value

9.3   Results

Figure 9-5 shows the results for three concepts compared against a model with no cement in lower apparent density bone. Figure 9-6 shows the results in the higher apparent density bone. The ratios given are those compared to the no cement result.

No Cement

137.9 N

A   B   C

369.1 N   756.5 N   337.7 N

(1:2.7)   (1:5.6)   (1:2.4)
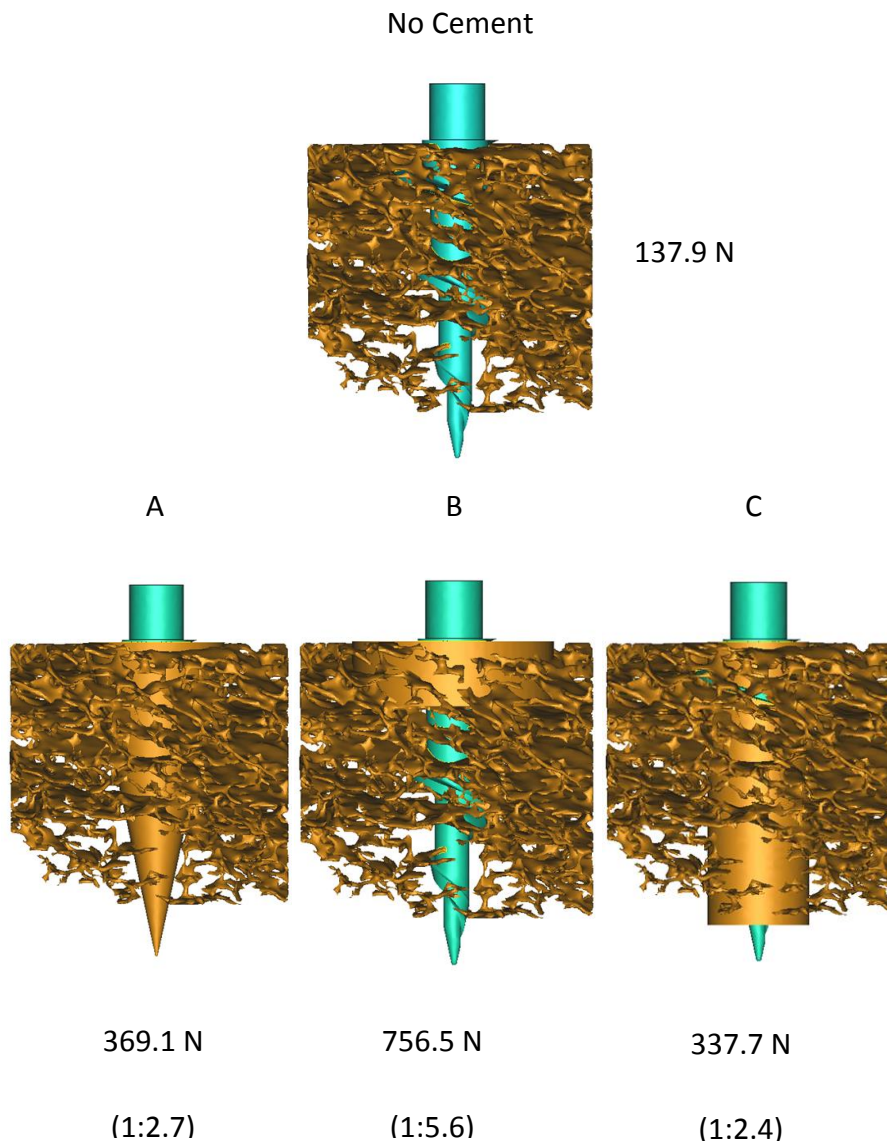
Figure 9-5: Shows the reaction forces for each concept at 0.2 mm in lower apparent density bone

No Cement

681.7 N

A   B   C

1596.5 N   7528.6 N   1600.9 N

(1:2.3)   (1:11)   (1:2.3)
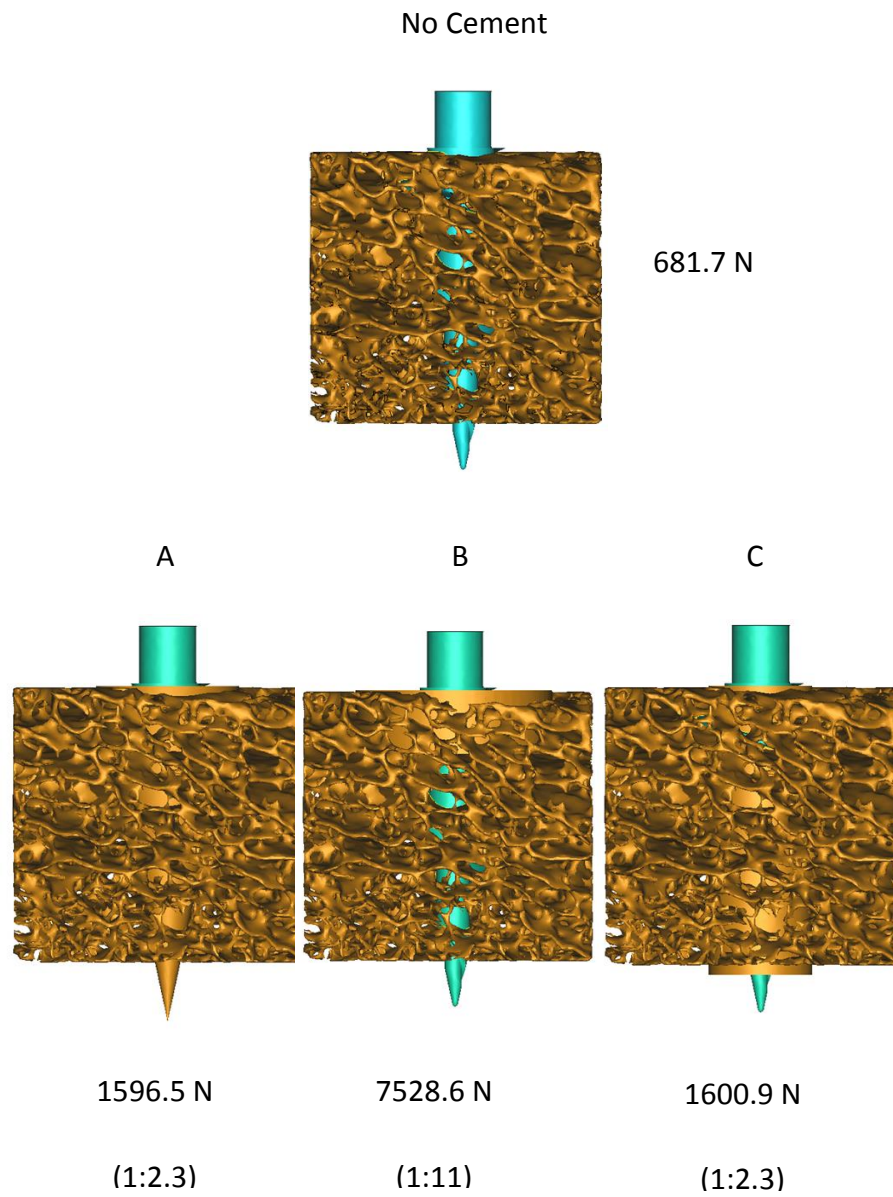
Figure 9-6: Shows the reaction forces for each concept at 0.2 mm in higher apparent density bone

The results demonstrated that in all cases cement at least doubled the reaction force. Concept B gave the largest increase in the strength, it increased the stiffness in low apparent density bone to a stiffness equivalent to that of the higher apparent density bone model. In the higher apparent density bone concept B increased the stiffness by an order of magnitude. It is believed that the reaction force in reality would be less due to the extra stiffness created by the one-piece body for the cement and bone. Even taking account the extra stiffness created by the one-piece bone and cement geometry it is believed augmentation in this case would increase pull-out force.

9.4   Conclusions

There is little difference between a cone (A) and a cylinder (C) of cement applied along the length of the thread. However, placing the cement at the top of anchor (Concept B) creates a significantly stronger union. There are two probable reasons: 1) the higher local BV/TV located towards the top of both pieces of bone and 2) the larger thread depth at the top of the anchor. The difference could be less apparent in parallel threaded screws due to the consistent thread depth.

This brief study has shown that there are benefits to using FEA as a tool to evaluate the mechanical aspects of cement distribution. It has also demonstrated that as expected augmentation will likely increase the holding power of anchors, although the increased artificial stiffness should be taken into account.

10 Final Conclusions and Future Work

10.1 Conclusions

This research has demonstrated the procedure for modelling implants in cancellous bone. It has shown the critical nature of modelling the microstructure of bone. Changing the direction of loading in the model leads to significant changes in the response of the construct, and this cannot be represented in continuum models, or in physical models using artificial cancellous bone. The results demonstrate that the fundamental variability in real bone can lead to large changes in behaviour over quite a small volume. It has shown how difficult it is to make predictions for pull-out forces, particularly in weak bone.

The importance of a cortical layer was re-confirmed. At the apparent densities simulated, engagement with the cortical layer increases pull-out force dramatically. Engaging the anchor even with a thin cortical layer can produce a significant improvement to pull-out strength.

It has been indicated that for a spicular structure, the well accepted linear relationship between thread length and pull-out force (Chapman *et al.,* 1996) may well not apply. There is likely a required length in a porous structure before a holding force can be achieved.

Contact settings are an essential parameter in analysis. This project has shown the importance of friction coefficient in models of anchor pull-out from a porous structure, and suggests that very low coefficients might lead to quite different mechanisms than those where friction is high. Any change in friction in-vivo could lead to a marked change in anchor performance.

In addition to established threaded anchor technologies, sonic-fusion and cement augmentation have been examined and compared with the conventional anchor application procedure.

Different methods of modelling sonic fusion and their results have been explored, discussed and evaluated. The difficulty in modelling sonic fusion over

threaded implants has been revealed but as the study has demonstrated, it is possible to import a complete model from a μ-CT scan. It can be concluded that using computer generated pin models rather than CT models is the most efficient way to model and evaluate the process, although there is naturally some difference between a model produced from a CT scan and a computer generated model. This difference arises because a better engagement or deeper penetration can be modelled using CAD.

The CT generated model aligns with preliminary laboratory results, indicating that the FEA model has been accurately produced.

It has been shown that if good engagement is made with bone, as in the case of concepts created, then sonic fusion can produce a strong holding power comparable with that of a threaded anchor. Although less stiff than a metal anchor, it is of sufficient strength and with the additional benefit of the material undergoing resorption. It has shown that sonic-fusion requires less drill penetration into the bone, meaning less of the bone structure is removed – vital for patients with poor bone quality.

Augmentation was demonstrated to improve anchor holding power. The research has shown that there are benefits to using FEA as a tool to evaluate the mechanical aspects of cement distribution. The results have proved the hypothesis that augmentation will likely increase the holding power of anchor, and its distribution will affect pull-out significantly.

Validation of the models has demonstrated that there is alignment between the physical and virtual for both the threaded anchor and sonic-fusion pin models. Emerging technologies were utilised to solve the problem of validation, previously something very difficult to achieve.

Rapid prototyping has confirmed the difference between modelling a continuum and modelling from a CT scan. The CT, meshing, and FEA processes were validated by comparison with mechanical testing. The results produced from the simulation correlated with the physical results.

10.2 Future Work

This research has established a process for accurate modelling of human trabecular bone. Over the period of the project increasing capability of software has been useful but also frustrating. Tasks which could not be carried out at the beginning of the project are now possible, and this continues to develop. Future models will be able to be made larger and take into account more bodies and greater contact.

Fluid dynamics could be of fundamental use to modelling sonic fusion and cement augmentation, using it to predict geometries created during a procedure. In the future, implant life, from insertion to pull-out could be completely modelled, using a combination of fluid dynamics and structural mechanics.

Published clinical work was examined during this project but no collaboration was present. Working with a surgical team would provide further insight into improving implants.

Finally, it can be suggested that in the future 3d printed models instead of PU foam could be used as a bone substitute. If a material similar to that of bone was used in conjunction with the appropriate printing process, an excellent bone substitute could be used. If an appropriate material was used correctly then only the challenges of print resolution would need to be overcome.

11 References

Abtahi, J., Tengvall, P., Aspenberg, P. Bisphosphonate coating might improve fixation of dental implants in the maxilla: a pilot study. Int J Oral Maxillofac Surg. 2010 Jul;39(7):673-7, 2010

Aldana, P. R., Roy, S., Postlethwait, R.A., and James, H.E. Ultrasound-aided fixation of a biodegradable cranial fixation system: uses in paediatric neurosurgery. J. Neurosurgery. Paediatrics 3(5): 420-424. 2009

Ashman, R.B., Cowin, S.C., Van Buskirk, W.C., Rice, J.C. A continuous wave technique for the measurement of the elastic properties of cortical bone. Journal of Biomechanics 17, 349-361, 1984

Asnis S.E. and Kyle R.F., Cannulated screw fixation: Principles and operative techniques, Springer, New York, 1996

Barber, A., Cawley, P. and Prudich, J.F. Suture Anchor Failure Strength – An In Vivo Study. Journal of Arthroscopic and Related Surgery, 1993

Barber, A., Herbert, M.A., Coons, D.A. and Boothby, M.H. Sutures and Suture Anchors. Journal of Arthroscopic and Related Surgery, 2006

Barber, A., Coons, D.A. and Ruiz-Suarez, M. Cyclic Load Testing of Biodegradable Suture Anchors Containing 2 High-Strength Sutures. Journal of Arthroscopic and Related Surgery, 2007

Barber, A., Herbert, M.A., Beavis, C. and Oro, F.B. Suture Anchor Materials, Eyelets, and Designs: Update 2008. Journal of Arthroscopic and Related Surgery, 2008

Bartucci, E.J., Gonzalez, M.H., Cooperman, D.R., Freedberg, H.I., Barmada, R., Laros, G.S., 1985. The effect of adjunctive methylmethacrylate on failures of fixation and function in patients with intertrochanteric fractures and osteoporosis. J. Bone Joint Surg. Am. 67, 1094–1107.

Bennani-Kamane, P. Finite Element Modelling of Screw Fixation in Augmented and Non-Augmented Cancellous Bone. School of Engineering & Design, Brunel University, London. PhD Thesis, 2013

Black, J. Biological Performance of Materials: Fundamentals of Biocompatibility. 2nd ed. Marcel Dekker, New York, 1992

Brighton, Carl T. and Robert M. Hunt. Histochemical localization of calcium in the fracture callus with potassium pyroantimonate: possible role of chondrocyte mitochondrial calcium in callus calcification. Journal of Bone and Joint Surgery, 68-A (5): 703-715, 1986

Brown C.J., MacInnes R.A., Day A., Hess B., Procter P., "An Approximate Model for Cancellous Bone Screw Fixation", Computer Methods in Biomechanics and Biomedical Engineering 16 (4): 443-450, 2013

Burguera, E.F, Xu, H.H.K., & Sun, L. Injectable Calcium Phosphate Cement: Effects of Powder-to-Liquid Ratio and Needle Size. Journal of biomedical materials research. Part B, Applied biomaterials 84(2): 493-502, 2008

Carter, D.R. and Hayes, W.C. The Compressive Behaviour of bone as a Two-phase Porous Structure, 1977

Chapman, J. R., Harrington, R. M., Lee, K. M., Anderson, P. A., Tencer, A. F. and Kowalski, D. Factors Affecting the Pull-out Strength of Cancellous Bone Screws J. Biomech. Eng. 118: 391-399, 1996

Chen, S.I., Lin, R.M. and Chang, C.H. Biomechanical investigation of pedicle screw-vertebrae complex: a finite element approach using bonded and contact interface conditions, Med Eng Phys. 25(4): 275-82, 2002

Ciarelli, M. J., Goldstein, S. A., Kuhn, J. L., Cody, D. D. and Brown, M. B. Evaluation of orthogonal mechanical properties and density of human trabecular bone from the major metaphyseal regions with materials testing and computed tomography. *J. Orthop. Res.,* 9, 674-682, 1991

Dalen, N., Hellstrom, L. and Jacobson, B. Bone mineral content and mechanical strength of the femoral neck. *ActaOrthop. Scand.,* 47, 503-508, 1976

Danelson, K.A., Gayzik, F.S., Yu, M.M., Martin, R.S., Duma, S.M. and Stitzel, J.D. Bilateral Carotid Artery Injury Response in Side Impact using a Vessel Model Integrated with a Human Body Model. Advanced Automotive Medicine 53: 271–279, 2009

Davis, B. L. Nonlinear Versus Linear Behaviour of Calcaneal Bone Marrow at Different Shear Rates, 2006

Di Lullo, G. A., Sweeney, S. M., Körkkö, J., Ala-Kokko, L, & San Antonio, J. D. Mapping the Ligand-binding Sites and Disease-associated Mutations on the Most Abundant Protein in the Human, Type I Collagen. J. Biol. Chem. 277 (6): 4223–4231, 2002

Diem, S.J., Blackwell, T. L., Stone, K. L., Yaffe, K., Haney, E. M., Bliziotes, M. M. and Ensrud, K. E. Use of Antidepressants and Rates of Hip Bone Loss in Older Women, 2007

Donaldson, F.E., Pankaj, P., Law, A.H. and Simpson, A.H. Virtual trabecular bone models and their mechanical response. Proc Inst Mech Eng H. 222(8):1185-95, 2008

Doube M, Kłosowski MM, Arganda-Carreras I, Cordelières F, Dougherty RP, Jackson J, Schmid B, Hutchinson JR, Shefelbine SJ. BoneJ: free and extensible bone image analysis in ImageJ. Bone 47:1076-9. doi: 10.1016/j.bone.2010.08.023, 2010

Dougherty, R. and Kunzelmann, K.H. Computing Local Thickness of 3D Structures with ImageJ. Microscopy and Microanalysis, 13 (Suppl. 02): 1678-1679, 2007

Ehrlich, P.J. and Lanyon, L.E. Mechanical Strain and Bone Cell Function: A Review. Osteoporosis International 13: 688-700, 2002

Geselevich, M. New Medical Techniques in Modern Surgery - Twelfth conference of the Board of the All-Union Scientific Society of Surgeons, 1971

Gibson, L. and Ashby, M. Cancellous bone, Cellular Solids: Structure & Properties, Pergamon Press, 1988

Glorieux, F.H. Osteogenesis Imperfecta, Best Practice & Research Clinical Rheumatology 22(1):85-100, 2008

Goldstein, S.A., Wilson, D.L., Sonstegarij, D.A. and Matthews, L.S. The mechincal properties of human tibial trabecular bone as a function of metaphyseal location. Journal of Biomechanics 16: 965-969, 1983

Goodship, A.E. and Cunningham, J.L. Pathophysiology of Functional Adaptation of Bone and Remodelling and Repair in Vivo. Bone Mechanic's Handbook 2nd Edition edited by S.C. Cowin. CRC Press, 2001

Gordon, M.D., Steiner, M.E. Anterior cruciate ligament injuries. In: Orthopaedic Knowledge Update Sports Medicine III, Garrick JG. (Ed), American Academy of Orthopaedic Surgeons, Rosemont, 2004

Grant, J.A., Bishop, N.E., Gotzen, N., Sprecher, C., Honl, M., Morlock, M.M. Artificial composite bone as a model of human trabecular bone: The implant–bone interface. Journal of Biomechanics 40: 1158–1164, 2007

Gundapaneni, D., Goswami, T. Thermal isotherms in PMMA and cell necrosis during total hip arthroplasty. J Appl Biomater Funct Mater. 19:0 [Epub ahead of print], 2014

Guo, X.E., Kim, C.H., Mechanical consequence of trabecular bone loss and its treatment: A three-dimensional model simulation. Bone 30: 404-411, 2002

Hara T., Tanck E., Homminga J., and Huiskes R., The influence of microcomputed tomography threshold variations on the assessment of structural and mechanical trabecular bone properties. Bone 31(1): 107-109, 2002

Hoddgskinson, R. and Currey, J.D. Effects of Structural Variation on Young's Modulus of non-human Cancellous Bone, Journal of Biomechanics 204:43-52, 1990

Jee, W.S.S. Integrated Bone Tissue Physiology: Anatomy and Physiology. Bone Mechanic's Handbook 2nd Edition edited by S.C. Cowin. CRC Press, 2001

Jonkers, I., Sauwen, N., Lenaerts, G., Mulier, M., Van der Perre, G., and Jaecques, S. Relation between subject-specific hip joint loading, stress distribution in the proximal femur and bone mineral density changes after total hip replacement. J. Biomech: 41(16): 3405-3413, 2008

Kim CH, Zhang H, Mikhail G, von Stechow D, Muller R, Kim HS, Guo XE, Effects of thresholding techniques on microCT-based finite element models of trabecular bone. Journal of Biomechanical Engineering 129(4):481-486, 2007

Kuhn, J.L., Goldstein, S.A., Choi, K., London, M., Feldkamp, L.A. and Matthews, L.S. Comparison of the trabecular and cortical tissue moduli from human iliac crests. Journal of orthopaedic research 7: 876-884, 1989

Lam, D.K., Sándor, G.K.B., Holmes, H.I., Carmichael, R.P. and Clokie, C.M.L. Marble Bone Disease: A Review of Osteopetrosis and Its Oral Health Implications for Dentists. *Journal of the Canadian Dental Association,* 73(9): 839-843, 2007

Langhoff, J.D, Kuemmerle, J.M, Mayer, J, Weber, U, Berra, M, Mueller, J.M, Kaestner, S.B, Zlinszky, K, Auer, J.A & von Rechenber, B. An Ultrasound Assisted Anchoring Technique (BoneWelding® Technology) for Fixation of Implants to Bone – A Histological Pilot Study in Sheep. Open Orthopaedics Journal: 3: 40-47, 2009

Li, S., Chien, S. and Branemark, P.I. Heat shock-induced necrosis and apoptosis in osteoblasts. J Orthopaedic Research; 17(6): 891-9, 1999

van der Linden, J.C., Verhaar, J.A., Weinans, H., A three-dimensional simulation of age-related remodeling in trabecular bone. Journal of Bone and Mineral Research 17: 688.696. 2002,

Mazzocca, A.D., Cole, B.J., Romeo, A.A. Arthroscopic Repair of Full-Thickness Rotator-Cuff Tears: Surgical Technique. Operative Techniques in Orthopaedics 12 (3): 167-175, 2002

McDonnell, P., Liebschner, M.A., Tawackoli. W. and McHugh, P.E. Vibrational testing of trabecular bone architectures using rapid prototype models. Med Eng Phys. 31(1):108-15, 2009

Melchels, F.P., Bertoldi, K., Gabbrielli, R., Velders, A.H., Feijen, J., Grijpma, D.W. Mathematically defined tissue engineering scaffold architectures prepared by stereolithography. J. Biomaterials 31(27):6909-16, 2010

Meyer, D. C., Mayer, J., Weber, U., Mueller, A., Koch, P.P., and Gerber, C. Ultrasonically Implanted PLA Suture Anchors Are Stable in Osteopenic Bone. Clinical Orthopaedics & Related Research 442: 143-148, 2006

Miller, S.C., de Saint-Georges, L., Bowman, B.M., and Jee, W.S. Bone lining cells: structure and function. Scanning Microscopy: 3(3):953-60, 1989

Moreau, J.L., Weir, M.D. & Xu, H.H. Self-setting collagen-calcium phosphate bone cement: mechanical and cellular properties. J Biomed Mater Res A. 91(2):605-13, 2009

Mueller, M.E., 1962. Die Verwendung von Kunstharzen in der Knochenchirurgie. Arch. Orthop. Unfall-chir 54, 513–522.

Müller-Richter, U.D.A., Reuther, T., Böhm, H., Kochel, M., Kübler, A.C. Treatment of Intracapsular Condylar Fractures With Resorbable Pins. Journal of Oral and Maxillofacial Surgery 69 (12): 3019–3025, 2011

Norris, J.B., Smith, R.T., White, K.L., Parks, B.G., O'Donnell, J.B. Effect of suture size and type on bone cut-out in transosseous tendon repairs. Journal of Arthroscopy 26, 2010

Oberg, E., Jones, F.D. and Horton, H.L. Working strength of bolts, Machinery's Handbook, Ryffel Industrial Press, 1987

Patel, P.S.D., Shepherd, D.E.T. and Hukins, D.W.L. Compressive properties of commercially available polyurethane foams as mechanical models for osteoporotic human cancellous bone. BMC Musculoskeletal Disorders 9:137, 2008

Patel, P.S.D., Shepherd, D.E.T. and Hukins, D.W.L. The effect of screw insertion angle and thread type on the pullout strength of bone screws in normal and osteoporotic cancellous bone models. Medical Engineering & Physics 32 822–828, 2010

Perren, S.M. Physical and biological aspects of fracture healing with special reference to internal fixation. Clinical Orthopaedics 138: 175-196, 1979

Ralston, S.H. Paget's Disease of Bone. New England J Med; 368:644-650, 2013

Rho, J.Y., Ashman, R.B. and Turner, C.H. Young's modulus of trabecular and cortical bone material: ultrasonic and microtensile measurements. Journal of Biomechanics 26: 111-119, 1993

Schneider, M., Seinige, C., Pilling, E., Rasse, M., Loukota, R., Stadlinger, B., Mai, R., Eckelt U. Ultrasound-aided resorbable osteosynthesis of fractures of the mandibular condylar base: an experimental study in sheep. Br J Oral Maxillofacial Surgery 50(6): 528-32, 2012

Seebeck, J., Goldhahn, J., Morlock, M.M., Schneider, E. Mechanical behavior of screws in normal and osteoporotic bone. Osteoporos. Int. 16 (suppl 2), S107–S111, 2005

Simpson, D.J., Brown, C.J., Yettram, A.L., Procter, P., and Andrew, G.J., "Finite Element Analysis of Intramedullary Devices: The Effect of Gap between Implant and Bone". Proc. IMechE, Part H: J. Engineering in Medicine, 222(H3): 333-345, 2008

Snyder *et al*. Role of Trabecular Morphology in The Aetiology of Age-related Vertebral Fractures, Calcif. Tissue Int 53: 14-22, 1993

Stolarski, T.S. Engineering Analysis with ANSYS Software. Butterworth-Heinemann, 2006

Tan, C.K., Guisasola, I., Machani B. *et al*. Arthroscopic stabilization of the shoulder: A prospective randomized study of absorbable versus nonabsorbable suture anchors. J. Arthroscopy 22:716-720, 2006

Turner, C.H., Rho, J., Takano, Y., Tsui, T.Y. and Pharr, G.M. The elastic properties of trabecular and cortical bone tissues are similar: results from two microscopic measurement techniques. Journal of biomechanics 32: 437-441, 1999

WHO Scientific Group, Prevention and Management of Osteoporosis. WHO Technical Report Series 921, 2003

Wikerøy, A.K., Høiness, P.R., Andreassen, G.S., Hellund, J.C., Madsen, J.E. No difference in functional and radiographic results 8.4 years after quadricortical compared with tricortical syndesmosis fixation in ankle fractures. J Orthop Trauma 24(1):17-23, 2010

Wirth, A.J., Muller, R., van Lenthe, G.H. The discrete nature of trabecular bone microarchitecture affects implant stability. Journal of Biomechanics 2011.12.024, 2012

Wysolmerski, J.J., Insogna, K.L. The Parathyroid Glands, Hypercalcemia, and Hypocalcemia. In Williams Textbook of Endocrinology. 11th ed. St. Louis, Mo: WB Saunders: chap. 266, 2008

Young, W.C. and Budynas, R.C. Roark's Formulas for Stress and Strain, 7th Edition. McGraw-Hill, 2002

Yakacki C.M, Griffis F, Poukalova M & Gall K. Bearing Area: A New Indication for Suture Anchor Pullout Strength? Journal of Orthopaedic Research 27: 1048-1054, 2009

11.1 Bibliography

S.C. Cowin. Bone Mechanic's Handbook 2nd Edition. CRC Press, 2001

S.E. Asnis and R.F. Kyle. Cannulated Screw Fixation: Principles and Operative Techniques. Springer, 1996

11.2 World Wide Web Uniform Resource Locators

http://bioserv.fiu.edu/~walterm/gen_bio_II/sum10_reviewmini_skeletal_muscle _organization.htm (2/12/2012)

http://classconnection.s3.amazonaws.com/795/flashcards/1195795/jpg/compac t_bone1329351421274.jpg (03/04/2013)

http://classconnection.s3.amazonaws.com/436/flashcards/844436/jpg/long_bon e1319071915389.jpg (03/04/2013)

http://bioserv.fiu.edu/~walterm/gen_bio_II/sum10_reviewmini_skeletal_muscle _organization.htm) (03/04/2013)

http://medicalpicturesinfo.com/cancellous-bone/ (01/04/2012)

http://www.spinewelding.ch/technology/ (01/04/2013)

http://www.wheelessonline.com/ (22/11/2013)

http://www.nhs.uk/conditions/osteoporosis/Pages/Introduction.aspx (12/01/2012)

http://inside.mines.edu/~apetrell/ENME442/Labs/1301_ENME442_lab6_lecture.pdf (24/11/2013)

http://cdn.overclock.net/a/a4/a4a47b78_ChsSwUE.png (25/11/2013)

http://www.stryker.com/en-us/products/Orthopaedics/SportsMedicine/UpperExtremity/Anchors/Titanium/TitaniumWedgeAnchor/index.htm (1/11/2012)

http://international.arthrocaresportsmedicine.com/files/technique_guides/A50_4001D.pdf (1/11/2012)

http://biomaterials.evonik.com/product/biomaterials/Specifications/evonik-specification-resomer-lr-706-s.pdf (9/11/2013)

http://www.fda.gov/medicaldevices/deviceregulationandguidance/howtomarketyourdevice/premarketsubmissions/premarketnotification510k/default.htm (12/11/2013)

http://www.conmed.com/products/shoulder-bio-mini-revo.php (01/04/2013)

11.3 Additional Sources

Time magazine March 12, 1945 | Vol. XLV No. 11

Solidworks 2013®, Dassault Sytems®, Waltham, Massachusetts (2012)

ANSYS, ANSYS® Academic Research, Release 13 (2012)

MicroMRI Inc,. USA, (2014)

Mimics®v14.0, Materialise NV, Leuven, Belgium (2012)

SkyScan® (Bruker-MicroCT), Belgium, 2014

(http://www.skyscan.be/products/1172.htm)

Appendix A

Materialise® instruction for the creation of cancellous bone models with implant insertion stage by stage.

Smooth

Smooth factor 0.7

Do not use compensation

Reduce triangles

Geometrical error 0.01

Flip Threshold angle 30

Ensure one shell

Mark shell, invert and delete other bits

Auto remesh

- Shape quality threshold 0.2 (then next time 0.3)

- Maximum geometrical error 0.02 (because small part and do not want triangles to be able to move very far)

- Do not control edge length

- Do not preserve surface contours

* using inspection to look at the number of triangles that have a shape quality of less than 0.2

Deal with intersecting and overlapping triangles

Delete intersecting triangles

Mark intersecting triangles (trial had 108)

select expand marked triangles and delete them

Mass hole filler

- Bad contour length of 5mm (or larger to ensure all are filled)

One was remaining so mark shell and invert again

Delete overlapping triangles

Mark overlapping triangles (trial had 8)

Select expand marked triangles and delete them

Mass hole filler as above

Second auto remesh

- Shape quality threshold to 0.3

- Maximum geometrical error 0.01

- Control edge length on, max edge length 0.3

Ensure one shell

Mark, invert and delete

Deal with intersecting and overlapping triangles

This time do not use hole filling as it may create more low quality triangles

Do it manually by marking, deleting and filling

Quality preserve reduce triangles

Use same parameters as automesh

Implanting Screw

*Can change the colour of the parts by selecting the surface and changing the colour in the lower menu. Cannot change internal colours of individual parts

** To ensure that the co-ordinate systems are the same go to edit update OCS to CS, method WCS

Auto Remesh

Remesh the screw to ensure that there are no local areas of high density mesh

- Shape quality threshold 0.3

- Max geometrical error 0.01

- Max edge length 0.2

Preserve surface contours

Create non-manifold assembly

Make sure screw is being inserted into the bone - not the other way round

Fix sharp triangles

- Mark and remove

- check filter distance and how this affects the geometry of the screw bone

interface

Auto Remesh

Using the same shape quality thresholds as have been used on the 2 components

previously

If they are different then for max geometrical error use the lowest of the two

parts and for max edge length use the largest.

Deal with intersecting and overlapping triangles

Delete intersecting triangles

Mark intersecting triangles (trial had 2)

Select expand marked triangles and delete them

Delete overlapping triangles

Mark overlapping triangles (trial had 11)

Select expand marked triangles and delete them

If deleting wee bits make sure the interface belongs to the screw.

Checking for holes at the interface

Remeshing > Create non-manifold curves

Curve list. Non manifold curves-3

3 is the number of surfaces that the edge belongs to. Normally this is 1 for a

triangle on a surface but is more at the interface when surfaces are joining. All of

these should be 'closed', if they are not there is a hole so fix it. Non-manifold

curves-4 should be ok.)

Other holes not at the interface can be found by bad edges in the normal view.

Appendix B

Abstract of the Presentation given at the Bio-Engineering 2012 Conference at Queen Mary University.

Bone fixation using Ultra-sonically inserted polymer pins – finite element modelling of pull-out forces

Hughes, C.M.[1], Brown, C.J. [†1], Behrens, A.[2], Robionek, B.[2] Procter, P.[1,3]

[1] School of Engineering and Design, Brunel University, Uxbridge, UB8 3PH, UK.
[2] Stryker Osteosynthesis, Professor Kunscher Strasse, Kiel, Germany.
[3] Stryker Osteosynthesis, Le Lumion, CH-1218 Grand Saconnex, Switzerland
† Author to receive correspondence

Keywords: ultra-sonic bone pins, finite element modelling, bone fixation.

Finite element models are used to simulate pull-out from cancellous bone of ultra-sonically bonded bio-resorbable polymer pins. The polymer is bonded to cancellous bone using Sonicfusion®, a process that uses ultrasonic energy to create shear forces between the bone and the polymer, resulting in localised melting where there is contact between the bone and pin. The intention of the technology is to decrease operation time for surgeons, whilst maximising interface contact area. The technique is currently clinically approved for use in hallux valgus correction procedures.

Using Mimics image processing software a finite element (FE) assembly mesh of the trabecular structure and the polymer pin is created from CT scans of Sonicfusion® implanted pins in desiccated and washed-out ovine bone. Mechanical testing is carried out to measure basic mechanical properties of the bone samples and the elastic-plastic properties of the pin used in the simulations. It was observed that when heated, melted and cooled, the polymer created a bond with the bone surface, enabling a bonded contact condition to be chosen for FE models. A displacement was applied to the superior surface of the pin and the results were used to compare directly with those from laboratory testing.

Preliminary results show good comparisons between the FE models and pull-out forces obtained in tests. The FE model can then be used to compare the effect of different cancellous bone structures on pin pull-out characteristics. In particular, observations are made about the way in which load is transferred in some of the cases modelled and the relevance of this to design optimisation.

Appendix C

Presented here is the author proof copy of a paper accepted by the American Society of Mechanical Engineers to the Journal of Medical devices in February 2014. It can be found online at:

http://medicaldevices.asmedigitalcollection.asme.org/article.aspx?articleid=183 3796&resultClick=3

Hughes, C.M., Bordush, A., Robioneck, B., Procter, P., and Brown, C.J. Bone Anchors - a Preliminary Finite Element Study of Some Factors Affecting Pullout. Journal of Medical Devices 13:1262. 2014

C. M. Hughes
School of Engineering and Design,
Brunel University,
Uxbridge UB8 3PH, UK
e-mail: chris.hughes@brunel.ac.uk

A. Bordush
Stryker Osteosynthesis,
24232 Schönkirchen, Germany
e-mail: Astrid.Bordush@gmail.com

B. Robioneck
Stryker Osteosynthesis,
24232 Schönkirchen, Germany
e-mail: Bernd.Robioneck@stryker.com

P. Procter
Stryker Osteosynthesis,
24232 Schönkirchen, Germany
e-mail: philip.procter@stryker.com

C. J. Brown[1]
School of Engineering and Design,
Brunel University,
Uxbridge UB8 3PH, UK
e-mail: chris.brown@brunel.ac.uk

AQ1

Bone Anchors—A Preliminary Finite Element Study of Some Factors Affecting Pullout

Bone anchors (or suture anchors) are used to provide attachment points for sutures to connect tissue such as tendons or ligaments to bone, and work by engaging a threaded portion—sometimes tapered—to the cancellous and/or cortical bone. Such repair is often needed after trauma, or as part of reconstructive surgery. This paper uses the finite element method to compare the pullout characteristics of one common type of bone anchor in different cancellous bone structures. Finite element models are created by using computed tomography (CT) scans of cancellous bone and building computer-aided design (CAD) models to define the cancellous bone geometry. Orthopedic surgeons will sometimes remove parts of the cortical shell and this paper also examines the mechanical effects of de-cortication. Furthermore, the importance of the connection between anchor and cortical layer is examined. One of the key outcomes from the model is that the coefficient of friction between bone and anchor determines potential mechanisms of pullout. The stiffness of anchors and the effect of the cortical layer are presented for different pullout angles to obtain the theoretical response. The results show the detailed modeling that includes the micro-architecture of the cancellous bone is necessary to capture the large variations that can exist. [DOI: 10.1115/1.4026901]

Introduction

The application of finite element (FE) analysis provides a cost-effective method for the comparative assessment of the design and performance of biomedical devices. This paper describes a process for modeling pullout of a bone anchor. Detailed definition of the cancellous bone architecture enables a preliminary assessment of key factors that affect the pullout performance.

Bone anchors, or suture anchors, are commonly small metal or polymer tapered screws used to secure sutures, and hence soft tissue to bone in both reconstructive and trauma surgery. While suture failures can occur, the successful procedure often relies on the anchor pull-out performance, particularly in weak or osteoporotic bone. Barber et al. [1] gives a good outline of the range of geometric anchor designs that are most often titanium alloy or stainless steel. However, the use of polymers [1,2], and bio-absorbable or bio-degradable anchors [3] is also increasing. The threaded helix has performed well under in vitro static conditions [1,2]. Conversely, "push-fit" type anchors often have a low pullout force due to small area engagement with the bone.

Cummins and Murrell [4] have examined clinical data on revision of rotator cuff repair and conclude that most failures are from suture tear, although there is some evidence of anchor loosening, while Bynum et al. [5] have examined the relative likelihood of each type of failure. They conclude that if a suture is placed so that the head of the anchor is significantly below the surface of the cortical bone—then pullout failure is likely to be a problem, whereas shallower placement is likely to lead to suture failure. Yakacki et al. [6] focused on the characteristics of the underlying bone, and investigated the effect of trabecular microstructure on suture anchor pullout. The study was based on pullout tests in human cadaver bone, and found the greatest correlation of pull-out force was with trabecular structure [7], measured via the Structural Materials Index (SMI). The study also found good correlation with trabecular thickness and bone mineral density but

little or weak correlation with trabecular number and connectivity density. Tingart et al. [8] support this view, also having carried out pullout tests on cadaver bone, while subsequent work by Poukalova et al. [9] suggests that it is the modulus of the underlying bone that determines the pullout strength. There is also other evidence to suggest that the bone stiffness plays a significant part in determining pullout [10–14]. The angle at which loading is applied is thought to have an influence, and Patel et al. [15] tested screws inserted at an angle in a PU foam material.

Huiskes and Chao [16] completed an excellent review of the beginnings and early applications of the FE method, while recent exponents [17,18] have developed a systematic approach to its use. The heterogeneous architecture of cancellous bone means that it can vary significantly. Bone Young's modulus has a strong correlation with volume fraction; as the volume fraction of cancellous bone changes over a cross section (sic), its stiffness can vary by orders of magnitude [19], dependant on the trabecular orientation of the bone and the tissue properties [20]. Therefore the representation of cancellous bone as a continuum is of limited use for small scale implants, such as bone anchors. Chen et al. [21] adopted a method to set the density of each individual element using the grey scale value from CT scans with the density value in turn related to the elastic modulus. The outcome is a continuum model with variable mechanical stiffness but no geometric peculiarities. Melchels et al. [22] evaluated various mathematically defined architectures for the FE lattice modeling including cube, diamond, gyroid, and an irregular salt-leached structure, and demonstrated that for the same porosity a cubic structure will have a higher stiffness than a gyroid structure, while Wirth et al. [18] compared CT-based models and continuum models for application with screws. In both high and low density structures they found a significant difference in bone-implant stiffness between models in which the bone/anchor interface is assumed to be contiguously connected, and concluded that continuum models are of limited use for peri-implant analyses. Brown et al. [23] have also examined the fundamental phenomena affecting pullout with simplified FE models that represent the cellular structure.

The main focus of the work presented in this paper is the relative pull-out performance of an idealized spiral anchor dependent

---

(a)

(b)
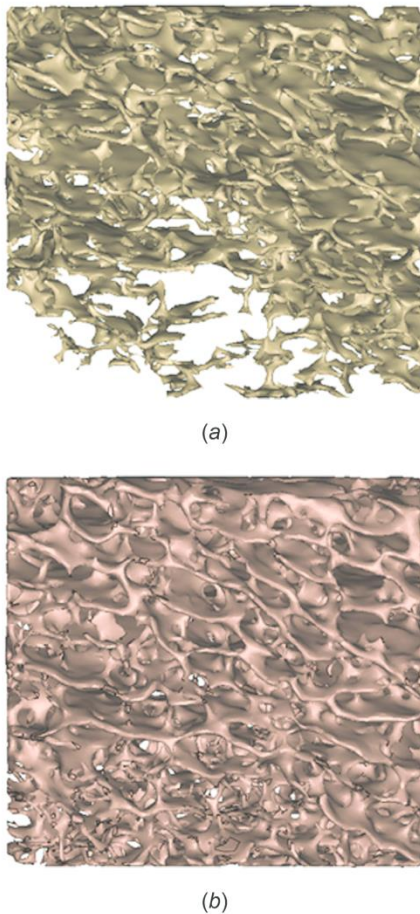
Fig. 1   (a) Image of low BV/TV. (b) Image of higher BV/TV.

78 on the underlying cancellous bone properties, and the important
79 effect of the cortical shell [14]. Two pieces of human cancellous
80 bone have been modeled, representing both "normal" and
81 "weaker" bone. The effect of connectivity with any cortical layer

82 present is considered. Modeling parameters such as friction and
83 contact are examined.
84   In clinical practice, loads are applied through a suture which
85 means that different loading angles can be applied to the direction
86 of pullout, and a second part of the study systematically examines
87 the consequence of angle of loading.

Materials and Methods   88

89   Ansys® [24] (Workbench version 13.0) was used to implement
90 all the FE analyses. FE modeling has evolved two common alter-
91 native strategies for detailed modeling of cancellous bone. The
92 first strategy uses voxels to create the building blocks of cancel-
93 lous bone and assembles the voxels as a solid, while the second
94 builds solids by modeling the surfaces and interpolates the surface
95 from a series of slices to form a solid. To determine pullout loads
96 for implants it is important to model the interacting surfaces of
97 bone and implant, and so this latter procedure is adopted here.

98   **Geometry.** A disc of bone was extracted from the femoral head
99 of a cadaver (adult female) and images were taken (μCT 1076,
100 SkyScan, Belgium—see Acknowledgment).
101   The bone has been orientated so that the upper surface (Fig. 1)
102 is parallel and near to the cortical shell. The "local" apparent bone
103 density measured by the ratio of Bone Volume (BV) to Total Vol-
104 ume (TV) (BV/TV) decreases through the depth of the sample.
105 The CT scan data was imported and processed using Mimics®
106 [25] (Materialise Mimics version 14.0) software to create surfa-
107 ces, and hence a volume of cancellous bone. The bone image was
108 cropped and a $10 \times 10 \times 11$ mm cancellous bone model created.
109   From the original volume, bone of different densities can be
110 created by modifying the threshold values in the software [26,27].
111 For this study two densities of bone have been created: one by
112 smoothing a closely approximated geometry of the original bone
113 (lower, Fig. 1(b)), and the other by eroding the smoothed geome-
114 try to give a bone of lower apparent density [28,29] (upper,
115 Fig. 1(a)). This method was chosen instead of finding two pieces
116 of bone with naturally different BV/TV, as it enables a direct
117 comparison between two similar bone structures. Tables 1 and 2
118 give the trabecular thickness and spacing measurements for both
119 cancellous bone models [30]. The smoothed bone model had an
120 overall apparent bone density of 17.5%, and this might represent
121 normal or healthy cancellous bone, while the eroded model had an
122 overall apparent bone density of 8.3%, and this might be more
123 appropriately described as weak or osteopenic bone. This study is
124 limited to this particular bone structure. For the sample with the
125 lower BV/TV ratio, the SMI (calculated using software ImageJ
126 1.46 with BoneJ plug-in 1.3.1. [30,7]) is 2.56, while for the higher
127 ratio the SMI is 2.03.

AQ2

Table 1   Trabecular thickness spacing and bone volume density data for the eroded model (all dimensions in mm). Tb.Th = trabecular thickness, Tb.Sp = trabecular spacing, and BV/TV = bone volume/total volume.

Region of bone	Tb.Th mean	Tb.Th S.D.	Tb.Th Max	Tb.Sp mean	Tb.Sp S.D.	Tb.Sp Max	BV/TV (%)
Bottom third	0.126	0.044	0.352	1.053	0.336	1.863	5.8
Middle third	0.143	0.050	0.381	1.026	0.372	2.176	8.5
Top third	0.154	0.061	0.419	0.917	0.304	1.816	10.6
Total	0.142	0.054	0.419	1.009	0.320	1.903	8.3

Table 2   Trabecular thickness spacing and bone volume density data for the smoothed model (all dimensions in mm). Tb.Th = trabecular thickness, Tb.Sp = trabecular spacing, and BV/TV = bone volume/total volume.

Region of bone	Tb.Th mean	Tb.Th S.D.	Tb.Th Max	Tb.Sp mean	Tb.Sp S.D.	Tb.Sp Max	BV/TV (%)
Bottom third	0.173	0.052	0.385	0.855	0.306	1.513	14.1
Middle third	0.192	0.062	0.468	0.762	0.336	1.850	17.7
Top third	0.203	0.072	0.528	0.670	0.269	1.556	20.7
Total	0.190	0.063	0.480	0.756	0.298	1.650	17.5

179

Fig. 2 Clockwise from top left: Isometric view of piece of bone, with anchor inserted, contact area shown on anchor, the final construct

Where appropriate a solid cortical shell was artificially created using CAD software, and therefore is an idealized body, i.e., there is no graduated change in apparent density between the upper surface and the cortical layer (Fig. 2). This was to ensure a controlled thickness of cortical shell could be used with the two cancellous bone BV/TV ratios.

Using CT manipulation software, it is possible to create a high resolution 3-D model and this is currently the most accurate method of simulating bone, and therefore often produces the most relevant and interesting results. Meshing was carried out using 3matic® (Materialise 3-matic version 6.1) software. Due to its inherent architecture and the presence of many spicules of bone, the limitations of the currently available software mean that the surface mesh has to be completed by inserting missing surface elements manually (i.e., the software does not give a fully automated process). Any intersecting or overlapping elements were deleted, and then replaced manually with similarly sized elements. The corrected mesh was then re-meshed using the software with the same mesh settings to ensure all elements were within the defined mesh resolution parameters. Higher mesh resolution settings or better geometric definition may occasionally prevent the creation of some intersecting and overlapping elements; conversely it tends to create a large number of ill-formed and hence ill-conditioned or "bad" elements within a certain volume. It is time-consuming and demanding to set-up and run each analytical model, and as models become more refined the need for the manual surface element insertion process increases dramatically.

Assembly. The spiral anchor used had a maximum external thread diameter of 5.36 mm and is shown in Fig. 3. Once the cancellous bone had been meshed, the anchor was placed into the two models using Boolean operations. Boolean operations allow a volume of bone identical to the anchor to be removed and be replaced by the anchor, thus ensuring a fit within the trabecular structure. The anchor was inserted vertically in the centre of the bone, and had the same position and orientation for each subsequent
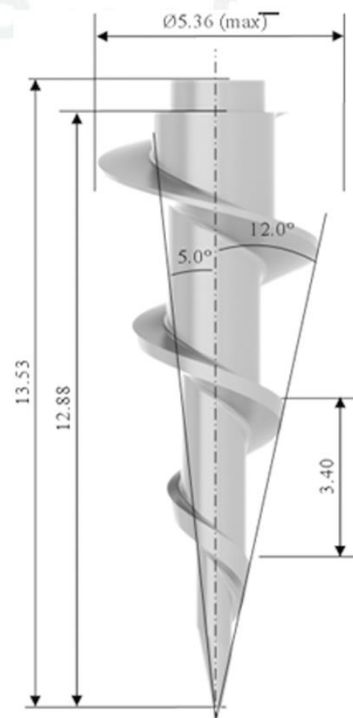
Fig. 3 Anchor with dimensions

analysis. The key dimensions of the anchor used are: maximum diameter of 5.36 mm, thread length of 12.88 mm, thread pitch of 3.4 mm, and a taper of 12 deg. The anchor dimension is based on a Stryker® Titanium Wedge anchor [31] but is similar in design essentials to other industry anchors such as the AthroCare® ParaFix Anchor [32].

Anecdotally, anchors can generate increased pullout resistance as they produce a radial stress field in the bone during the insertion process. This has not been modeled here. In weak bone, the radial stress field is very low, and while the ensuing results may be conservative we feel this is justified. Furthermore, the consequences of the anchor insertion process on the bone are unknown, and while it is possible that bone fragments might cause local damage and weakening of trabecular struts, an effect similar to that produced by impaction grafting might also ensue, giving increased strength. Again, this has not been modeled here.

The term "fully engaged" is used to indicate when the thread of the anchor is embedded in the cortical shell. Alternatively, the cortical shell may still generally be present and important [14] but removed at the anchor location through drilling or other surgical procedure—de-cortication. To model this, a cylinder of cortical bone equal to the cortical thickness and of diameter slightly greater than the anchor has been removed. This allows the anchor to engage in the cancellous bone alone without connection to the cortex.

In total, eight different geometries were explored for each apparent density resulting in sixteen meshes. The geometries for each cancellous bone apparent density were

- one without any cortical layer,
- one with a non-engaged cortical layer with five cortical thicknesses of 0.25, 0.5, 1.0, 1.5, and 2.0 mm, respectively, and
- two with anchors fully engaged with a cortical layer of 0.5 mm and 1.5 mm, respectively.

We consider this represents the smallest stiffness and a range of increasing stiffness of underlying bone.

Material Properties. In this preliminary study the elastic and strength properties used for bone elements [33–35] and titanium alloy are assumed to be the same in tension and compression. The bone elements have Young's modulus = 17 GPa, Poisson's ratio = 0.3, yield strength = 100 MPa, and ultimate strength 120 MPa. The values chosen fall within a range of measured values given in the literature for "normal" bone [35]. The material properties used for titanium alloy [24] are Young's modulus = 96 GPa, Poisson's ratio = 0.3, yield strength = 930 MPa, and ultimate strength 1070 MPa.

Contact. The interface between the bone and anchor is a frictional contact. Previous experience [23] has shown the results to be more appropriate to physical studies when compared to the alternative bonded model. This is because under bonded contact no contact shear stress or sliding occurs between the surfaces, resulting in a significantly stiffer structure. A frictional coefficient of 0.6 [23] was normally used—a more detailed comment on the variation of pullout mechanism with frictional contact is given below. A bonded contact was used between the cancellous bone and the idealized cortical layer.

Loading. The elements of the cancellous bone block were fully restrained on the four vertical sides (i.e., those outer surfaces lying in the z–x and z–y planes—the cortical layer lying in the x–y plane). For every simulation a linear ramped displacement in the appropriate direction of 0.2 mm was applied to the cylinder at the top of the anchor (eyelet strength was not a point of interest for this study and so was replaced with a cylinder to simplify the FE mesh and consequently reduce solver time). In clinical practice the loading on the eyelet varies in direction depending on tendon attachment location. Therefore the four different angles of loading in the positive z–y plane only are: vertical (0 deg), 45 deg, 72.5 deg, and horizontal (90 deg). This latter is not a practical case but provides a limit analysis. The forces given as "pullout" forces are in fact the reaction forces at the directional displacement of 0.2 mm.

Convergence tests are difficult for these models. Approximately one million volume elements are used for a volume of about 1100 mm³, and each of these models can take significant time (of the order of days) to load and complete the run. This number of elements is close to the limit of computational ability available to the authors at this time. Hence, further refinement is not achievable as it would involve taking a significantly smaller piece of bone around the screw. Other issues related to the creation of the models arise (see comments mesh generation above). Further coarsening is also not acceptable, as the mesh is graded to give adequate geometric definition of the screw/bone interface—a factor which in our experience is also important to give a solution with the contact elements used. Larger elements may lead to a failure to produce any solution.

Results

Contact area between the anchor and the bone will vary for the same anchor in different apparent densities of bone with the same structure and topography. Figure 4(a) shows the contact area between the bone and implant on the implant, while Fig. 4(b)

High density

Low density

(a)   (b)
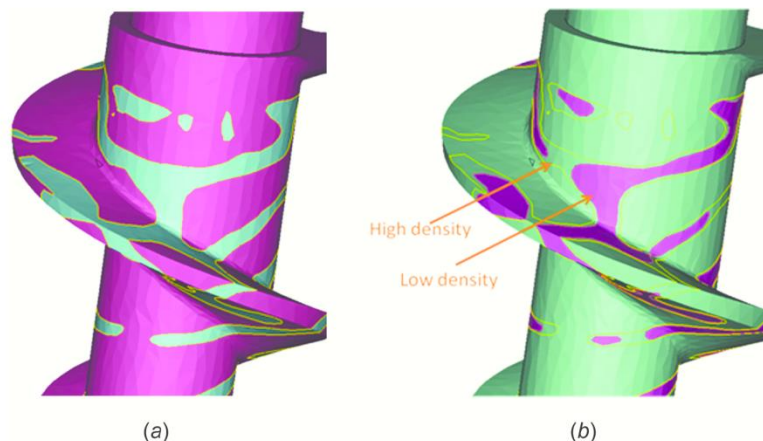
Fig. 4   (a) Contact region in higher apparent density bone. (b) Contact region in lower apparent density bone.
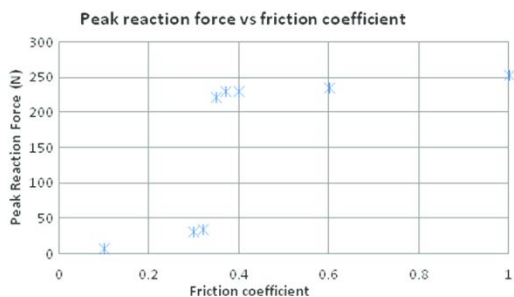
Fig. 5   Variation of peak reaction force with friction coefficient

Figure 6 shows the position of the upper surface of the anchor with increasing pull-out displacement—i.e., for the initial position and four subsequent consecutive displaced positions during the pull-out process. The range from blue to red indicates increasing displacement normal to the upper surface that is being viewed. On the left, there is rotation of the upper surface visible where the friction coefficient is low; on the right, there is no rotation where the friction coefficient is 0.6.

The pullout force output (Fig. 7 et seq.) is given as the peak reaction force at a vector displacement of 0.2 mm. A value of 0.2 mm was used as this was the largest mean trabecular thickness of either bone model; values beyond 0.2 mm would be likely to

shows the same plot of the area in contact using a computer-eroded bone model, with the outline of the original contact area given in the same figure. In some cases the contact area of a particular trabecular strut slightly decreased, while in others it has been removed entirely. The higher apparent density model had a contact area of 16.28 mm², and this decreased to 10.13 mm² for the lower apparent density model.

Small changes in friction coefficient between 0.3 and 0.4 can lead to large changes in pullout force (Fig. 5). Above 0.4 the rate of increase of pullout force is small for increasing friction coefficients. A friction coefficient of 0.3 or below can lead to low values of pullout force.
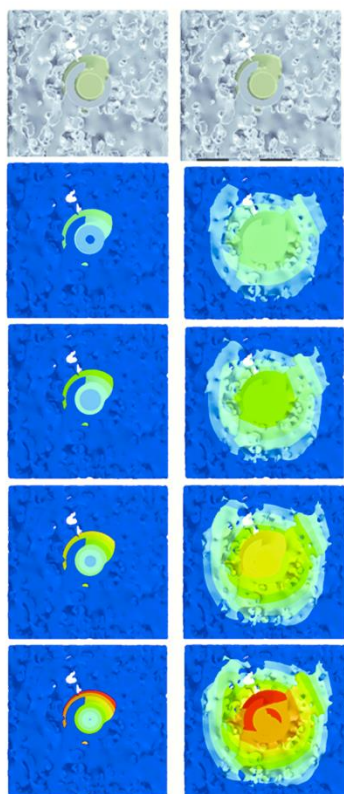
Fig. 6   Upper surface of anchor at increasing load. Left: low friction coefficient. Right: higher friction coefficient.

Fig. 7   Variation of reaction force with cortical thickness for two apparent densities, with engaged and non-engaged anchors (a) vertical load, (b) load at 45 deg, (c) load at 72.5 deg, and (d) load horizontal

274 indicate large deflections in the trabecular struts beyond the scope
275 of the present analysis. Figure 7(a) is for vertical pullout, while
276 Fig. 7(b) is for loading inclined at 45 deg, Fig. 7(c) is for 72.5 deg,
277 and Fig. 7(d) is for 90 deg. Four sets of results are presented and
278 two bone apparent densities each with two cortical shell condi-
279 tions are given—when the anchor thread is engaged with the corti-
280 cal layer and when it is not engaged (i.e., when the cortex has
281 been "over-drilled").
282   The patterns of displacement on a slice through the centre of
283 the construct under vertical pullout (Fig. 8(a)) and lateral pullout,
284 respectively (Fig. 8(b)) show the changes in stress within the bone.
285   The developing number of elements in contact (Fig. 9) while
286 increasing the loading shows quite marked differences between
287 pullout and cut-out for the same anchor in the same piece of bone.

288 Discussion

289   The results show the relative magnitudes of pullout force for
290 different anchor/bone configurations. Validation of implant pull-
291 out force is difficult in real bone because of its variable material
292 properties, while substitute materials produce unrepresentative
293 loads. Nevertheless, the numerical values from the FE model are
294 consistent with the order of magnitude of those data presented in
295 the literature [1] for the pullout of suture anchors, where mean
296 pull-out values of between 220 N and 710 N are given.

(a)

(b)
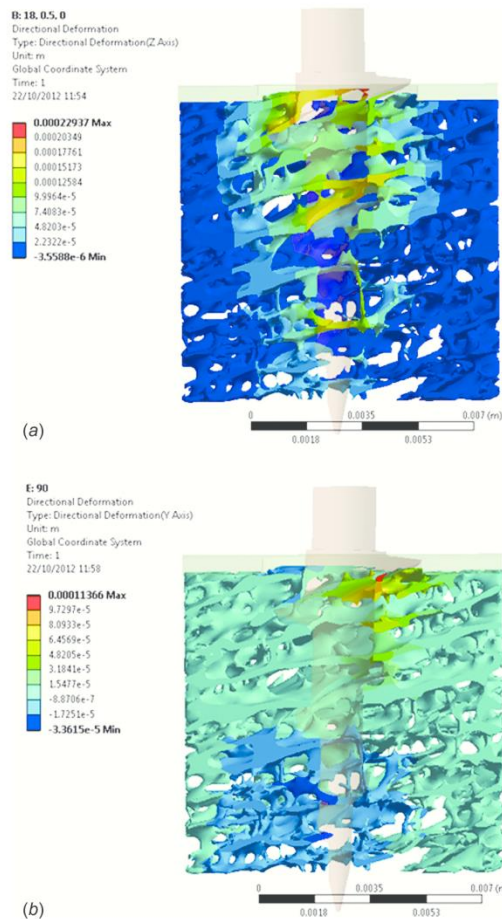
Fig. 8 Slice showing deformation under (a) vertical load and (b) horizontal load
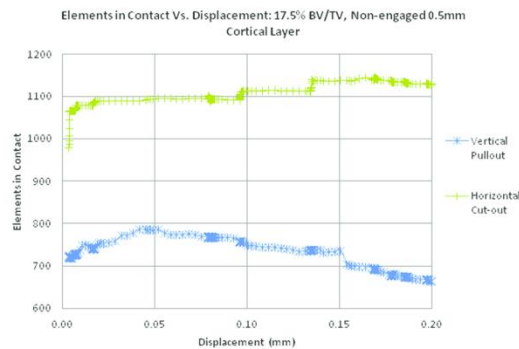
Fig. 9 Elements in contact with increasing displacement for vertical and horizontal loads

Figure 4 shows the relatively small area of an implant that 297
actually connects to the bone structure. Even so, contact area does 298
not appear to relate directly to pullout force, although Yakacki 299
et al. [36] suggest otherwise. However, greater contact area is 300
likely to be associated with bone of higher apparent density, for 301
which there is strong evidence of increased pullout force [36,37]. 302
There is generally a very small part of the anchor in contact with 303
the cancellous bone. 304
    The marked effect of changing friction coefficient has been 305
shown in the results. We suggest that this may be due to different 306
modes of pullout represented in the model. On the left of Fig. 6, 307
the friction coefficient is low, and an "un-screwing" phenomenon 308
can be observed through the rotation of the top of the screw. On 309
the right with higher friction, there is no screw rotation and the 310
upper surface of the bone is moved towards the viewer as a rigid 311
body, even though sliding between surfaces in the model is still 312
allowed. That this phenomenon can be observed in the model is 313
somewhat surprising. In previous work on screw fixation [23] we 314
have examined the importance of friction coefficient and deduced 315
it might not be a critical factor, but approximate models, espe- 316
cially those that use continua to represent cancellous bone, are 317
unlikely to be able to exhibit this unscrewing behavior. There is 318
little change in pullout force for a range of friction coefficients 319
between 0.35 and 0.6. in vivo, friction coefficients may change 320
with time as surfaces are lubricated to a greater or lesser degree. 321
    This rotation effect with low friction has been demonstrated for 322
a pull-out displacement applied to the upper surface of the screw, 323
and normal to the bone outer surface, and it may be that as the 324
loading is inclined this effect will be minimal. Furthermore, any 325
"clamping" effect on the anchor that may be present from inser- 326
tion procedures and the resultant radial stress field has been omit- 327
ted, although the magnitude of this in bone of low apparent 328
density is unknown. Nevertheless, the fact that this potential 329
mechanism is demonstrated in the FE model gives further support 330
for the validation of such a model. Higher coefficients of friction 331
have been used in the remaining modeling to be more representa- 332
tive of normal behavior. 333
    The angle of pull-out has been investigated (Fig. 7), and it is 334
varied from an angle normal to the surface (Fig. 7(a)) to one par- 335
allel to the bone upper surface (Fig. 7(d)) with two other angles in 336
between (Figs. 7(b) and 7(c)). The key observation from the 337
results for the different parameters in the study is that, as 338
expected, the pull-out is most strongly influenced by the apparent 339
density of the underlying bone. With a density of 17.5%, the pull- 340
out force at a given displacement is generally at least double that 341
of the lower 8.3% apparent density. 342
    As expected, the pullout force is greater if there is a cortical 343
shell present [14,21] even if the anchor is not engaged with the 344
cortex. However, this effect diminishes for non-engaged anchors 345
as the cortex becomes thicker, and from 0.5 mm to 2 mm there is a 346

(a)

(b)
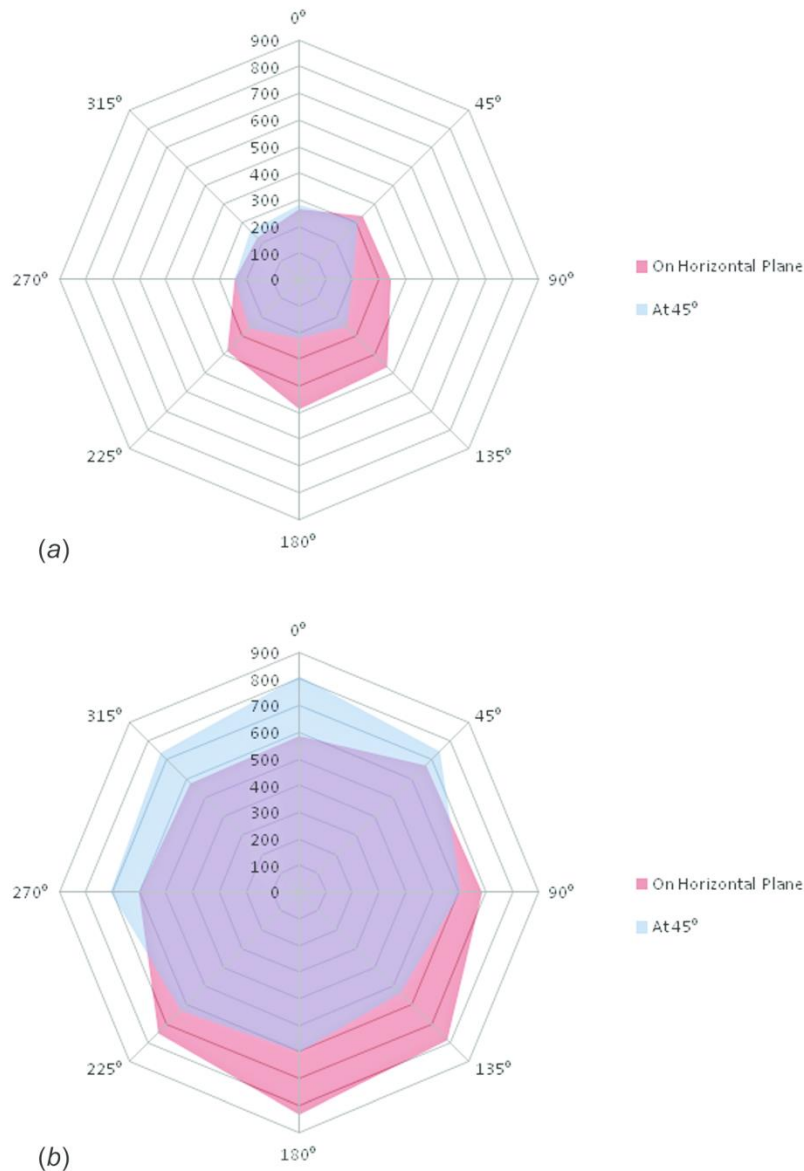
Fig. 10   (*a*) Variation of reaction force (N) with angle for low apparent density bone. (*b*) Variation of reaction force (N) with angle for higher apparent density bone.

negligible increase in force for both bone densities. Nevertheless the importance of maintaining even a minimal cortical layer is evident.

For pullout angles of zero, up to about 45 deg the importance of connecting to a cortical layer—even of limited thickness—can be remarkable. In the bone of higher apparent density there is little effect for thin cortical layers because the cancellous bone is relatively stiff, but for a cortical layer of about 1.5 mm the pullout force is significantly increased. In the bone of lower apparent density the cortical layer has an immediate effect, and even the 0.5 mm layer will increase pullout force for low angles of inclination.

Instead of a direct pullout through failure at the bone anchor interface, the anchor is also engaged in cut-out as it tries to move through the bone so that at 90 deg the mechanism is almost entirely cut-out. For vertical pullout, the deformation is almost the same at any position around the anchor, while for the lateral load it is evident that significant deformation is happening in the cancellous bone adjacent to the top of the anchor, and this pattern is shown in Fig. 8.

In the early stages of loading, the number of contacts increases (Fig. 9) as the tiny gaps between the anchor surface and adjacent bone elements are closed. As the anchor is pulled further, more contacts are generated under lateral loading than under vertical

PROOF COPY [MED-13-1262]

loading. Finally, the number of contacts under lateral loading decrease as the tip of the anchor moves away from the bone.

While combined vertical and horizontal loading has been examined in one selected plane, the choice of this plane was arbitrary. To check that this choice has no effect, the direction of the lateral load is changed by 45 deg on the x–y plane to give seven other directions (eight in total). Figure 10 shows a plot of pullout forces when the force is horizontal, and when pullout is inclined at 45 deg to the horizontal for both low and higher apparent density bone. The reaction load can change quite markedly depending on the direction of pull. In the lower apparent density bone, the mean pullout force for loads on the horizontal plane is 344 N (CV = Coefficient of Variation = Standard deviation/mean = 28.9%) but the minimum value is 223 N, and the maximum 489 N—a ratio of 2.19:1. As might be expected, the variation is less when the pullout is at 45 deg to the plane, with a mean of 255 N (CV = 13.7%), a minimum of 200 N, and a maximum of 314 N—a ratio of 1.57:1. As the angle to the horizontal plane increases this ratio should decrease, so that at 90 deg to the horizontal plane the ratio must be unity. In the bone of higher apparent density the variation is not as great. The CV values are both 14%, and the mean values show much less divergence. Nevertheless, such variation could never be detected in any models that use a continuum representation of cancellous bone.

This small element of the study shows the sensitivity of pullout force to local bone structure and the importance of including this feature in any models that are created for screw pull-out. The potential consequences for both in vivo applications and in vitro testing are quite important. First, there is going to be a large variation in pull-out force in the in vivo configuration. Further studies are needed to consider how such variation can be mitigated, but it is clear that the parameters identified here (e.g., bone apparent density, screw pull-out angle) will have a fundamental effect. Second, it indicates that any tests carried out in vitro in bone of low apparent density will have a potentially large variation in results. While definition of bone parameters is useful (e.g., Tables 1 and 2) this is not sufficient to describe the key parameters; again further studies are needed.

Conclusion

This study has shown the importance of friction coefficient in models of anchor pullout from a porous structure, and suggests that very low coefficients might lead to quite different mechanisms than those where friction is high. Any change in friction in vivo could lead to a marked change in performance.

The study has also re-confirmed the importance of a cortical layer. At the angles and apparent densities simulated, engagement with the cortical layer increases pullout force dramatically. Engaging the anchor even with a thin cortical layer can produce a significant advantage to pull-out strength.

Finally, we have shown the critical nature of modeling the microstructure of bone. Changing the direction of loading in the model leads to significant changes in the response of the construct, and this cannot be represented in continuum models, or in physical models using artificial cancellous bone. These results demonstrate that the fundamental variability in real bone can lead to large changes in behavior over quite a small volume.

Acknowledgment

References

[1] Barber, A., Herbert, M. A., Coons, D. A., and Boothby, M. H., 2006, "Sutures and Suture Anchors," J. Arthroscopic Relat. Surg., ■, pp. ■–■.

[2] Barber, A., Herbert, M. A., Beavis, C., and Oro, F. B., 2008, "Suture Anchor Materials, Eyelets, and Designs: Update 2008," J. Arthroscopic Relat. Surg., ■, pp. ■–■

[3] Tan, C. K., Guisasola, I., Machani, B., Kemp, G., Sinopidis, C., Brownson, P., and Frostick, S., 2006, "Arthroscopic Stabilization of the Shoulder: A Prospective Randomized Study of Absorbable Versus Non-Absorbable Suture Anchors," Arthroscopy, 22, pp. 716–720.

[4] Cummins, C. A., and Murrell, G. A., 2003, "Mode of Failure for Rotator Cuff Repair With Suture Anchors Identified at Revision Surgery," J. Shoulder Elbow Surg., 12(2), pp. 128–133.

[5] Bynum, C. K., Lee, S., Mahar, A., Tasto, J., and Pedowitz, R., 2005, "Failure Mode of Suture Anchors as a Function of Insertion Depth," Am. J. Sports Med., 33(7), pp. 1030–1034.

[6] Yakacki, C. M., Poukalova, M., Guldberg, R. E., Lin, A., Saing, M., Gillogy, S., and Gall, K., 2010, "The Effect of the Trabecular Microstructure on the Pullout Strength of Suture Anchors," J. Biomech., 43, pp 1953–1959.

[7] Hildebrand, T., and Rüegsegger, P., 1997, "Quantification of Bone Microarchitecture With the Structure Model Index," Comput. Methods Biomech. Biomed. Eng., 1(1), pp. 15–23.

[8] Tingart, M. J., Apreleva, M., Lehtinen, J., Zurakowski, D., and Warner, J. J., 2004, "Anchor Design and Bone Mineral Density Affect the Pullout Strength of Suture Anchors in Rotator Cuff Repair: Which Anchors Are Best to Use in Patients With Low Bone Quality?," Am. J. Sports Med., 32(6), pp. 1466–1473.

[9] Poukalova, M., Yakacki, C. M., Guldberg, R. E., Lin, A., Saing, M., Gillogly, S. D., and Gall, K., 2010, "Pullout Strength of Suture Anchors: Effect of Mechanical Properties of Trabecular Bone," J. Biomech., 43(6), pp. 1138–1145.

[10] Asnis, S. E., Ernberg, J. J., Bostrom, M., Wright, T. M., Harrington, R. M., Tencer, A., and Peterson, M., 1996, "Cancellous Bone Screw Thread Design and Holding Power," J. Orthop. Trauma, 10(7), pp. 462–469.

[11] Chapman, J. R., Harrington, R. M., Lee, K. M., Anderson, P. A., Tencer, A. F., and Kowalski, D., 1996, "Factors Affecting the Pullout Strength of Cancellous Bone," J. Biomech. Eng., 118, pp. 391–398.

[12] Larsson, S., and Procter, P., 2011, "Optimising Implant Anchorage (Augmentation) During Fixation of Osteoporotic Fractures: Is There a Role for Bone-Graft Substitutes?," Inj. Int. J. Care Inj., 42, pp. S72–S76.

[13] Ramaswamy, R., Evans, S., and Kosashvili, Y., 2010, "Holding Power of Variable Pitch Screws in Osteoporotic, Osteopenic and Normal Bone: Are All Screws Created Equal?," Injury, 41, pp. 179–183.

[14] Seebeck, J., Goldhahn, J., Morlock, M. M., and Schneider, E., 2005, "Mechanical Behavior of Screws in Normal and Osteoporotic Bone," Osteoporosis Int., 16, pp. S107–S111.

[15] Patel, P. S. D., Shepherd, D. E. T., and Hukins, D. W. L., 2010, "The Effect of Screw Insertion Angle and Thread Type on the Pullout Strength of Bone Screws in Normal and Osteoporotic Cancellous Bone Models," Med. Eng. Phys., 32, pp. 822–828.

[16] Huiskes, R., and Chao, E. Y. S., 1983, "A Survey of Finite Element Analysis in Orthopedic Biomechanics: The First Decade," J. Biomech., 16(6), pp. 385–409.

[17] Helgason, B., Taddei, F., Pálsson, H., Schileo, E., Cristofolini, L., Viceconti, M., and Brynjólfsson, S., 2008, "A Modified Method for Assigning Material Properties to FE Models of Bones," Med. Eng. Phys., 30(4), pp. 444–453.

[18] Wirth, A. J., Muller, R., and van Lenthe, G. H., 2012, "The Discrete Nature of Trabecular Bone Microarchitecture Affects Implant Stability," J. Biomech., 45(6), pp. 1060–1067.

[19] Goldstein, S. A., Wilson, D. L., Sonstegarij, D. A., and Matthews, L. S., 1983, "The Mechanical Properties of Human Tibial Trabecular Bone as a Function of Metaphyseal Location," J. Biomech., 16, pp. 965–969.

[20] Keaveny, T. M., Morgan, E. F., Niebur, G. L., and Yeh, O. C., 2001, "Biomechanics of Trabecular Bone," Annu. Rev. Biomed. Eng., 3, pp. 307–333.

[21] Chen, S. I., Lin, R. M., and Chang, C. H., 2003, "Biomechanical Investigation of Pedicle Screw-Vertebrae Complex: A Finite Element Approach Using Bonded and Contact Interface Conditions," Med. Eng. Phys., 25(4), pp. 275–282.

[22] Melchels, F. P. W., Bertoldi, K., Gabbrielli, R., Velders, A. H., Feijen, J., and Grijpma, D. W., 2010, "Mathematically Defined Tissue Engineering Scaffold Architectures Prepared by Stereolithography," Biomaterials, 31(27), pp. 6909–6916.

[23] Brown, C. J., MacInnes, R. A., Day, A., Hess, B., and Procter, P., 2013, "An Approximate Model for Cancellous Bone Screw Fixation," Comput. Methods Biomech. Biomed. Eng., 16(4), pp. 443–450.

[24] ANSYS, ANSYS® Academic Research, Release 13, 2012.

[25] Mimics®, v14.0, Materialise NV, Leuven, Belgium.

[26] Hara, T., Tanck, E., Homminga, J., and Huiskes, R., 2002, "The Influence of Microcomputed Tomography Threshold Variations on the Assessment of Structural and Mechanical Trabecular Bone Properties," Bone, 31(1), pp. 107–109.

[27] Kim, C. H., Zhang, H., Mikhail, G., von Stechow, D., Muller, R., Kim, H. S., Guo, X. E., 2007, "Effects of Thresholding Techniques on MicroCT-Based Finite Element Models of Trabecular Bone," J. Biomech. Eng., 129(4), pp. 481–486.

[28] Guo, X. E., and Kim, C. H., 2002, "Mechanical Consequence of Trabecular Bone Loss and Its Treatment: A ThreeDimensional Model Simulation," Bone, 30, pp. 404–411.

[29] van der Linden, J. C., Verhaar, J. A., and Weinans, H., 2002, "A ThreeDimensional Simulation of AgeRelated Remodeling in Trabecular Bone," J. Bone Miner. Res., 17, pp. 688–696.

[30] Doube, M., Klosowski, M. M., Arganda-Carreras, I., Cordelières, F., Dougherty, R. P., Jackson, J. S., Schmid, B., Hutchinson, J. R., Shelbelline, S. J., and

185

PROOF COPY [MED-13-1262]

Bone, J., 2010, "Free and Extensible Bone Image Analysis in ImageJ," Bone, **47**(6), pp. 1076–1079.

[31] See http://www.stryker.com/en-us/products/Orthopaedics/SportsMedicine/Upper Extremity/Anchors/Titanium/TitaniumWedgeAnchor/index.htm (last accessed November 1, 2012).

[32] See http://international.arthrocaresportsmedicine.com/files/technique_guides/A50_4001D.pdf (last accessed November 1, 2012).

[33] Ashman, R. B., Cowin, S. C., Van Buskirk, W. C., and Rice, J. C., 1984, "A Continuous Wave Technique for the Measurement of the Elastic Properties of Cortical Bone," J. Biomech., **17**, pp. 349–361.

[34] Turner, C. H., Rho, J., Takano, Y., Tsui, T. Y., and Pharr, G. M., 1999, "The Elastic Properties of Trabecular and Cortical Bone Tissues are Similar: Results From Two Microscopic Measurement Techniques," J. Biomech., **32**, pp. 437–441.

[35] Rincon Kohli, L., 2003, "Identification of a Multiaxial Failure Criterion for Human Trabecular Bone," PhD thesis, Faculté Sciences et Technique de l'Ingénieur, Institut de Genie biomedical, Section de Genie Mécanique, Ecole Polytechnique Federale de Lausanne, Lausanne, Switzerland.

[36] Yakacki, C. M, Griffis, F., Poukalova, M., and Gall, K., 2009, "Bearing Area: A New Indication for Suture Anchor Pullout Strength?," J. Orthop. Res., **27**, pp. 1048–1054.

[37] Asnis, S. E., and Kyle, R. F., 1996, *Cannulated Screw Fixation: Principles and Operative Techniques*, Springer, New York.

AQ5

186